
Study of Aerofoils at High Angle of Attack, in Ground Effect.

*A thesis submitted in fulfilment of the requirements for the degree of
Master of Engineering*

Daniel J. Walter

B.Eng. (Hons)

SCHOOL OF AEROSPACE, MECHANICAL & MANUFACTURING ENGINEERING

PORTFOLIO OF SCIENCE, ENGINEERING & TECHNOLOGY

RMIT UNIVERSITY

September 2007

Abstract

Aerodynamic devices, such as wings, are used in higher levels of motorsport (Formula-1 etc.) to increase the contact force between the road and tyres (i.e. to generate downforce). This in turn increases the performance envelope of the race car. However the extra downforce increases aerodynamic drag which (apart from when braking) is generally detrimental to lap-times. The drag acts to slow the vehicle, and hinders the effect of available drive power and reduces fuel economy. Wings, in automotive use, are not constrained by the same parameters as aircraft, and thus higher angles of attack can be safely reached, although at a higher cost in drag. Variable geometry aerodynamic devices have been used in many forms of motorsport in the past offering the ability to change the relative values of downforce and drag. These have invariably been banned, generally due to safety reasons. The use of active aerodynamics is currently legal in both Formula SAE (engineering competition for university students to design, build and race an open-wheel race car) and production vehicles. A number of passenger car companies are beginning to incorporate active aerodynamic devices in their designs.

In this research the effect of ground proximity on the lift, drag and moment coefficients of inverted, two-dimensional aerofoils was investigated. The purpose of the study was to examine the effect ground proximity on aerofoils post stall, in an effort to evaluate the use of active aerodynamics to increase the performance of a race car. The aerofoils were tested at angles of attack ranging from 0° – 135° . The tests were performed at a Reynolds number of 2.16×10^5 based on chord length. Forces were calculated via the use of pressure taps along the centreline of the aerofoils. The RMIT Industrial Wind Tunnel (IWT) was used for the testing. Normally 3m wide and 2m high, an extra contraction was installed and the section was reduced to form a width of 295mm. The wing was mounted between walls to simulate 2-D flow. The IWT was chosen as it would allow enough height to reduce blockage effect caused by the aerofoils when at high angles of incidence. The walls of the tunnel were pressure tapped to allow monitoring of the pressure gradient along the tunnel. The results show a delay in the stall of the aerofoils tested with reduced ground clearance. Two of the aerofoils tested showed a decrease in C_l with decreasing ground clearance; the third showed an increase. The C_d of the aerofoils post-stall decreased with reduced ground clearance. Decreasing ground clearance was found to reduce pitch moment variation of the aerofoils with varied angle of attack.

The results were used in a simulation of a typical Formula SAE race car. For a car travelling at 55km/h, the use of active aerodynamics was found to improve steady state cornering by 9% to 1.89g (wings @ 10°), or alternatively its braking by 10% to 2.04g (wings @ 45°). With the wings in the

low-drag position (0° AoA) the addition power requirement would be only 26.0W. However given the added complexity an active aerodynamic system would add the design, manufacture and testing of a Formula SAE race car, it is unlikely that such a system could be considered worthwhile.

Declaration

I, Daniel Walter declare that:

- the work included in this thesis is my own except where due acknowledgement has been made;
- the work in this thesis has not been submitted previously, in whole or in part, to qualify for any other academic award;
- the content of this thesis is the result of work which has been carried out since the official commencement date of the approved research program;
- any editorial work, paid or unpaid, carried out by a third party has been acknowledged;
- ethics procedures and guidelines have been followed.

Daniel Walter

26 – March - 2007

Acknowledgements

Firstly I would like to thank my family. Their continuing support and encouragement have allowed me to complete this project.

Thankyou to my Supervisors, Prof. Simon Watkins and Dr Angelo Tempia for their guidance and support throughout the project. Thankyou for the time spent reading and commenting on the drafts for this thesis. Their enthusiasm and aptitude have enriched this project as well as the minds of their students.

RMIT Racing was more than just the inspiration for this project; the team provided access to data for this project, and provided an environment for the development of tomorrow's automotive leaders. I look forward to the new developments you will bring to the FSAE.

The RMIT technical staff are a valuable resource and this project would not have happened without their guidance and assistance. Thankyou to Gil Atkin for his assistance in the construction and installation of the mechanism to support the aerofoils and the construction, installation and removal of the 2D test section for the RMIT Industrial Wind Tunnel. Thankyou to both Adrian Reivers and Mark Overend for the measurement of the aerofoil models.

Thankyou to the Formula SAE Tire Test Consortium (FSAE TTC) and the Calspan Tire Research Facility (TIRF) for access to, and the use of relevant tyre data.

Table of Contents

Abstract.....	i
Declaration.....	iii
Acknowledgements.....	iv
Table of Figures	iv
Table of Equations	vii
Nomenclature	viii
Chapter 1 Introduction.....	1
1.1 Preamble	1
1.2 Properties of aerofoils	3
1.3 The effects of high angles of attack	4
1.4 The ground effect	6
1.5 Wind-tunnel testing techniques	24
1.5.1 Two-dimensional flow simulation	24
1.5.2 Ground effect simulation.....	26
1.5.3 Correction factors	29
1.5.4 Data acquisition	31
1.5.5 Size of model	33
1.6 The use of aerodynamic devices on automobiles.....	9
1.6.1 Vehicle requirements for maximum performance	11
1.7 The Formula SAE competition.....	21
1.7.1 Formula SAE design considerations	21
1.8 Scope and objectives of this investigation.....	22
Chapter 2 Apparatus and testing method employed	24
2.1 Preamble	24

Table of Contents

2.2 Experimental design.....	24
2.3 Two-dimensional tunnel design and construction.....	35
2.4 Aerofoils used for testing	40
2.5 Instrumentation and measurement procedure.....	43
Chapter 3 Results and discussion.....	47
3.1 Preamble	47
3.2 Correction method.....	47
3.3 Pressure contours	48
3.4 Individual aerofoil results	52
3.4.1 Lift coefficient variation	53
3.4.2 Drag coefficient variation	59
3.4.3 Moment coefficient variation	65
3.5 Aerofoil comparison.....	72
3.6 Discussion.....	74
3.6.4 Discussion of errors	43
3.6.5 Discussion of results.....	75
Chapter 4 Implications of results.....	80
4.1 Preamble	80
4.2 Wing size.....	80
4.3 Aspect ratio	81
4.4 Flow interaction	83
4.5 Vehicle weight	84
4.6 Tyres	84
4.7 Vehicle aerodynamic characteristics	85
4.8 Potential performance benefit.....	85
4.8.1 Pre-stall 3-D wing coefficients.....	85

Table of Contents

4.8.2 Post-stall 3-D wing coefficients	87
4.8.3 Potential forces and benefit from system	88
Chapter 5 Conclusions and recommendations.....	93
5.1 Preamble	93
References and bibliography	96
Appendix 1 Calibration.....	106
A1.1 Dynamic Cobra probe calibration.....	106
A1.2 DPMS calibration	107
A1.3 Tunnel calibration.....	110
Appendix 2 Errors	114
A2.1 Aerofoil geometry.....	114
A2.2 Measurement of AoA	116
A2.3 Pressure measurement.....	116
A2.4 Measurement of ground clearance	117
A2.5 Measurement of flow velocity.....	117
A2.6 Environmental variables.....	117
A2.7 Repeatability study.....	118

Table of Figures

Figure 1.1 Variation of C_l and C_d vs AoA (R.Sheldahl P. Klimas, (1981))	5
Figure 1.2 Variation of C_l with Ground Clearance (Zhang et al, 2002) for a Tyrell 026 aerofoil.	7
Figure 1.3 Example of tyre drive force and traction vs speed	12
Figure 1.4 Friction ellipse, adapted from Milliken (1995).....	13
Figure 1.5 Lateral Weight Transfer	14
Figure 1.6 Lateral Coefficient variation with vertical load - Data courtesy of TIRF and TTC (2005) and used with permisssion.....	15
Figure 1.7 Longitudinal Coefficient variation with vertical load - Data courtesy of TIRF and TTC (2005) and used with permisssion.....	15
Figure 1.8 Aerodynamic requirements through a corner.....	17
Figure 1.9 Attack angles suited to different requirements (R.Sheldahl P. Klimas, (1981)).....	20
Figure 2.1 Test schedule for one aerofoil.....	34
Figure 2.2 2-D tunnel installed in IWT	35
Figure 2.3 Aerofoil model.....	37
Figure 2.4 Aerofoil slide mount on slide rail	38
Figure 2.5 Aerofoil shapes tested	42
Figure 3.1 Overlay of pressure contour.....	50
Figure 3.2 Pressure contours for different AoA	51
Figure 3.3 Pressure contours for different ground clearances	52
Figure 3.4 Lift coefficient variation - Clark Y	53
Figure 3.5 Lift coefficient variation - 6-Series	54
Figure 3.6 Lift coefficient variation - 6-Series with Gurney	54
Figure 3.7 Lift coefficient variation with AoA as a function of non-dimensionalised ground clearance - Clark Y.....	55

Figure 3.8 Lift coefficient variation with AoA as a function of non-dimensionalised ground clearance - 6 Series	56
Figure 3.9 Lift coefficient variation with AoA as a function of non-dimensionalised ground clearance – 6-Series with Gurney	56
Figure 3.10 Lift coefficient variation with ground clearance as a function of AoA - Clark Y	57
Figure 3.11 Lift coefficient variation with ground clearance as a function of AoA - 6 Series.....	58
Figure 3.12 Lift coefficient variation with ground clearance as a function of AoA – 6-Series with Gurney.....	58
Figure 3.13 Drag coefficient variation - Clark Y	59
Figure 3.14 Drag coefficient variation - 6-Series.....	60
Figure 3.15 Drag coefficient variation - 6-Series with Gurney.....	60
Figure 3.16 Drag coefficient variation with AoA as a function of non-dimensionalised ground clearance - Clark Y.....	61
Figure 3.17 Drag coefficient variation with AoA as a function of non-dimensionalised ground clearance - 6 Series	62
Figure 3.18 Drag coefficient variation with AoA as a function of non-dimensionalised ground clearance – 6-Series with Gurney	62
Figure 3.19 Drag coefficient variation with ground clearance as a function of AoA - Clark Y	63
Figure 3.20 Drag coefficient variation with ground clearance as a function of AoA - 6 Series.....	64
Figure 3.21 Drag coefficient variation with ground clearance as a function of AoA - 6-Series with Gurney	64
Figure 3.22 Moment coefficient variation - Clark Y	65
Figure 3.23 Moment coefficient variation - 6-Series.....	66
Figure 3.24 Moment coefficient variation - 6-Series with Gurney.....	67
Figure 3.25 Moment coefficient variation with AoA as a function of non-dimensionalised ground clearance - Clark Y.....	68
Figure 3.26 Moment coefficient variation with AoA as a function of non-dimensionalised ground clearance - 6 Series	68

Figure 3.27 Moment coefficient variation with AoA as a function of non-dimensionalised ground clearance - 6-Series with Gurney	69
Figure 3.28 Moment coefficient variation with ground clearance as a function of AoA- Clark Y	70
Figure 3.29 Moment coefficient variation with ground clearance as a function of AoA - 6 Series.....	71
Figure 3.30 Moment coefficient variation with ground clearance as a function of AoA - 6-Series with Gurney	71
Figure 3.31 Lift coefficient comparison	72
Figure 3.32 Drag coefficient comparison	73
Figure 3.33 Moment coefficient comparison	74
Figure 3.34 Drag variation displaying error	44
Figure 4.1 Drag coefficients of rectangular plates as a function of 1/AR (Hoerner, 1965).....	87
Figure 4.2 Total downforce vs speed	89
Figure 4.3 Total drag vs speed	90
Figure 4.4 Speed histogram for an FSAE circuit.....	91
Figure A 1 DPMS during calibration.....	108
Figure A 2 Velocity contour of 2-D section.....	110
Figure A 3 Velocity contour of 2-D section (more refined)	111
Figure A 4 Pressure tapped tunnel wall	112
Figure A 5 Tunnel pressure gradient.....	113
Figure A 6 Aerofoil point cloud	114
Figure A 7 Aerofoil splines	115
Figure A 8 Aerofoil overlay.....	116
Figure A 9 Pressure tap layout for repeatability study.....	119
Figure A 10 Normalised pressure acquired per channel	121
Figure A 11 Pressure variation between runs per channel	122

Table of Equations

Equation 2.1 Pressure coefficient	46
Equation 4.1 Aspect ratio for rectangular wings.....	81
Equation 4.2 End plate effect on wing AR (Hoerner, 1965)	82
Equation 4.3 Pre-Stall lift coefficient for a 3-D wing (Katz, 1995).....	85
Equation 4.4 Pre-stall lift slope of a 3-D wing for AR >6 (Katz, 1995)	86
Equation 4.5 Pre-stall lift slope of a 3-D wing for AR <4 (Anderson, 2001)....	86
Equation 4.6 Pre-stall drag coefficient for 3-D wing (Katz, 1995).....	86
Equation 4.7 Induced drag for 3-D wing (Katz,1995)	86
Equation 4.8 Lift coefficient for post-stall 3-D wing	88
Equation 4.9 Drag coefficient for post-stall 3-D wing	88

Nomenclature

2-D	Two Dimensional
3-D	Three Dimensional
α	Angle of attack
α_{L0}	Angle of attack increment due to aerofoil camber
δ	Boundary layer thickness
δ^*	Boundary layer displacement thickness
AoA	Angle of Attack
AR	Aspect Ratio
c	Chord
CoG	Centre of Gravity
CoP	Centre of Pressure
C_{sf}	Coefficient of Skin Friction
$C_{L\alpha}$	Lift slope of aerofoil
C_d	Drag Coefficient (Aerofoil)
C_D	Drag Coefficient (Wing)
C_{D_i}	Coefficient of induced drag
C_{D0}	Coefficient of viscous drag
C_{D90}	Drag coefficient at 90° angle of attack
C_l	Lift Coefficient (Aerofoil)
C_L	Lift Coefficient (Wing)
C_m	Pitch Moment Coefficient (Aerofoil)

Nomenclature

C_M	Pitch Moment Coefficient (Wing)
DPMS	Dynamic Pressure Measuring System
FSAE	Formula SAE
IWT	Industrial Wind Tunnel
Re	Reynolds Number
SAE	Society of Automotive Engineers

Chapter 1 Introduction

1.1 Preamble

In this chapter the use of wings on race cars is introduced via the literature and the broad objective of the work is described. After reviewing relevant literature the chapter concludes with a set of specific objectives defining the research.

Early cars did not regularly travel fast enough for aerodynamically generated forces to have major effects on the stability of the vehicle. As technology improved, speeds rose, and the need of a better understanding of the aerodynamics of the vehicle was required. Unless certain design measures are taken, the airflow around the basic geometry of an automobile will tend to generate lift and a nose-up pitching moment. This tendency can lead to high speed instability; the contact force between the tyres and the road is reduced, thus reducing traction.

Aerodynamic devices such as wings are used in higher levels of motorsport (Formula-1 etc.) to increase the contact force between the road and tyres (i.e. to generate downforce). This in turn increases the performance envelope of the race car. A side effect of the extra downforce is increased aerodynamic drag which (apart from when braking) is generally detrimental to lap-times. The drag acts to slow the vehicle, and hinders both available drive power and fuel economy. As is well known, the angle between the flow

direction and the chord of an aerofoil is known as the angle of attack (AoA). By altering a wing's AoA, the lift/drag relationship and magnitude can be altered. This would allow high downforce when required (cornering and braking) and low drag when downforce was not required (usually driving in a straight-line at relatively high speed). A system that would enable this to happen could provide the benefits of wings, without the drag-induced power/economy cost when driving at high speed.

Variable geometry aerodynamic devices have been used in various forms of motorsport in the past, but were invariably banned usually for safety reasons. The use of active aerodynamics is currently legal in both Formula SAE (FSAE), an engineering competition for university students to design, build and race an open wheel race car described later in section 1.7, and production road going vehicles. A number of car companies are beginning to incorporate active aerodynamic devices in their designs.

While some research has been done with aerofoils at very high AoA, (R.Sheldahl P. Klimas, 1981) the majority of data on different aerofoils have been collected for aeroplanes, and as such do not include data beyond the normal operating envelope of aircraft (i.e. at AoA well beyond the stall of the aerofoil). The effect of the close proximity of a ground plane (simulating the road surface) is important in ground based vehicle research due to the close proximity to the ground at the front, and the vehicle body at the rear (J. Katz, 1995).

The combination of high AoA and ground effect is not a situation commonly encountered in aviation thus studies have not been conducted, and banning variable geometry aerodynamic devices in “mainstream” motorsport has stopped automotive studies. This investigation intends to look into the combined effects of ground effect and high AoA in an effort to quantify the potential gains that may come from an active aerodynamic system, and to investigate the potential for FSAE cars.

1.2 Properties of aerofoils

When an aerofoil passes through a fluid, such as air, the fluid exerts a force on the aerofoil that is a function of aerofoil geometry, speed and AoA. The general characteristics of the forces an aerofoil experiences as it passes through a fluid are fairly well understood, and will not be described here. The reader is directed to references such as Hoerner, (1965) or Anderson, (2005) for more insight into this.

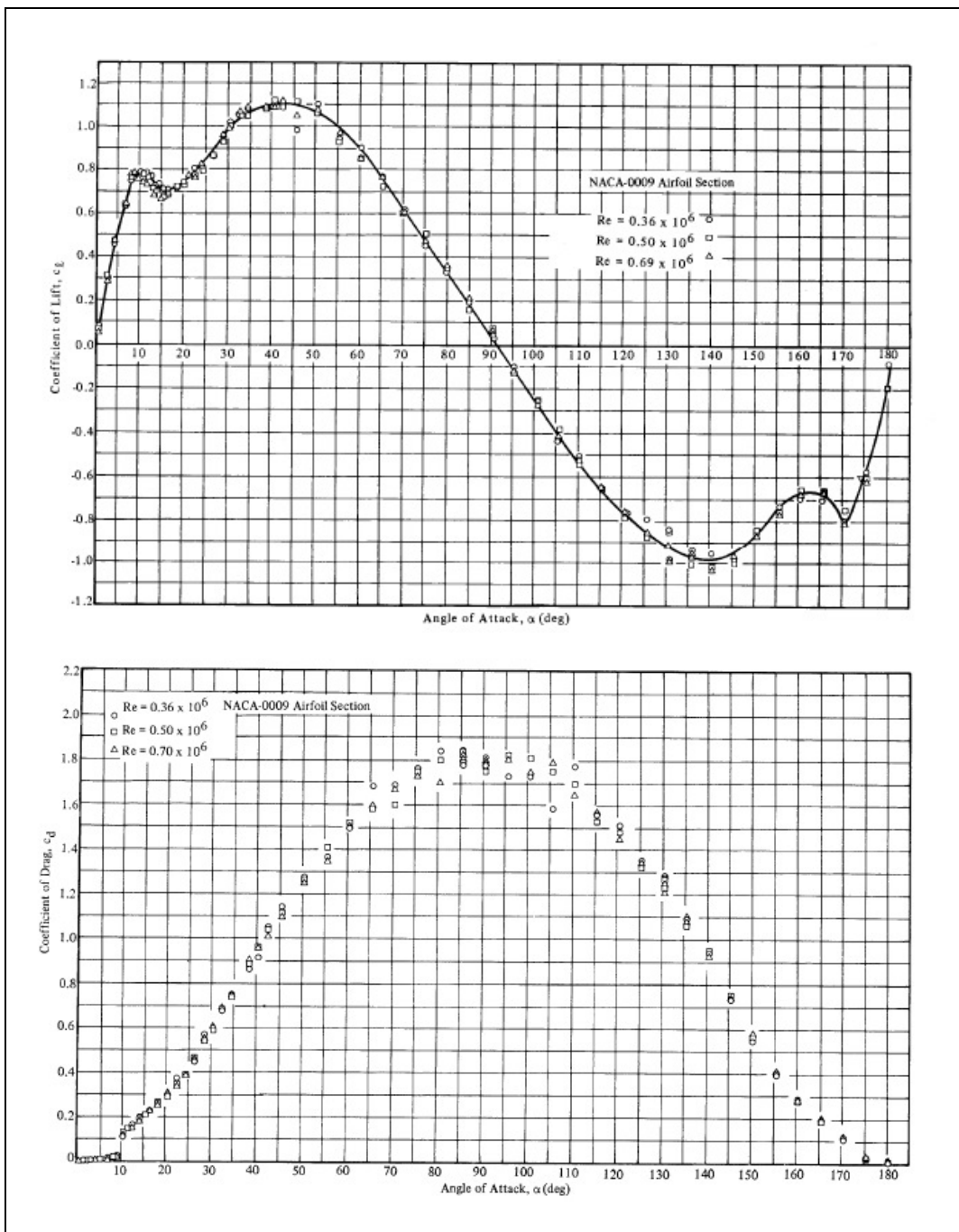
In the past, aerofoils were designed through a process of trial and error. Data were published for different families of aerofoil (NACA etc). Users would generally choose an aerofoil from a catalogue. These days, aerofoils are generated to suit the given purpose using inverse methods. This allows designers to tailor the aerofoil shape for a given application, and even for a different location along the wing. This method is ideal for automotive use, especially for the design of the rear wing where the flow direction has been disturbed by the body. Katz & Dykstra (1992) found the effects of the body on approach streamline direction of the wing (AoA) need to be taken into account

when designing/selecting a wing. Later Katz & Dykstra (1994) and Katz (1995) described the use of the inverse method for wings on cars.

1.3 The effects of high angles of attack

As the AoA is increased, the lift produced by the wing will also initially increase and the wing-tip (free) vortex strength increase proportionally to the lift produced. At some point the flow across the suction side of the wing will separate, and the wing will stall. At this point, further increase in AoA will generally lead to a decrease in the amount of lift the aerofoil can provide, before increasing again, albeit with increased drag, see Figure 1.1.

The majority of research data that have been collected over the years has been for the aviation industry, and thus rarely contains data for an AoA of over 32 degrees as most aerofoils have stalled by this point. One of the few examples that shows the lift and drag coefficient from 0° to 180° AoA is R.Sheldahl P. Klimas, (1981) shown in Figure 1.1. Some recent research has been done with the F-18 HARV and X-29A aerofoils at AoA up to 66 deg (L Bjarke et al 1992) however their paper focussed on the flow around the aircraft forebody and vortex production, rather than the flow over the aerofoil.

Figure 1.1 Variation of C_L and C_d vs AoA (R.Sheldahl P. Klimas, (1981))

Helicopter blades can sometimes reach high AoA (inboard) thus some early work (e.g. Hoerner, (1975)) has been done on the characteristics of certain aerofoils over a large range of AoA (up to 180 deg). Another field

where aerofoils reach high AoA is wind turbines. The Sandia company in the USA has conducted some research into this area (R.Sheldahl P. Klimas, 1981). The results for their study were broadly similar to the trends found by Hoerner (1975). The general trend found in both studies was that while the shape of the aerofoil was important for the pre-stall characteristics, post-stall the behaviour of the aerofoil is very similar to that of a flat plate, and geometry is less significant. Once deeply stalled, the aerofoil behaves as a bluff body. The flow separates from the leading and trailing edge, and the shape of the aerofoil has little effect on the forces generated. Based on this concept, Lindenburg, (2000) developed an empirical method for calculating drag on aerofoils at high AoA by substituting with formulae for simple geometries. A good approximation was found by treating the aerofoil as the combination of an ellipse and a wedge.

1.4 The ground effect

When a wing travels in close proximity to the ground, it experiences an increase in lift, and decrease in induced drag. This is known as ground effect. The presence of the ground acts to reduce both the induced angle and induced drag (S.F. Hoerner 1965). Ground effect can be broken into two primary contributors, span dominated and chord dominated effects (E. van Opstal et al. 2003).

- Span – related to reducing wingtip vortex effect on lift and drag.

- Chord – related to cushion/venturi effect between wing and ground of close proximity.

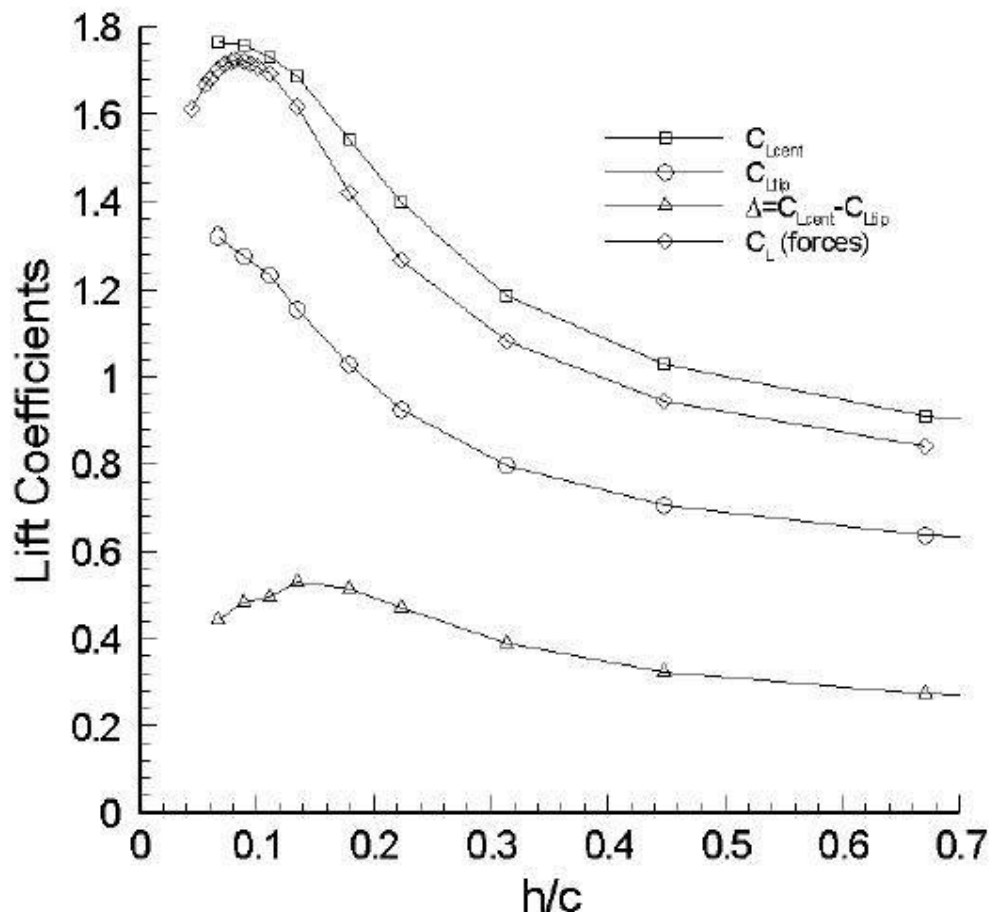


Figure 1.2 Variation of C_l with Ground Clearance (Zhang et al, 2002) for a Tyrrell 026 aerofoil.

Zhang et al (2002) performed an experimental study of the tip vortices from a single element inverted-aerofoil (from a Tyrrell 026 Formula One car) operating in ground effect. It was found that when a thick symmetrical wing or wing with inverted camber is brought close to the ground, the vertical force produced will increase (compared to free-stream) to a maximum, then

decrease again. See Figure 1.2. This force reduction at very close proximity is due to separation on the suction side of the wing, due to the venturi effect of the flow between the wing and ground.

Due to the relevance to both ground and air transport, numerous works have been done on the ground effect and the general consensus is that the ground may be thought of as a plane of reflection.

The simulation of ground in a wind tunnel is important as it has consequences on the aerodynamics of the model. In the case of wings, the ground has an effect on the induced AoA of the wing. In the context of aircraft, ground effect is usually only relevant for take-off and landing where AoA is generally small.

Wings in automotive use are not constrained by the same parameters as aircraft, and thus the higher AoA can be safely reached, although at a higher cost in drag. The aeroplane is relying on the wing for support as well as control. In the case of the automobile, support is provided by the tyres so the wing can operate in a larger envelope. In the passenger car context drag is usually the most studied parameter. The close proximity of the vehicle underbody to the ground can lead to interaction of the vehicle and ground boundary layer.

1.5 The use of aerodynamic devices on automobiles

While the added downforce from inverted wings on race cars can be beneficial for traction, wings can alter the flow over the whole car owing to the up-wash generated by the wing. This may have adverse effects on other systems relying on air flow. The front wing is subject to the cleanest flow, being forward of the body disturbance. The front wing is also mounted in close proximity to the ground, and thus can make use of ground effect. The front wing must also be designed with consideration to the wake produced, and its interaction with other components.

Sidepods and engine intake are usually downstream of the front wing, and already subject to fairly turbulent air due to interference with rotating wheels and suspension components. The design of the front wing, in particular the wing tips should keep low pressure vortices from interfering with these components.

Cooper et al (1998 and 2000) and Visconti et al (2000) completed studies on the use of under-body diffusers, showing downforce proportional to flow rate through the diffuser. Katz & Dykstra (1992) demonstrated that the up-wash of the front wing can diminish diffuser effectiveness by reducing the flow-rate.

The rear wing is usually mounted over the rear wheels (due to rule and flow restrictions), and this tends to increase the height of the Centre of Gravity (CoG) and Centre of Pressure (CoP). A higher wing will be subject to cleaner

flow, but will have adverse effects on the dynamic lateral response of the vehicle increasing inertial roll moment in cornering. Despite the relative distance between front and rear wing, interaction is still possible, depending on body shape (Katz 1995). The flow over the rear wing will no doubt have some degree of pitch, and this should be taken into account in the design AoA.

While not a problem in closed cockpits, buffeting of the driver's helmet can cause undue strain on the driver, reducing concentration and effectiveness. Vortices should not directly interact with the helmet in the range of yaw expected.

Quite a lot of research has been done on the flow conditions induced by rolling wheels. Mercker et al (1991) carried out full scale wind tunnel tests on a passenger car with moving belt. Wickern et al (1997) acted to determine the proportion of drag from wheels, specifically "fan-moment". Mears et al (2002) studied the air flow about an exposed racing wheel. Knowles et al (2002) studied the near wake of 40% champ car wheels.

The position of the vehicle's CoP is important for stability, not just in yaw but also pitch, as shown in the study by Dominy et al (2000). The location of the CoP relative to the CoG affects the yaw stability of the vehicle. Milliken (1995) suggests if the CoP is aft of the CoG, the car will exhibit "weather-cock stability." This promotes stability in yaw against cross-winds. As the vehicle speed increases, the lift/downforce will affect weight-bias and thus the handling of the car. This can lead to reduction in traction of one axle, altering

the understeer/oversteer gradient. Howell & Le Good (1999) investigated the effect of lift on the stability of passenger cars; performance is degraded if the vehicle suffers from lift and a nose-down pitching moment, due to the reduced traction at the rear axle with increased speeds. A compromise must be made when locating the design location for the vehicle CoP, taking into account both side force and lift, to achieve longitudinal stability.

1.6.1 Vehicle requirements for maximum performance

The lateral acceleration performance envelope of a high performance automobile is typically limited by the traction available from the tyres. Longitudinal acceleration is limited by traction of the driven/braked wheels and by the capabilities of the drive/brake systems. For example, as a car accelerates from a standing start, the engine may be able to provide enough torque to break traction, thus the longitudinal acceleration is limited by the traction of the tyres. As the car speeds up, a point will be reached where the torque potential from the engine is no longer enough to break traction, and the car will then be power limited. In the example shown in Figure 1.3, the tyre becomes traction limited when the car is in 2nd gear.

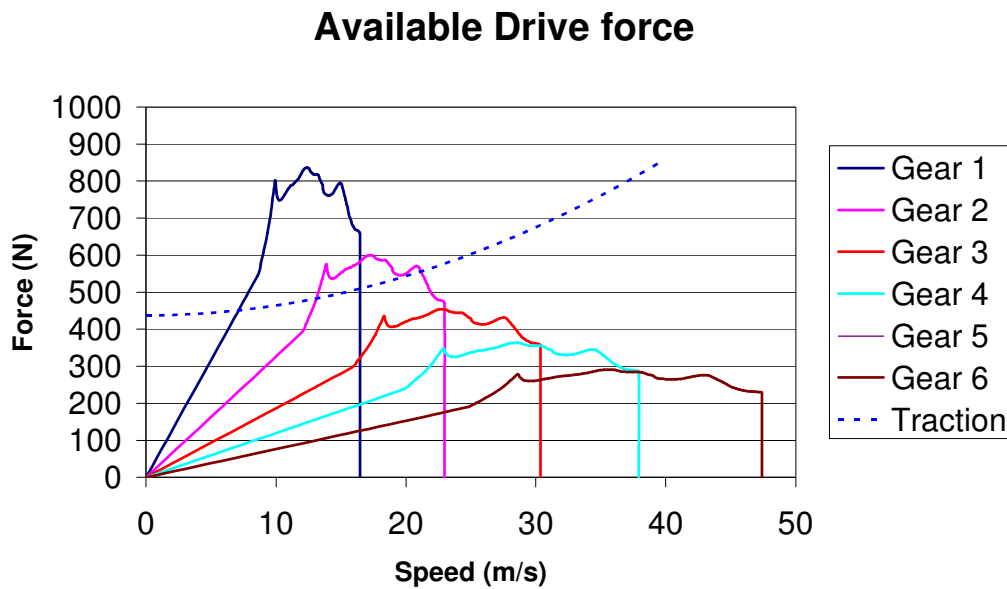


Figure 1.3 Example of tyre drive force and traction vs speed

The situation is similar in longitudinal braking. Provided the braking system can provide enough torque to lock the wheels, the vehicle will be traction limited. If the brake system is not powerful enough (due either to poor design or fade) the deceleration will be limited by the capability of the brake system.

Further constraints are also placed on a vehicle in combined longitudinal and lateral acceleration. The force available from a tyre is governed by a concept known as the friction ellipse (Milliken 1995), where the longitudinal and lateral friction coefficients (μ_x , μ_y) are plotted against each other. When the tyre is operating at high levels of lateral traction, longitudinal traction is severely limited. Equally maximum longitudinal traction limits the potential for lateral traction.

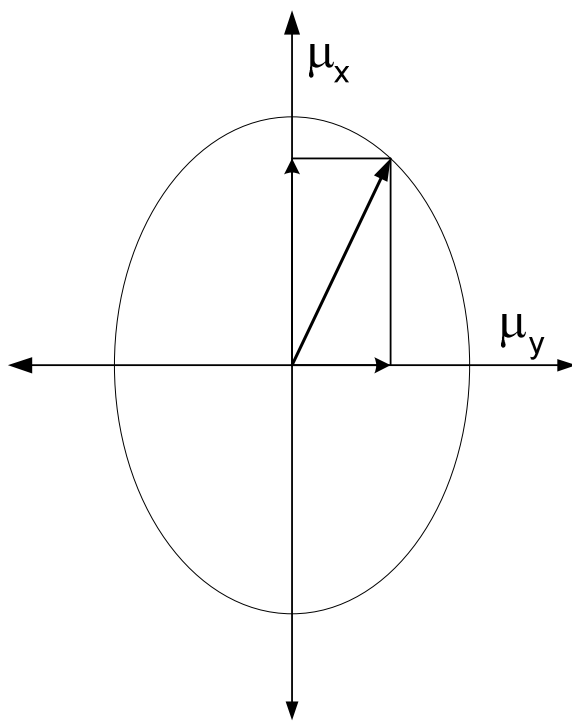


Figure 1.4 Friction ellipse, adapted from Milliken (1995)

Generally speaking, longitudinal and lateral forces available from a tyre are proportional to the normal force on a tyre. This relationship is not linear, and tends to reduce with increased load. This characteristic tends to reduce the performance envelope of the car during acceleration. When a car accelerates (laterally or longitudinally) the weight distribution between the four tyres will change. This reaction force from the inertia of the car acts at the CoG, which is above the ground (where the tyres act).

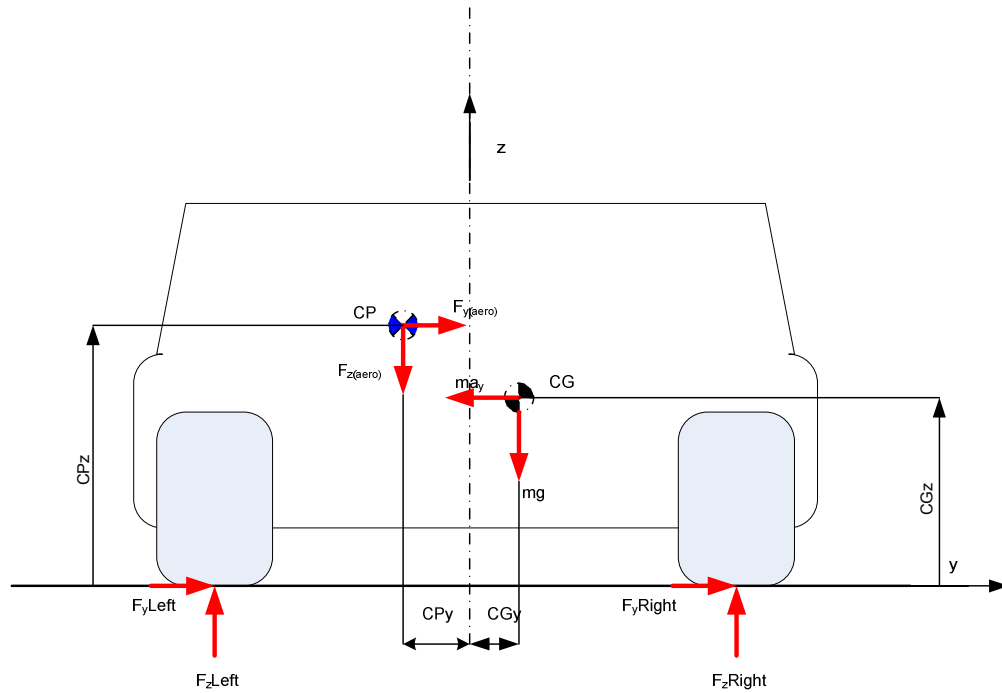


Figure 1.5 Lateral Weight Transfer

For example in the case of a car turning to the left, the left wheels will experience reduced normal force, and the right side higher. This means the right side will have increased lateral capability, however due to the tyre characteristic; the total car lateral capability is reduced. This is because the additional lateral grip gained by the right wheels is less than the grip lost by the left, leaving a net loss of grip. Figure 1.6 shows this effect for a racing tyre, typical of those used by FSAE vehicles. These data were collected by the Calspan Tire Research Facility (TIRF) and are provided by the FSAE Tire Test Consortium (TTC).

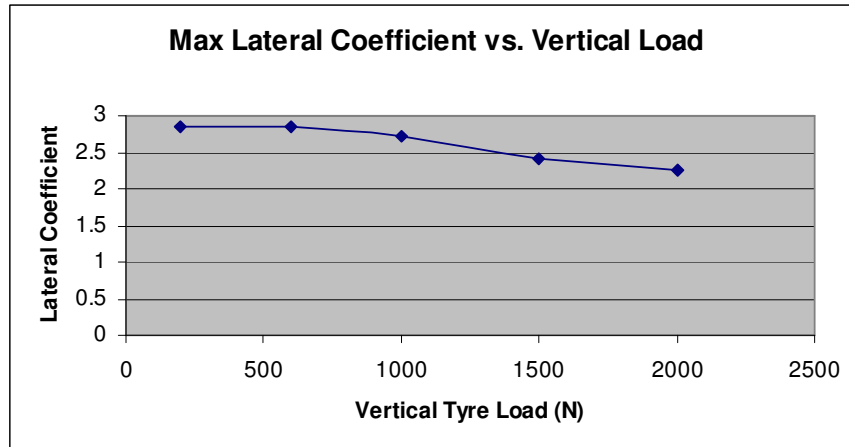


Figure 1.6 Lateral Coefficient variation with vertical load - Data courtesy of TIRF and TTC (2005) and used with permission

This load proportionality is similar in the longitudinal direction. Figure 1.7 shows the effect of different loading on the longitudinal performance of the racing tyre.

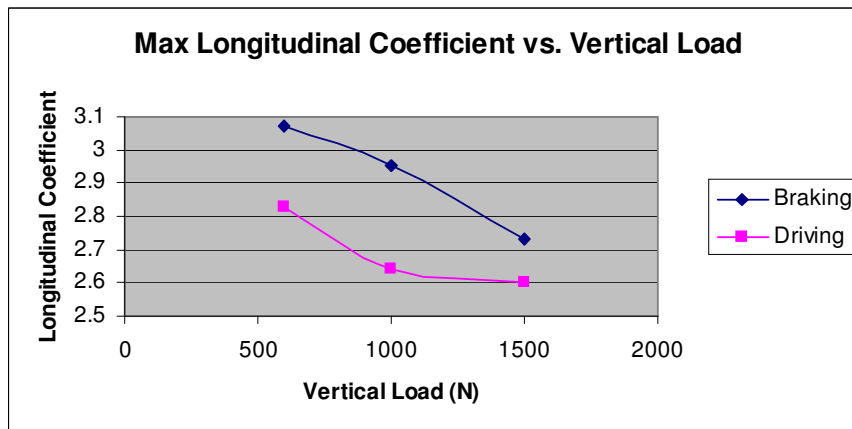


Figure 1.7 Longitudinal Coefficient variation with vertical load - Data courtesy of TIRF and TTC (2005) and used with permission

The force requirements of a race car vary greatly as it travels around a track, as illustrated in the following example: Consider a vehicle travelling at speed as it approaches a corner. The driver applies the brakes while still travelling in a straight line to maximise the longitudinal acceleration possible. At this point the priority of the driver is to decelerate as rapidly as possible. Depending on driving style, the driver will typically still be braking as the car enters the corner, ideally moving around the perimeter of the tyre's friction ellipse, decreasing longitudinal braking force while increasing lateral. The driver then begins to exit the corner, slowly increasing longitudinal acceleration while straightening the car to decrease lateral acceleration. The car then accelerates away until the next corner. The effectiveness of the driver / car partnership can be seen with a plot of lateral vs longitudinal acceleration (G-G Plot). If the driver is able to maintain the car on the limit, the majority of time will be spent on the perimeter of the performance envelope; the tyres will always be working to optimum traction, providing lowest times around the circuit.

The ideal aerodynamic configuration is different for each section of the track, particularly cornering. Refer Figure 1.8 for an example.

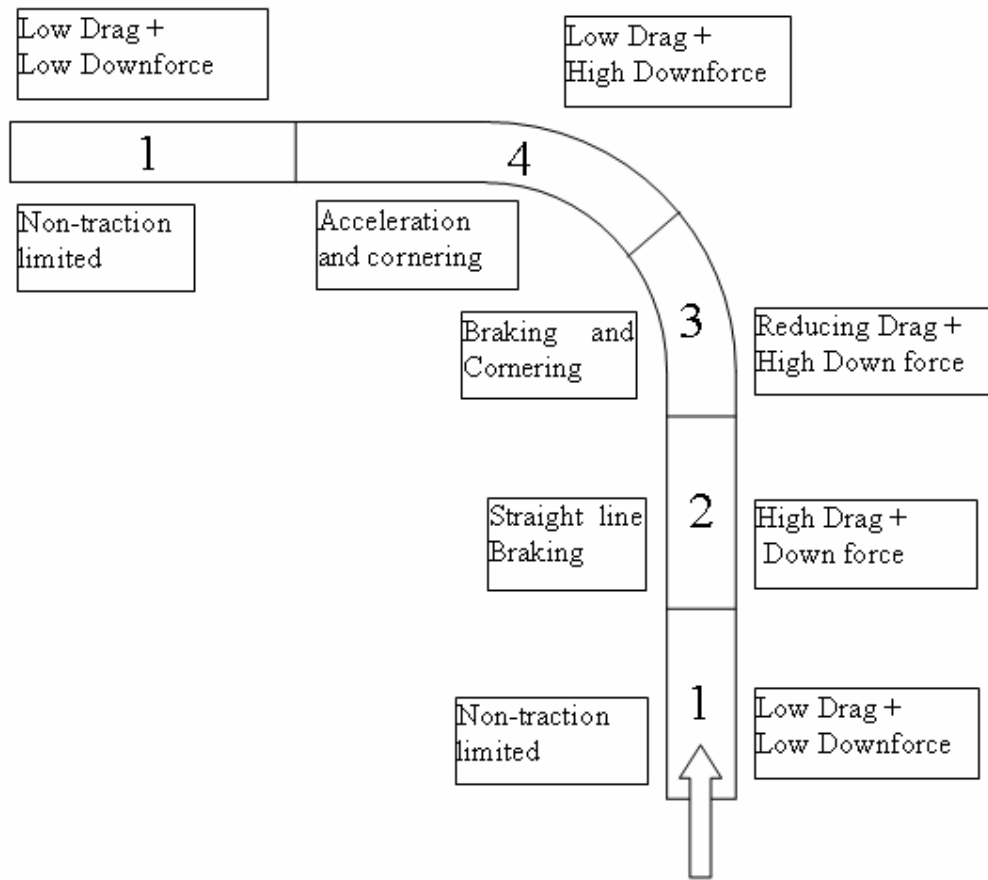


Figure 1.8 Aerodynamic requirements through a corner

When travelling in a straight line and not traction limited (Sector 1), the vehicle requires low drag and only enough downforce to allow stability at the speed. The AoA of the wing could theoretically be altered at different speeds to allow a tailoring of downforce/drag ratio to minimise time.

When braking in a straight line (Sector 2), the requirement is for drag, as it will assist the tyres in slowing the vehicle. Downforce will also aid the braking by increasing the potential grip of the tyres. Additionally active aerodynamics (defined here as the ability to change AoA) can potentially

assist the efficiency of the brake system by distributing the vehicle mass more evenly across the 4 wheels. Careful consideration of the location of the CoP of the aerodynamic configuration can cause a pitching moment to counter the moment caused by the longitudinal acceleration, reducing the weight transfer.

As the car enters the corner (Sector 3), the requirement for drag reduces and more lateral traction, requiring increased downforce, is required.

During corner exit (Sector 4) the configuration should provide downforce to aid traction, with minimal drag to impede the acceleration out from the corner.

Once the car is no longer traction limited (Sector 1) the aero configuration can be returned to a low drag, low downforce configuration.

Considering these requirements, and looking at the typical characteristics of an aerofoil, different ranges of AoA can be chosen for each segment of the corner.

At low AoA, the aerofoil will exhibit low drag and low downforce characteristics, good for the straight when not traction limited (Sector 1).

Angles of attack around 90 deg could provide maximum drag with perhaps some downforce, suitable for straight-line braking (Sector 2).

The AoA between 35 and 60 deg will provide a range of low to high drag with high downforce for corner entry (Sector 3).

The AoA just prior to stall provides high downforce with low drag, suitable for corner exit (Sector 4).

Considering the aerofoil characteristic shown previously in Figure 1.1 with reference to the requirements stated previously,

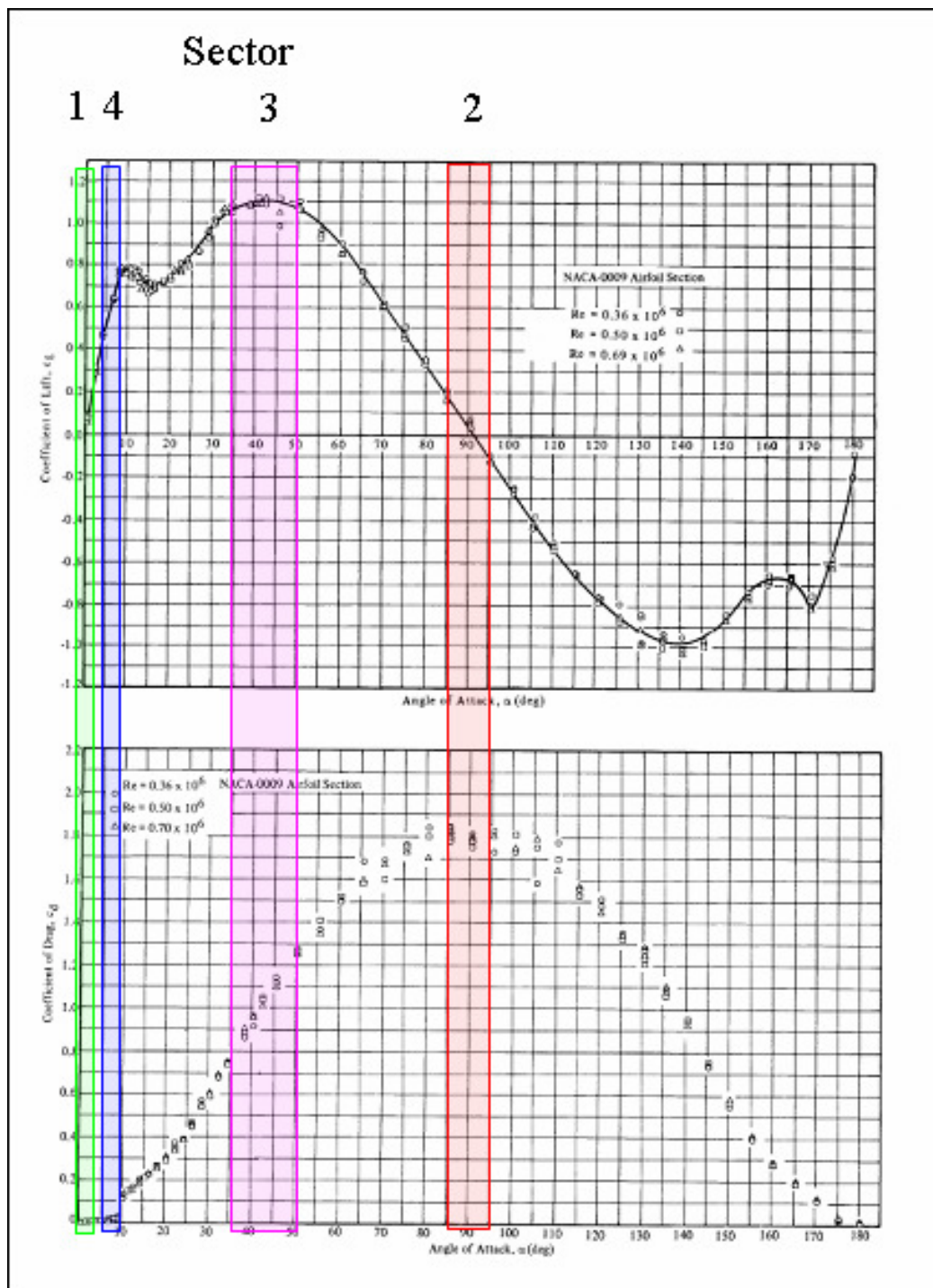


Figure 1.9 shows ranges of AoA suitable for the different track Sectors discussed.

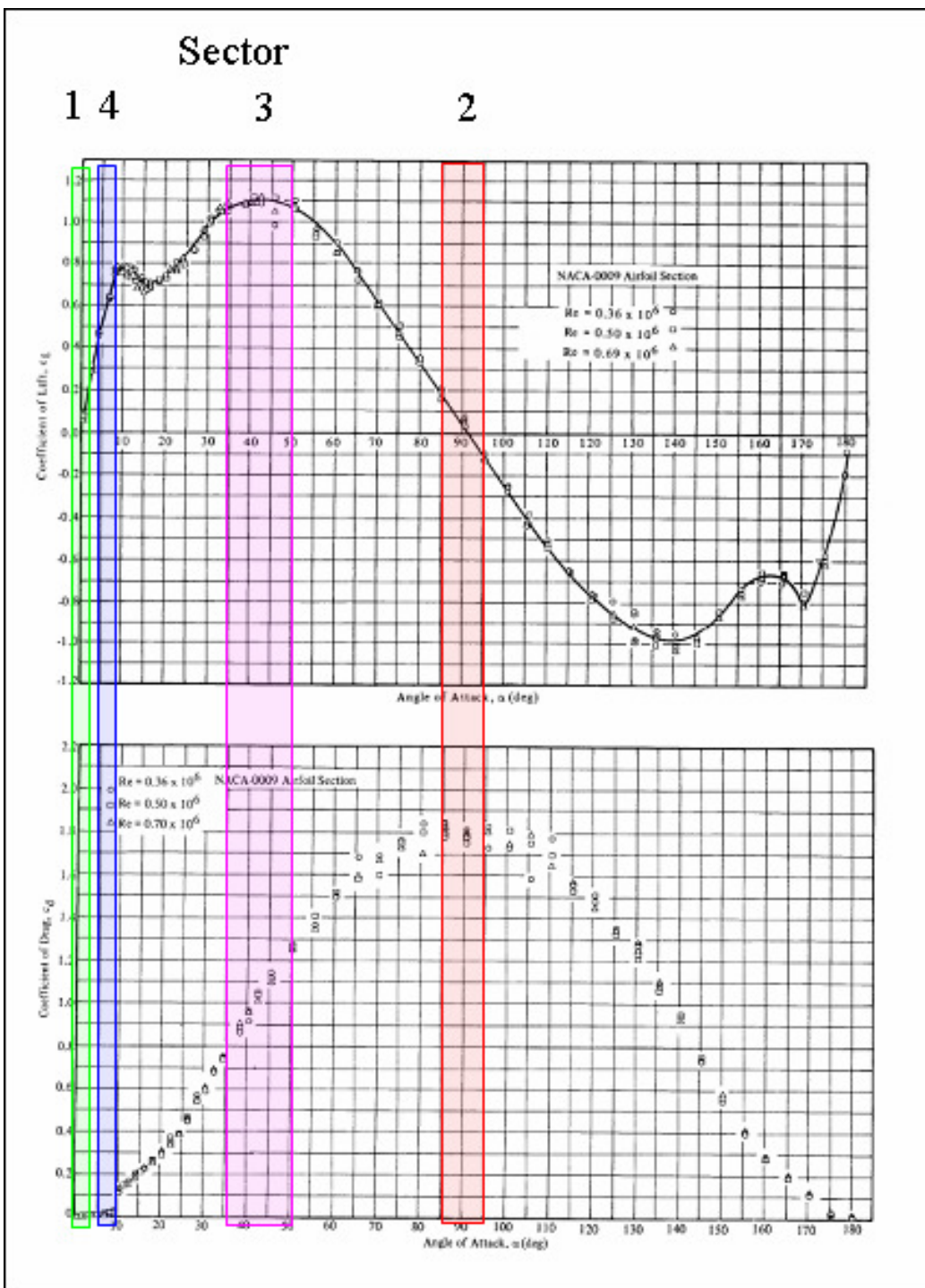


Figure 1.9 Attack angles suited to different requirements (R.Sheldahl P. Klimas, (1981))

1.7 The Formula SAE competition

FSAE is a class of racing developed to allow students to design, build and race cars in inter-university competition. A series of rules or “Formula” was developed to allow safe competition by the Society of Automotive Engineers (SAE). Teams compete in different events to earn competition points. The events are designed to test all different aspects of the car, from the dynamic on-track capability to the cost, marketability and design.

1.7.1 Formula SAE design considerations

The design of a complex system such as a race car will always include compromise to find the optimal solution. FSAE is one of the few forms of racing where active aerodynamic devices are not banned. Here the previously outlined advantages of active aerodynamics could be exploited. Jawad et al (2001) and McKay & Gopalarathnam (2002) did studies comparing the trade off between downforce and drag on the performance of a FSAE car, while Wordley & Saunders (2006) provided an analysis of the aerodynamic limitations and requirements for a FSAE racer and did analysis into the potential performance benefit of using wings. They showed there is benefit to be gained by fixed wings in the class of racing and the preceding arguments (Section 1.6.1) has argued that variable AoA has the potential to further increase these benefits. However there has to date been little work on the effect of a wide range of AoA on suitable aerofoils in ground effect.

1.8 Scope and objectives of this investigation

As the FSAE rules permit active aerodynamics, there are a number of issues that need to be resolved, for the first of which would be to obtain relevant aerodynamic data. This first step in the design process is to consider the aerodynamic potential such a system could provide.

The main research questions this investigation will answer are:

- How do the drag and lift forces vary with AoA in the range of 0° - 135° in ground effect?
- How does the Centre of Pressure location move with varied AoA within this range, in the presence of ground?
- How can this information potentially be used to enhance the performance of a Formula style car?

The scope of this investigation is limited to a 2-D study. In reality, the wings would be exposed to three dimensional (3-D) flows; however this would increase the number of variables to be explored greatly. Wings in automotive use typically use endplates to reduce 3-D effects, and ground proximity also tends to reduce these effects. Jasinski & Selig (1998) suggested that considering the restriction of the free vortex due to ground proximity and end-plates, it can be assumed that the flow over a large proportion of the wing is two-dimensional.

Race cars typically use multi-element wings. The multi-element design allows for much higher lift than is possible from a single element wing of similar dimensions. This investigation has been limited to the effects on a single element wing. The effective study of a multi-element type would require

a lot more time owing to the increased number of setup variables and complexity of flow. A benefit of the single element is the simplicity of the design. The mechanism to actively control a single element wing would be a lot simpler than that for a multi-element, thus easier to implement in both FSAE and production vehicles.

In any investigation, there are always different approaches that can be taken. Numerical, analytical and experimental approaches all have their advantages and disadvantages. CFD initially appeared suited to this investigation owing to the large number of tests, however the experimental method was chosen primarily due to the presence of separated and complex flows that if solved by other means, would still require experimental validation (Gharib 1996). Great advances have been made in CFD, however as this is a preliminary investigation in this specific scenario it was felt some experimental work was required to provide a means of verification and validation of numerical results. Further study could include the use of CFD to more rapidly view the outcomes of different configurations.

The effects of ground proximity will require simulation for this investigation. While a moving ground would most closely simulate the physical reality, this is both difficult and expensive to implement for 2-D simulations. The method chosen to simulate the ground will be a slightly raised floor in the tunnel section. While a boundary layer will be present on the floor, this will be greatly reduced due to the large contraction ratio at the inlet to the 2-D section, and the floor.

Chapter 2 Apparatus and testing method employed

2.1 Preamble

In this chapter the equipment and methods used in the investigation are discussed, along with the errors inherent to the setup.

It was decided to test relatively small chord aerofoils, and a Clark Y, 6-series (63-412) and a modified 6-series (63-412 with Gurney Tab) were chosen. These were mounted in a specially constructed 2-D wind tunnel and were able to rotate about a pivot point and to also be translated such they came into ground effect. The tunnel, aerofoils and methods are described herein. Additional detailed information about the equipment and calibration can be found in Appendix 1.

2.2 Wind-tunnel testing techniques

Wind tunnels have long been used as a means of replicating flows to allow testing in a controlled manner. Many different techniques are available to replicate/simulate conditions found in real world scenarios.

2.2.1 Two-dimensional flow simulation

Simulating two-dimensional flow allows the reduction of variables, and can provide a solution directly comparable to that from an analytical or

computation method. This is often done by spanning the aerofoil across the tunnel section, taking care to seal the wing tips to the walls. Sometimes a dedicated tunnel, with a narrower section, is constructed for this purpose. In reality, *pure* two-dimensional flow is difficult to achieve due to boundary layer growth on the tunnel side boundaries, however very close approximations are possible.

The addition of an endplate to a wing design helps reduce wingtip vortex strength and effect on the wing. The presence of an endplate will effectively increase the aspect ratio (AR) of the wing, thus flow will begin to approximate two-dimensional flow near the centre. A lot of work has been done to try and equate plate size and shape to a change in AR. Early work such as Hoerner (1975) show the effects of basic geometries. Some more modern works, using current geometries and race car wings are Jasinski & Selig (1998) and Soso & Selig (2002), both finding the area of the endplate was the most significant variable affecting the effective AR. Soso & Selig (2002) also found the height of the endplate to be much more important than the chord.

Installing two parallel inserts in a wind tunnel section can provide a reasonable way of simulating two-dimensional flow. The benefits of this method are the cost and ease of manufacture / installation compared to making a dedicated two-dimensional tunnel. The drawback of this method is flow partially bypassing the test section and travelling either side, instead of through it. The problem becomes more prevalent as the blockage in the two-

dimensional section increases as the AoA increases. While this effect can be measured and calibrated for, it does pose a limit to the testing the tunnel will be able to perform.

An alternate method of simulating two-dimensional flow in a relatively large test section is to install a second contraction within the tunnel to force all air to pass through the narrowed section. While potentially more expensive and complex than parallel inserts, this method avoids the problem of flow bypassing the section. It should not be assumed that a section of this design can necessarily provide higher airspeeds as the increased blockage restriction does put extra load on the tunnel fan and motor. Suitable diffuser design may not be possible for the two-dimensional section as the original test section may not be long enough to accommodate the length of both the two-dimensional section and additional diffuser. The losses that come from separation at the end of the two-dimensional section limit the maximum speed capable of being attained in the section. Providing the modified tunnel is capable of supplying the required flow velocity, this arrangement can be a convenient method to achieve two-dimensional flow.

2.2.2 Ground effect simulation

The main difficulty in replicating moving ground effect is the boundary layer that will grow on any fixed surface in the flow. This ground boundary layer is not present in reality for moving vehicles, where the model moves relative to the ground and air.

One of the earliest means of simulating the ground effect was to use symmetry. In this method, an identical inverted model was mounted beneath the model being tested, so as to mirror it. The ground plane was assumed to be a plane exactly between the two models. While this method may be accurate in replicating the time-averaged effects of ground effect, it does not fully capture dynamic effects, as fluid is able to pass across the plane of symmetry. This method is also more expensive as two models have to be built and they both have to be mounted and adjusted for each configuration or angle change. Care also needs to be taken to ensure the models actually do mirror each other (i.e. AoA) and the simulated moving ground plane should ideally coincide with a plane of symmetry of the tunnel.

A simpler setup for testing in ground effect is to use a fixed ground. This can simply be the floor of the tunnel, or a raised section. The ground plane in this setup becomes influenced by the boundary layer on the floor or raised section. If a raised section is used, this boundary layer can be reduced from that of the tunnel. Several disadvantages occur with the method. The boundary layer will grow down the section, thus the ground plane is effectively on an angle and is also effectively displaced away from the physical ground. There are other complex additional effects, as discussed in Barlow et al (1999)

Another method closely related to the fixed floor is the raised ground board. This method also suffers from a boundary layer on the surface of the board, however it is usually reduced compared with the normal tunnel floor

boundary layer due to the short length preceding the model. This setup also suffers from the problem of airflow bypassing the test-section and flowing beneath the board. Differences in blockage above and below the board can lead to circulation. This problem is often countered by using a flap at the end of the board; however this needs to be calibrated, and adjusted each run. This method has been used quite a lot in the past. Ranzenbach & Barlow (1994) and again in (1996) studied 2-D aerofoils in ground effect using a raised ground plane to simulate the ground reflection.

Boundary layer suction has been used in the past to remove the boundary layer from the section floor and tangential blowing has been used to re-energise the boundary layer. Both suction and blowing have been used in conjunction with the moving belt system.

The method that most closely models the real world is the moving ground plane. This setup usually includes a belt that is speed controlled to match the flow speed within the tunnel. While a moving floor with upstream boundary layer suction will simulate the ground effect most closely, the cost of the installation and setup can make this testing prohibitive. In the case of two-dimensional studies, the use of moving floor is made more difficult due to the need for a dynamic seal between the tunnel and the floor.

Moving ground effect is particularly difficult to simulate. Numerous methods of varying complexity have been tried over the years. While some methods are better than others, all suffer from compromises. The effect on accuracy of moving ground compared to stationary has been studied quite

thoroughly. Hoerner (1965) has details of early wind tunnel testing of different ground simulation techniques, and compares the effects of different types of ground simulation. Howell & Hickman (1997) compare the difference between fixed and moving ground, concluding that fixed is usually sufficient, unless trying to find absolute drag figures, or investigate flow around wheels. Barber et al. (2002) compared the differences between different methods (experimental and numerical) of ground effect simulation, concluding the moving ground simulation most accurate. Wickern et al. (2005) investigates the effect of ground simulation on induced drag. The investigation found that better ground simulation increased the flow rate under the car, thereby effecting base-drag and rear lift. This paper also includes a literature review of other papers on wind tunnel ground simulation.

2.2.3 Correction factors

The blockage ratio (defined as the model cross-sectional area divided by the tunnel cross-sectional area) will be important when deciding the model size. If the model is relatively large, the flow around the model will be overly constrained by the tunnel test section, yielding results that do not reflect the nature of flows in an open field. Blockage is a problem in both open and closed jet tunnels, although the effects are different. Many works have investigated blockage effects, for example Ramamurthy et al. (1989) who investigate corrections for blockage when the model is bluff. An empirical expression was developed to aid in correction. Discrepancies for blockage ratios below 0.1 were negligible.

The thickness of the boundary layers on the walls, floor and ceiling of the tunnel will generally increase from start to end of the section. This causes variation in the static pressure along the axis of the tunnel, (Barlow et al. 1999). The variation in pressure from the front to the rear of the model can generate an extraneous thrust force. This force is proportional to the geometry of the model, especially the length.

The presence of the closed section has an effect on the direction of the flow around a model in the section. In the free field, on-coming air is able to change direction well before reaching the model, whereas in the tunnel, the flow direction is controlled to some degree. This effectively increases the camber of the model measured (Barlow et al 1999).

Aeronautical wind tunnel testing tends to be done with blockage ratios of less than 0.05, while automotive tunnels, dealing with primarily bluff shapes can have blockage ratios up to 0.1. Higher blockage automotive tunnels exist, however these tend to be open jet, and active systems are used to effectively reduce the blockage effects (Hucho, 1998). The main effect of blockage in the tunnel is an increment in the flow velocity experienced by the model. It is generally accepted that provided the blockage is less than 7.5 %, the errors in the corrected results will be negligible (Rae & Pope, 1984), and beyond this an “engineering estimation of the necessary corrections is possible” (Katz & Walters, 1995).

2.2.4 Data acquisition

The measurement of the aerodynamic forces can be done in a number of ways. The earliest method and one that is still in use today is the use of force balances. In early days the forces were measured with scale balances, however these days strain-gauge force balances are commonly used. This method represents the best option when the model can be completely supported by the balance, so that all forces generated are transmitted. This method is not as suitable for two-dimensional studies. The model in a two dimensional (2-D) study usually has a seal at either end to inhibit flow passing the wing tips. The model is usually mounted from outside the section, so some means of support will need to pass through the walls of the tunnel, the hole for which also requires sealing. The problem with the sealing of the model is that it may affect the amount of force that is transmitted to the force balance; thus the model may be partially supported by the seals.

A more appropriate method for obtaining force measurements in two-dimensions is through the use of pressure taps. The contour of pressure for the aerofoil can be found, then the lift and drag forces can be calculated by resolving and integrating the pressure across the surface. This method was used by K.E.Stalwell et al (2003) for tests on a wind generator section. Care must be taken to provide enough resolution at the leading edge of the aerofoil where there is potential for high pressure gradients. The pressure taps should ideally be slightly staggered, so the pressure measured by a tap is not influenced by the disturbance of preceding taps (Roach & Turner 1988).

Staggering taps also assists in allowing higher tap density at the leading edge. If staggered taps are used, care should be taken to ensure there is no gradient in velocity across the width of the aerofoil i.e. the flow must be two-dimensional. This method is more tolerant of different model supports. The drag force found using this method underestimates the actual force as it only measures the pressure drag; the method does not allow for the calculation of the drag caused by skin-friction. While methods such as laser interferometry (Mateer et al 1996) allow measurement of the skin friction, generally the skin friction drag is low compared to the pressure drag, especially for bluff bodies, where the focus of this study lies.

Another method for calculating the drag forces generated by an object in airflow is the velocity deficit method (e.g. see Houghton and Carruthers, 1982). In this method a probe is traversed in a plane across the wake of the object at different distances downstream. The velocity magnitude and direction at each point on the plane is compared to the flow without the object. Any difference in flow momentum will have been caused by the object, and can be equated to a force on the object. This method requires appropriate sensors and traversing gear that can be quite expensive. It also requires more time than the other methods, as many more samples have to be taken. This can lead to errors if there are transient effects, or the tunnel is unable to maintain constant speed for the time required to traverse the plane.

2.2.5 Size of model

The actual size of the model is an important variable for the experiment. Some factors in the decision of chord length are:

Reynolds number required and tunnel speed range available;

Blockage Effect in test section as previously described.

Signal/noise ratio of acquisition equipment;

The Reynolds number of the flow is possibly the most important factor when deciding on scale and flow speed. It is possible a smaller model will be cheaper to make, however for dynamic similarity the tunnel speed will need to be increased to match the Reynolds number of the scenario being modelled. In this situation, the limiting factor could well be the top speed of the tunnel.

Although usually not as big an issue as Reynolds similarity and blockage, some thought should also be given to the signal-noise ratio of the sampling equipment. If the outputs from the model are too small, the data may be significantly corrupted from background-noise.

2.3 Experimental design

In order to get a good understanding of the behaviour of the aerofoils a series of wind tunnel tests were conducted. The AoA was varied from 0 to 135 deg. This shows a range of behaviour, from pre-stall through stall to post-stall

and inversion (post 90 deg). The aerofoils were pivoted about the 0.25 chord position.

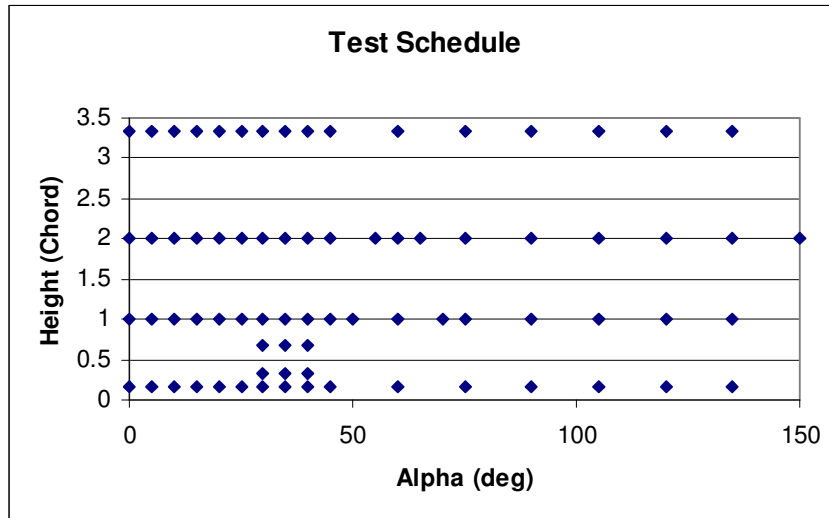


Figure 2.1 Test schedule for one aerofoil

As shown in Figure 2.1 the ground clearance was varied from 0.17 to 3.33 chord heights for all AoA tested. This gives an indication of the behaviour in and out of ground effect. Some additional tests were run close to the stall in close ground effect to give better resolution of this region. The ground clearance was taken as the gap between the lowest point on the aerofoil surface (not the pivot) and the ground. Refer to Figure 2.2 for a schematic of the setup parameters measured for each test.

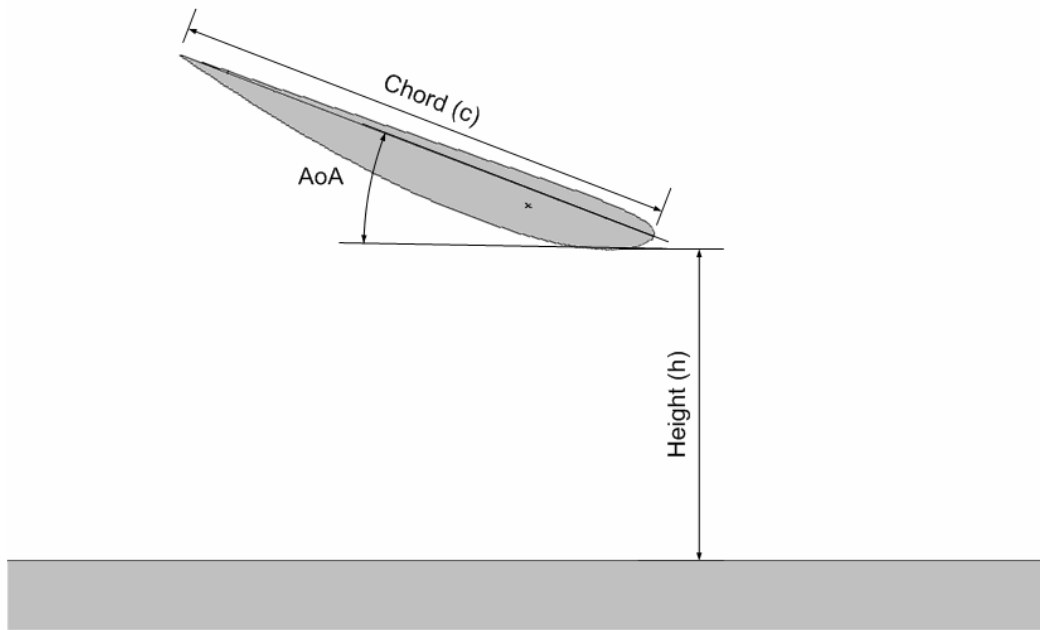


Figure 2.2 Aerofoil position parameters

2.4 Two-dimensional tunnel design and construction

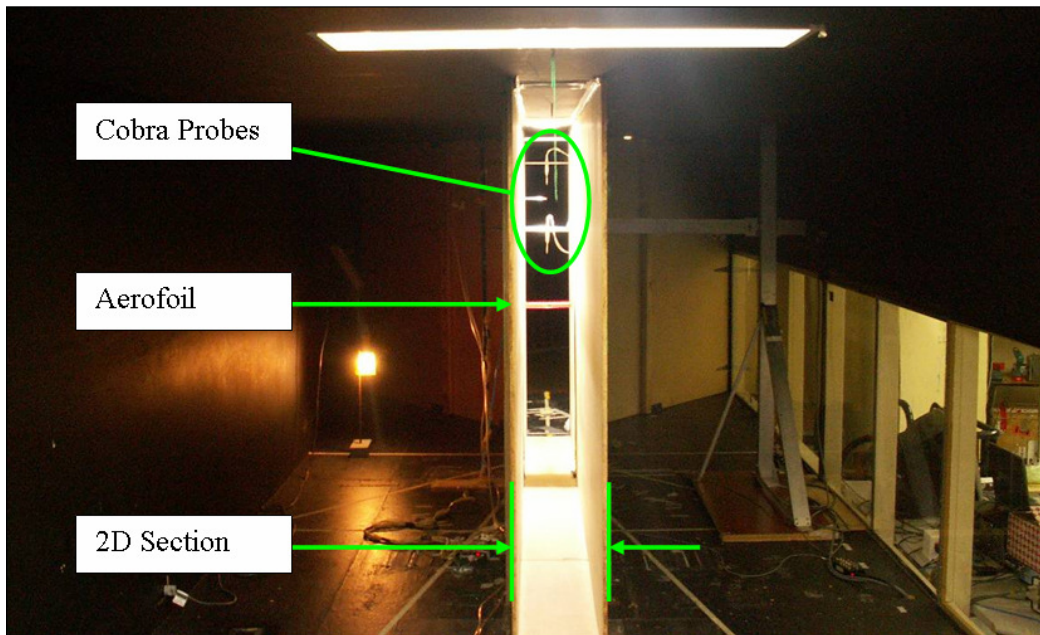


Figure 2.3 2-D tunnel installed in IWT

The RMIT Industrial Wind Tunnel (IWT) was used for 2-D testing of the aerofoils (see later). Normally the IWT has a test section 3m wide, 2m high and 9m long. An extra contraction was constructed and installed reducing the section width to 295mm.

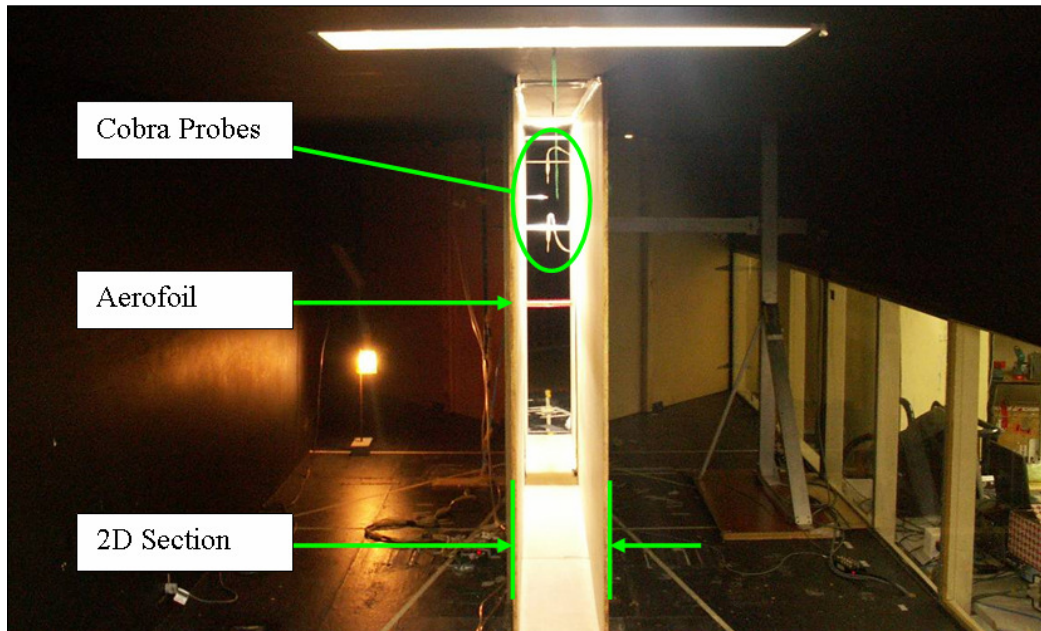


Figure 2.3 is a view looking upstream in the IWT section. The light area in the middle of the photo is the 2-D section. The additional contraction is visible in the background, either side of the 2-D section. The aerofoil model is visible in the centre mounted horizontally in the section. Two Cobra probes are visible in the section, above the aerofoil. Although a smaller wind tunnel was available, the IWT was chosen as it would allow enough height to reduce blockage effect caused by a horizontally located aerofoil at an incidence of 90° . The chosen aerofoils had chords of 150mm, thus the constructed tunnel will experience a maximum blockage of 7.5%. Constructed from 16mm thick MDF sheets, the walls for the new contraction and section were fixed to the ceiling and floor of the original (full sized) test section. Additional bracing

(50X150mm Pine) was also installed to reduce the tendency for the walls to bow in the middle during use. Care was taken to seal the gaps at the wall edges. The walls of the tunnel were pressure tapped to allow monitoring of the pressure gradient along the tunnel. Slots in the tunnel allowed the aerofoil to be restrained outside the tunnel, and the pressure tubes to exit. These slots were fitted with foam to allow rotation for AoA changes and vertical translation of the aerofoil while still sealing the tunnel. The aerofoils were supported by two steel frames. The aerofoil design allowed for mounting and pivoting about an axis at the 0.25 chord location. The Clark Y aerofoil is shown in Figure 2.4. Each mount was passed through a hole in a sliding mount (Refer Figure 2.5) and located with a grub screw. The mount was then able to be adjusted vertically, and then a bolt could be tightened to clamp the slide rail. This setup allowed the ground clearance and AoA of the aerofoils to be varied independently.



Figure 2.4 Aerofoil model



Figure 2.5 Aerofoil slide mount on slide rail

The air velocity in the tunnel was measured with a Dynamic Cobra Probe (Refer to Section A1.1 for more details on the Dynamic Cobra probe and its calibration). Dynamic Cobra probes provide pressure and velocity measurements.

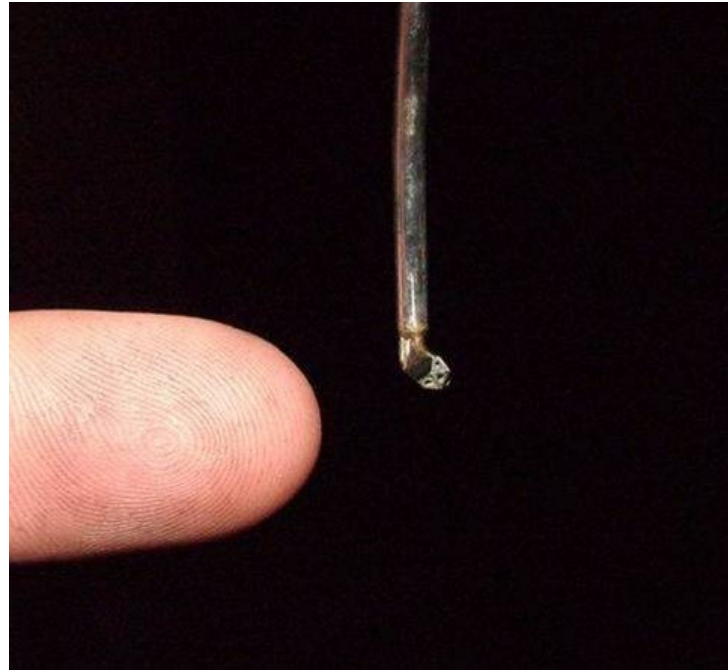


Figure 2.6 Dynamic Cobra head



Figure 2.7 Dynamic Cobra probe - side view (TFI catalogue)

The probe (refer Figure 2.6 and Figure 2.7) can take measurements for flow directions within an acceptance cone of $\pm 45^\circ$. The probe accuracy for velocity measurement is listed as $\pm 0.3\text{m/s}$ for velocities between 2 – 100m/s. This equates to $\pm 1.36\%$ at 22m/s. Flow angles are accurate to $\pm 1.0^\circ$.

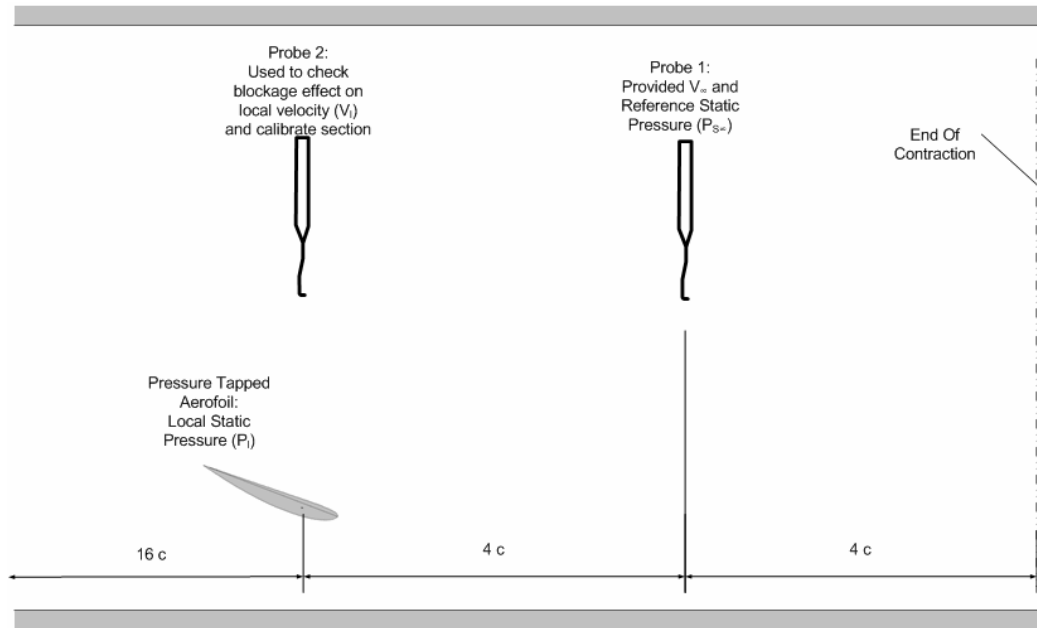


Figure 2.8 Cobra Probe positions in tunnel

One probe was mounted forward of the wing to provide data for V_∞ . Prior to testing (refer Figure 2.8- Probe 1), a Cobra probe was traversed across a vertical plane in the section where the wing was to be mounted (refer Figure 2.8- Probe 2). This provided a map of the flow velocity within the section, allowing it to be calibrated. Refer to Section A1.3 for more on the calibration.

2.5 Aerofoils used for testing

The design of a custom aerofoil is beyond the scope of this project, and thus appropriate shapes were chosen. Considering this is an early study in this area, it was decided that the actual specific profiles tested were not particularly important, provided the profiles differed in camber. The decision was made to use a set of pre-existing wings that had been manufactured for a

previous project. The models were made to be used in a small wind-tunnel (295mm wide x 300mm high x 1000mm long section) to allow undergraduates to study the pressure contours of a pre-stall aerofoil. The wing models had already been pressure-tapped, and using these models significantly reduced the cost and labour required for the project. The models all had a span of 295mm and chord of 150mm. They were all pivoted at 25% chord. They were manufactured in two halves (top and bottom), pressure-tapped, then glued together and painted. The pressure-taps generally ran down the centreline of the model (refer Figure 2.4) however a number of taps near the leading on the Clark Y model were staggered left and right of the centreline, no more than 0.04c. The pressure tap locations are displayed in Figure 2.9.

The first aerofoil to be tested had a Clark Y profile. This profile was chosen as it is a shape that is well documented and understood. The Clark Y typically exhibits slow stall characteristics, and limited CoP migration, however the drag tends to be higher and lift lower than other aerofoil shapes (Scott 2001).

The second profile tested was that of a 6-Series aerofoil, designated 63-412. The 6-series aerofoils were specifically designed using inverse methods to maintain laminar flow over most of the section, thus reducing drag for a certain operating range. This is an advantage of the 6-series, coupled with higher maximum lift co-efficient. Disadvantages include rapid stall characteristics and higher drag when not operating in design range (Scott 2001).

The third profile to be tested was the second profile with the addition of a “Gurney Tab” to the trailing edge. The Gurney tab effectively increases the camber of the aerofoil, altering the lift and drag characteristics. While more efficient means of achieving this are available, the Gurney tab is a quick and simple way, and is commonly used in race cars (Katz 1995) for tuning purposes, where a slight increase in drag is a tolerable for increased downforce. The tab used had a height of 0.067 chord.

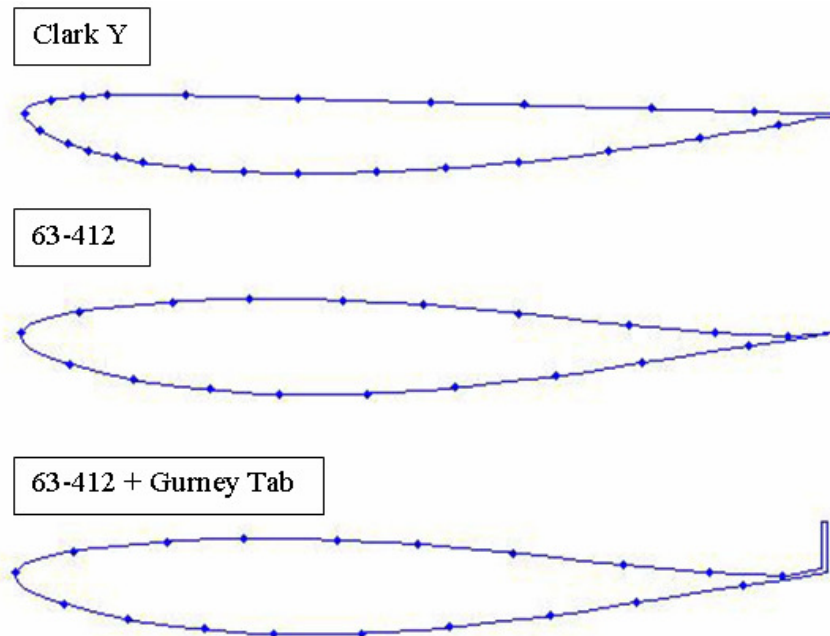


Figure 2.9 Aerofoil shapes tested with pressure tap locations

The aerofoil profiles were checked with the aid of a 3-D co-ordinate measuring machine. See section A2.1 for more details.

2.6 Discussion of errors

As with any investigation, the potential exists for errors to contaminate the results. The magnitude of these errors and the repeatability of results will be discussed here. For more detailed information on the individual errors refer to section Appendix 2.

The geometry of both aerofoils was tested and both aerofoils were found to be within 2% of the published shape, and two-dimensional to within 1%. The AoA was measured with the aid of a protractor fixed to the aerofoil pivot. Measurement was accurate to within +/- 0.5°. The ground clearance was measured with the aid of purpose built spacers, cut to the appropriate lengths. The clearance achieved with this method would be subject to a maximum error of +/- 0.001 Chord.

Pressure measurement was performed with a DPMS. Testing has shown the DPMS is accurate to +/- 0.3 % of full range. Flow velocity was measured with the aid of a Dynamic Cobra probe. This is accurate to +/- 1.36% for the velocity tested.

To give a visual indication of the potential magnitude of errors Figure 2.10 shows a plot with error bars superimposed on a datum point.

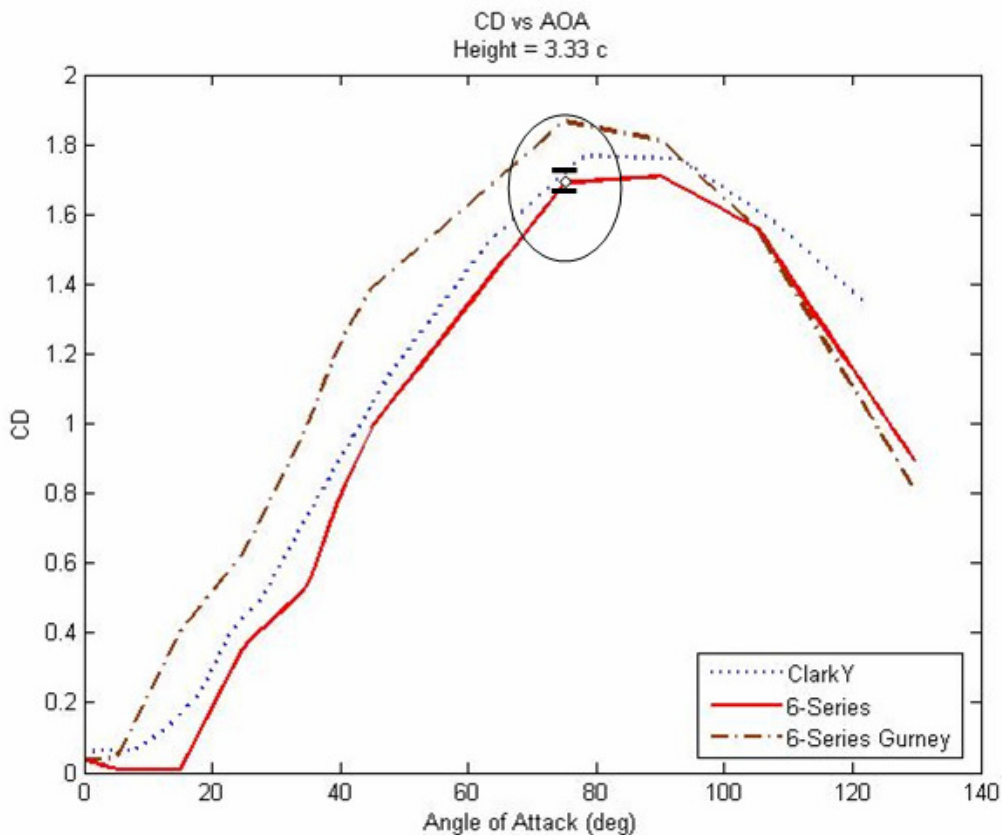


Figure 2.10 Drag variation displaying error

Only the error bars for the coefficient are shown, as the errors for AoA and ground clearance are not visible on this scale. It can be seen that the errors are relatively minor compared to the trends seen in the plot, thus it is safe to conclude the trend is due to physical phenomena, not errors.

In an effort to get an idea of the repeatability of the study, a number of trial runs were repeated at different times throughout the study. The coefficients from each of the runs were very similar. The standard deviation of lift coefficient for the tests was 1.9%, the drag coefficient standard deviation

was 1.4% and the standard deviation of the moment coefficient was 3%. Details of this study are in section A2.7

2.7 Instrumentation and measurement procedure

The forces acting on the wing were calculated by instrumenting the wing section with pressure-taps, and integrating across the surface for the force. A Dynamic Pressure Measuring System (DPMS) was used to acquire the pressure data. The DPMS allowed simultaneous measurement of the pressures from the taps on the aerofoil model. More details on the DPMS can be found in Section A1.2. Each test was sampled at 1,250 Hz for 6.963 seconds, and then averaged to provide time-averaged values. The sample frequency was chosen to provide a time period longer than expected dynamic effects (aerofoil vortex shedding for example) and enough resolution while not providing an overly large amount of data.

The velocity was measured with a Dynamic Cobra probe. As with the pressure data, velocity was sampled at 1,250 Hz for 6.963 seconds, and then averaged to provide time averaged values. Data from the Cobra probe were used to non-dimensionalise the pressure data. Pressure coefficients for the aerofoil pressure taps were calculated by using the relationship in Equation 2.1.

$$C_P = \frac{P_l - P_{s\infty}}{\frac{1}{2} \rho V_\infty^2}$$

Equation 2.1 Pressure coefficient

Where:

P_l = Local pressure (Pressure Tap)

$P_{s\infty}$ = Reference static pressure

$\frac{1}{2} \rho V_\infty^2$ = Reference dynamic pressure.

The ground clearance was measured with the aid of purpose built spacers, cut to the appropriate lengths. AoA was measured with a protractor fixed to the aerofoil pivot. The protractor was fitted to the mounting shaft of the model, on the outside of the tunnel section. Graph paper was fixed to the outside of the tunnel, aligned vertically with the aid of a plumb-bob. AoA was measured by comparing the angle on the protractor with the graph paper. This setup allowed the AoA to be checked at different heights.

Chapter 3 Results and discussion

3.1 Preamble

This chapter presents the results from the experimental investigation. The effects of high AoA on an aerofoil pressure contour are shown, as are the effects of ground proximity. The pressure contours are used to calculate the lift, drag and moment coefficients for each of the aerofoils, and the variation of these coefficients with both AoA and ground clearance is displayed.

3.2 Correction method

All the data represented have been corrected for instrument and tunnel calibration. Refer to Appendix 1 for details on calibration.

While results can be adjusted for the effects of blockage and there are many differing correction methods available, it is preferred that blockage be kept as small as possible. The blockage ratio experienced in this investigation varied from 0.009 (0° AoA) to 0.075 (90° AoA). The geometry of the aerofoils tested is such that the blockage ratio will be below 0.05 for AoA up to 42°, beyond the stall of all aerofoils. While 7.5% is a relatively high blockage ratio for a bluff body, the error induced will be minimal, as suggested by Rae & Pope (1984).

The tunnel had pressure taps installed to allow measurement of the static pressure along the length of the test section, so as to calculate the effects of horizontal buoyancy due to pressure gradient. Refer to Section A1.3 for more details on the calibration of the tunnel with regard to buoyancy. The effects were found to be negligible compared to the lift and drag.

The effects of streamline curvature interference on the results of this investigation will be minimal. The floor will affect the oncoming stream, however this is desired. The model will be far enough away from the ceiling (c/h ranges from 0.07 – 0.1) that the effect would be negligible.

3.3 Pressure contours

The forces acting on the wing were calculated from the surface pressures, resolving and integrating across the surface for the force. The pressures were first calibrated to suit the calibration of the sensors in the DPMS. The velocity of the tunnel was used to non-dimensionalise the data. This velocity was captured with a Dynamic Cobra probe, and was adjusted for both tunnel and probe calibration. The pressure data were converted to non-dimensional pressure coefficients (CP) and plotted as a function of x/c .

The non-dimensionalised pressure data were then used to integrate the pressure contour across the aerofoil surface. The axial and normal forces acting on the aerofoil were calculated, along with the moment. The moment was taken to act about a point at 25% chord. The axial and normal forces

were then used to calculate the lift and drag, depending on AoA via trigonometry.

Calculations were done with the aid of MatLab, which streamlined and automated the compression and analysis of data. Over 140 different runs were tested. Rather than display all pressure contours, only those pertinent to the discussion will be displayed.

In order to examine the validity of the experimental setup and results, a pressure contour from the best known aerofoil, the Clark Y was compared to literature, see Figure 3.1.

Figure 3.1 shows a pressure contour as a sample overlayed on some contours from the literature (Riegels, 1961). The contour is slightly different towards the leading edge of the aerofoil, with both top and bottom showing slightly higher pressure magnitudes. Following this the geometry of the aerofoil was then checked, and found to be accurate (see section A2.1 for details on the geometry measurement). The second tap from the leading edge on the lower (suction) side of this model was found to be faulty, and is shown here for completeness; it was not used in the calculations. This would help explain the unexpected gradient change in this region.

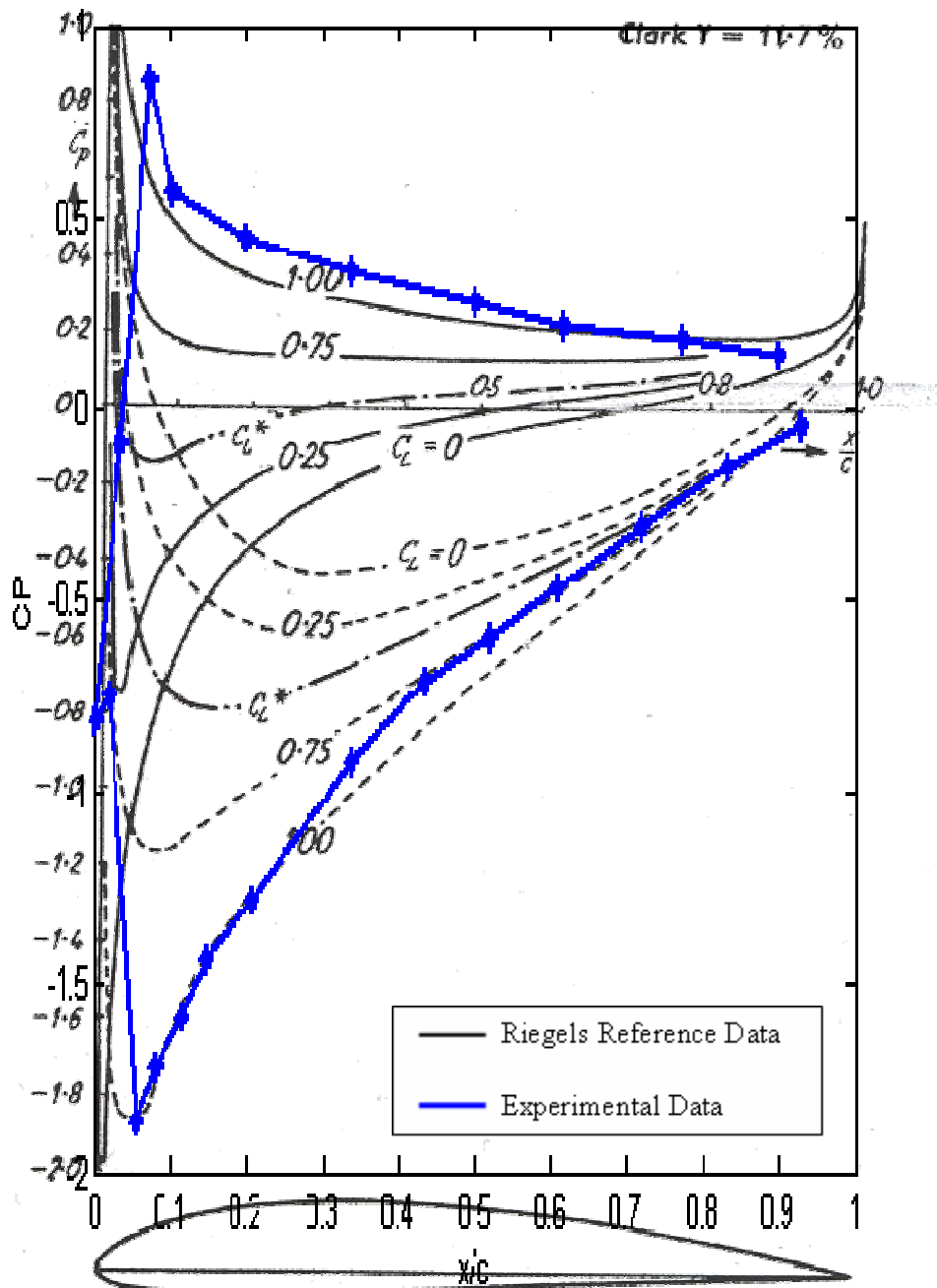


Figure 3.1 Overlay of pressure contour

The variation of pressure distribution with various AoA for the 6-series aerofoil is shown in Figure 3.2.

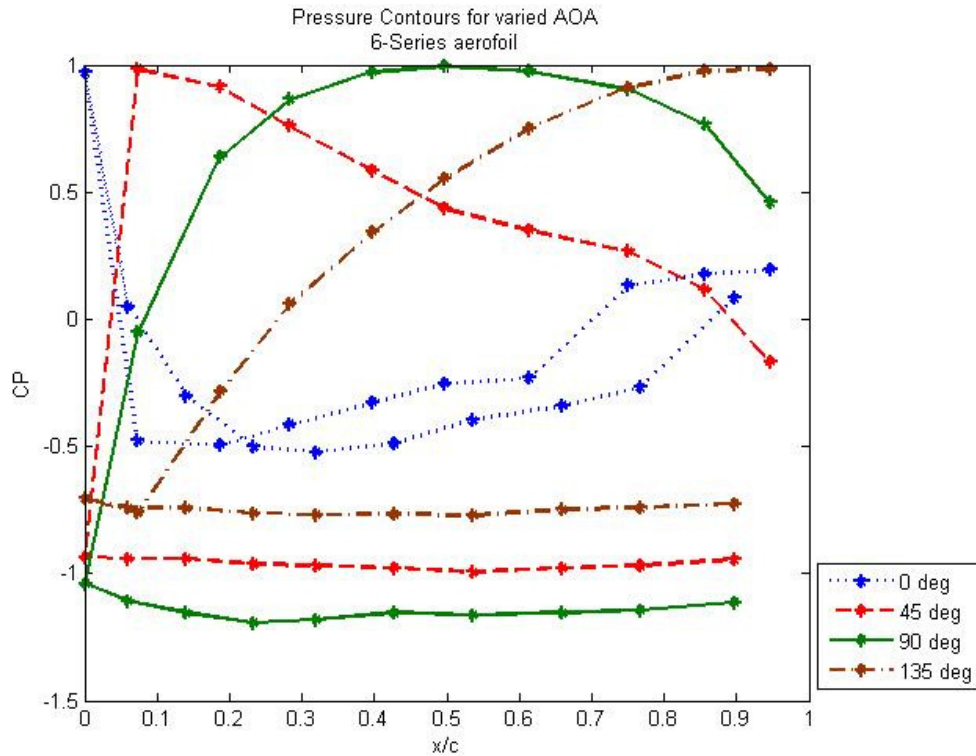


Figure 3.2 Pressure contours for different AoA

As would be expected, the stagnation point moves rearward after the stall. The pressure on the lower side of the aerofoil also varies in the general manner expected, with the maximum negative pressure occurring at 90° AoA. This general trend is the same for all the aerofoil shapes tested.

Figure 3.3 shows the variation of pressure distribution with ground clearances for a set AoA.

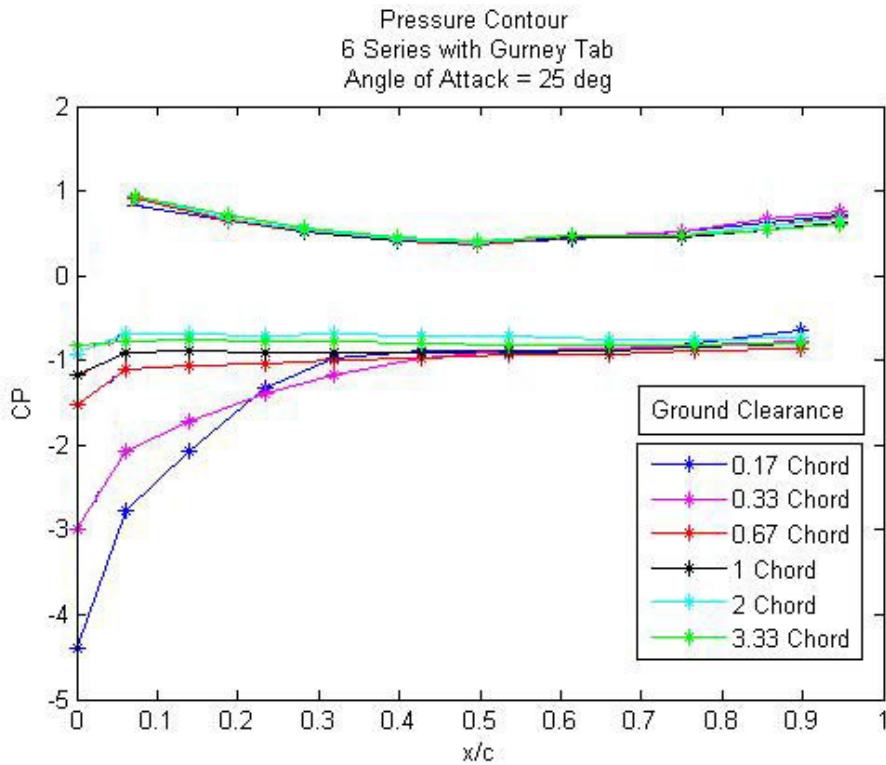


Figure 3.3 Pressure contours for different ground clearances

As can be seen in Figure 3.3 the majority of change with varied clearance occurs on the underside of the aerofoil, specifically the suction at the leading edge. This trend was also seen in the other aerofoil shapes.

3.4 Individual aerofoil results

The contours from each run were simplified to a C_l , C_d and C_m . These points were then used to generate a surface for lift, drag and moment, as shown in the following sections. This surface was constrained to pass through the points tested; spline interpolation was used between points. The test results are also plotted with the surface, and are shown with a marker.

3.4.1 Lift coefficient variation

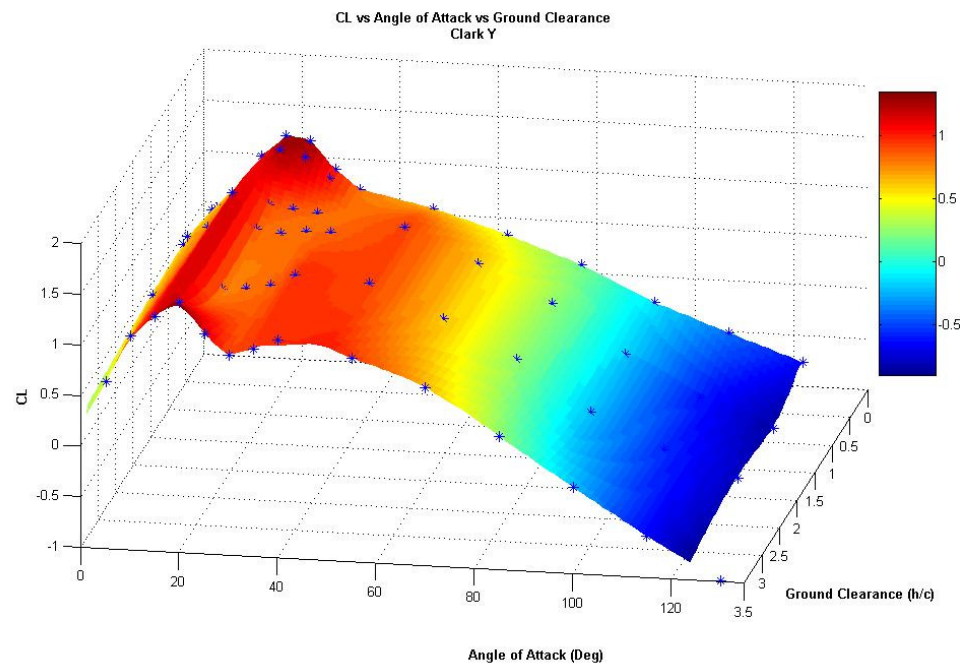


Figure 3.4 Lift coefficient variation - Clark Y

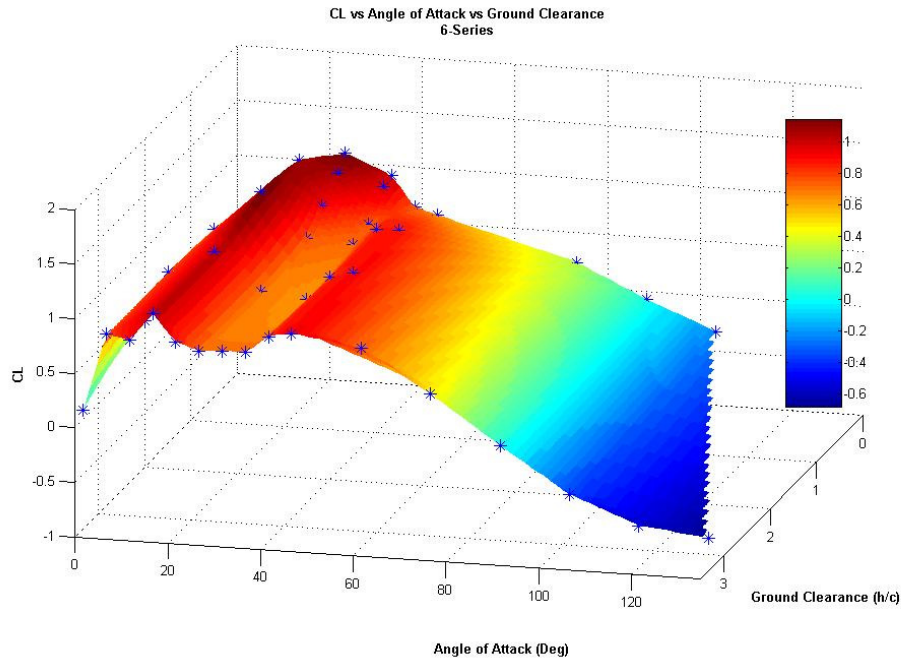


Figure 3.5 Lift coefficient variation - 6-Series

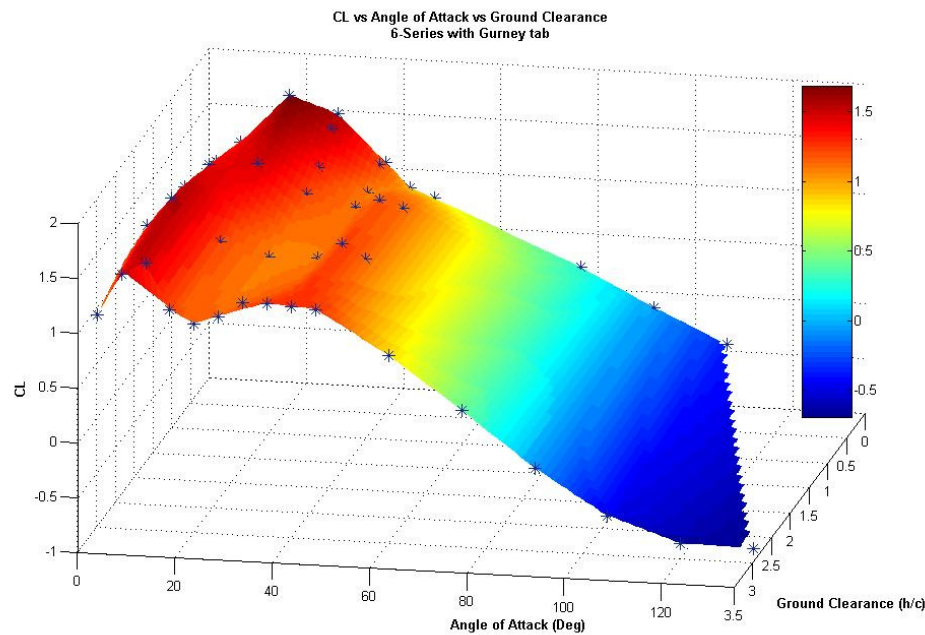


Figure 3.6 Lift coefficient variation - 6-Series with Gurney

The lift co-efficient varied with both AoA and ground clearance. Decreasing ground clearance tended to increase the magnitude of the lift coefficient across all AoA. Of particular interest was the effect close ground clearance had on the stall characteristic. It appears that the close ground clearance tended to inhibit or greatly reduce the severity of the stall.

3.4.1.1 Lift variation with angle of attack

To facilitate the interpretation of the surface plots, cross plots were made using spline interpolation and are presented in the next series of figures. These cross plots were generated from the 3D surface plot, thus the datum points are not shown. The actual datum points are shown in the surface plots previously.

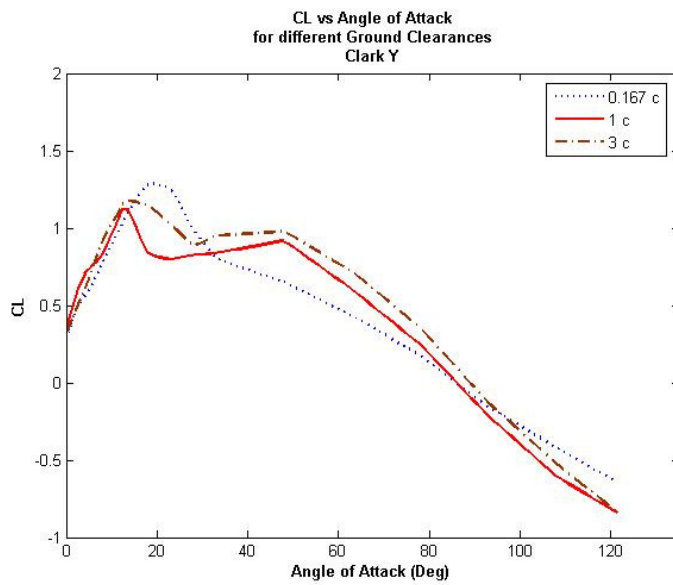


Figure 3.7 Lift coefficient variation with AoA as a function of non-dimensionalised ground clearance - Clark Y

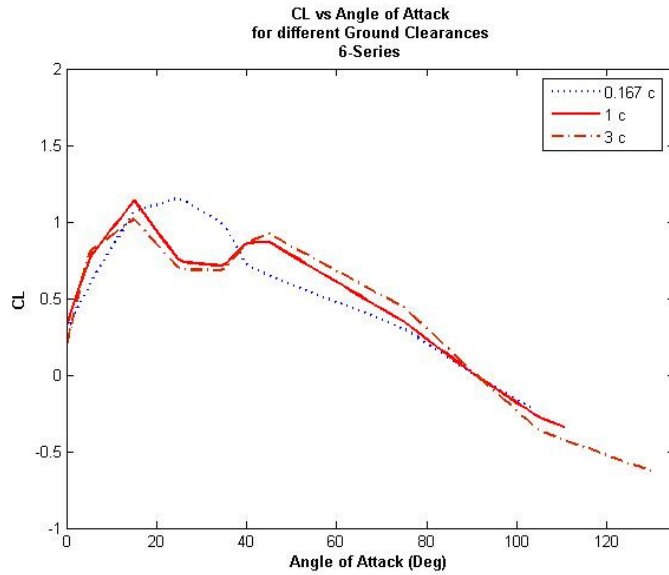


Figure 3.8 Lift coefficient variation with AoA as a function of non-dimensionalised ground clearance - 6 Series

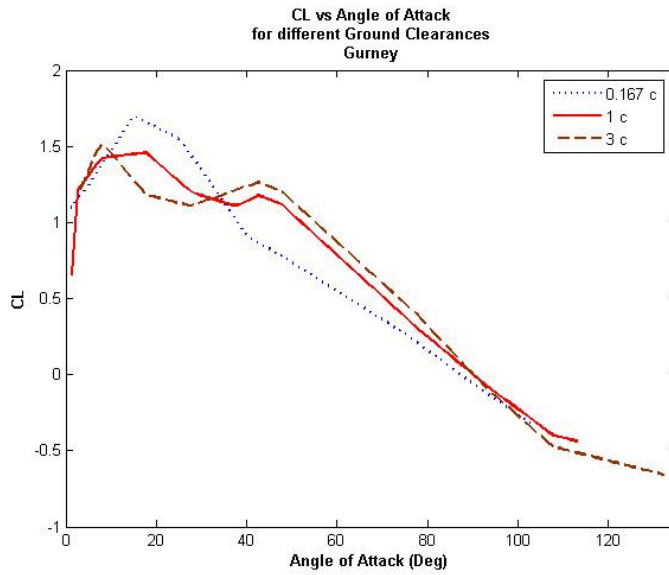


Figure 3.9 Lift coefficient variation with AoA as a function of non-dimensionalised ground clearance – 6-Series with Gurney

Figure 3.7 to Figure 3.9 show the lift vs AoA curves for differing heights. In all aerofoils, the stall tends to occur between $10^\circ - 30^\circ$ AoA. The effect on the stall characteristic is clearly seen in the curve at 0.167 chord compared to the curve at 3 chord lengths. All aerofoils show the stall occurring later when the aerofoil is in close ground proximity compared to when outside ground effect.

3.4.1.2 Lift variation with ground clearance

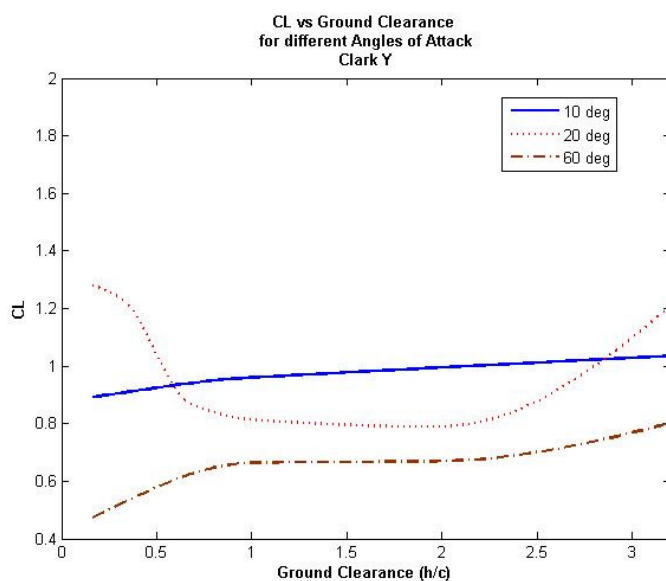


Figure 3.10 Lift coefficient variation with ground clearance as a function of AoA - Clark Y

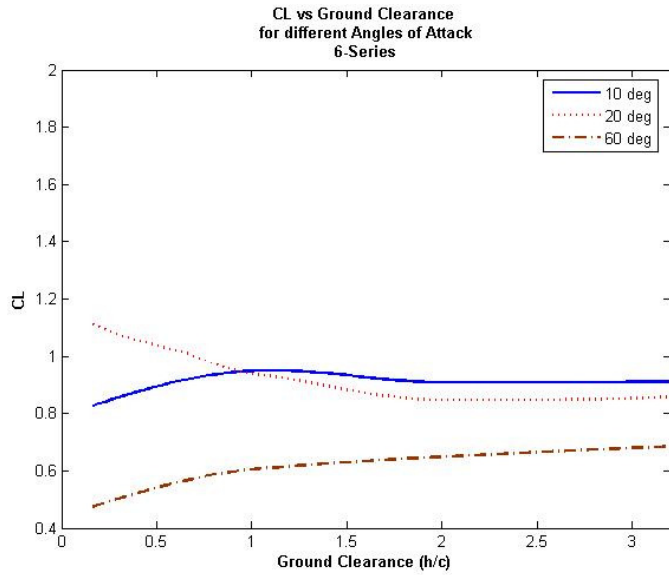


Figure 3.11 Lift coefficient variation with ground clearance as a function of AoA - 6

Series

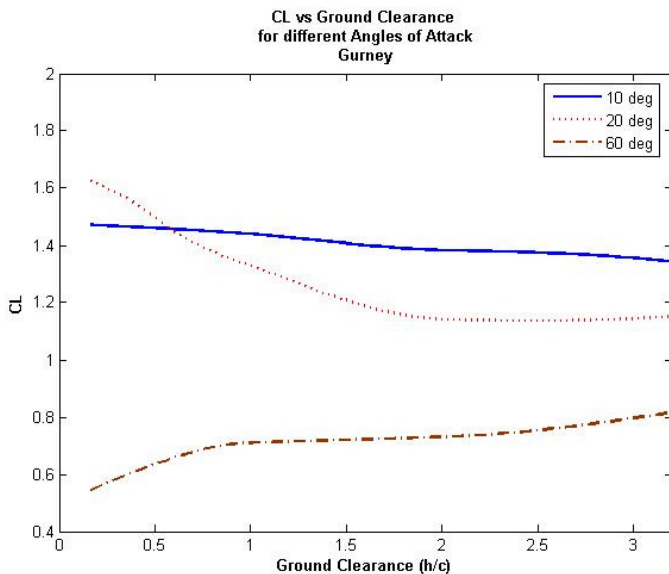


Figure 3.12 Lift coefficient variation with ground clearance as a function of AoA – 6-

Series with Gurney

Figure 3.10 to Figure 3.12 show the lift vs clearance curves for differing AoA. Of note is the trend of the post-stall curves at 60 deg, showing increasing lift with increasing clearance, contrary to the expected pre-stall trend of decreasing lift with increasing clearance. Both the Clark Y and 6-Series show some decrease in lift with decreased clearance. This is different to expectation and may be a result of the ground simulation.

3.4.2 Drag coefficient variation

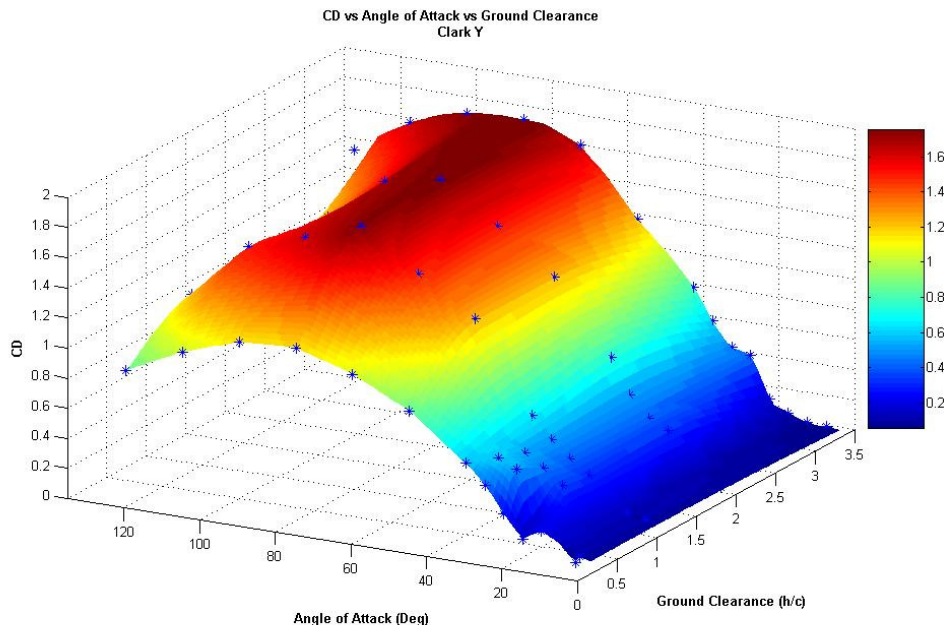


Figure 3.13 Drag coefficient variation - Clark Y

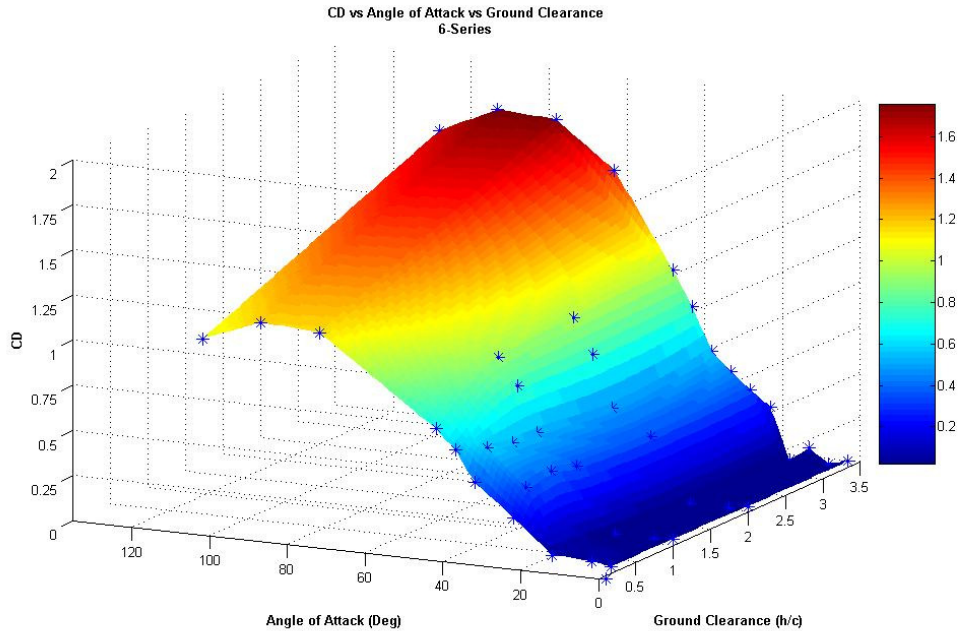


Figure 3.14 Drag coefficient variation - 6-Series

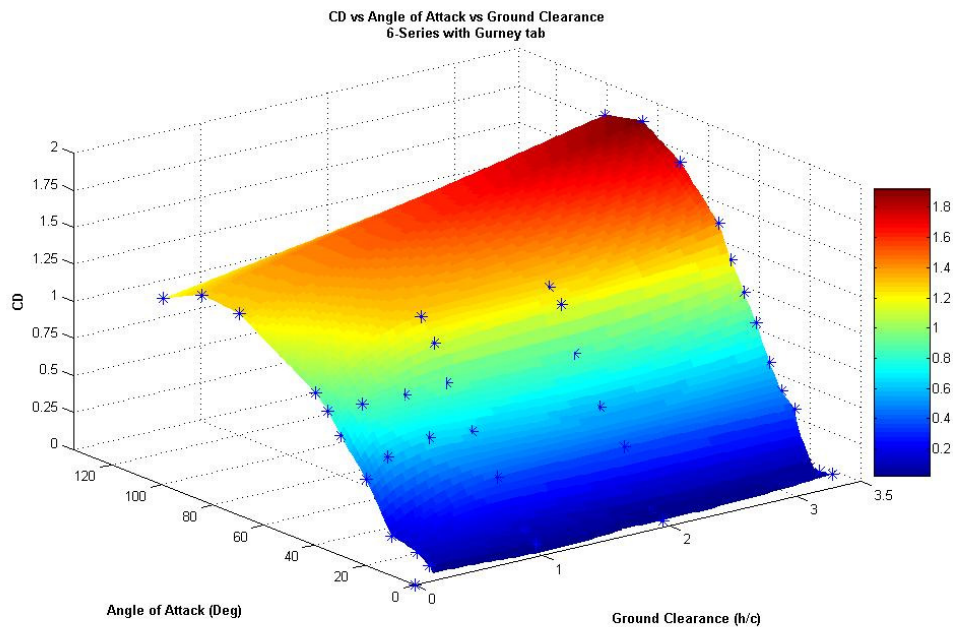


Figure 3.15 Drag coefficient variation - 6-Series with Gurney

The drag coefficient followed an expected trend, increasing rapidly from stall to a maximum at approximately 90°. It can be seen that the magnitude of the drag co-efficient was reduced with decreasing ground clearance.

3.4.2.1 Drag variation with angle of attack

As with the lift coefficient, cross plots were made using spline interpolation to facilitate the interpretation of the surface plots. The cross plots are presented in the next series of figures. These cross plots were generated from the 3D surface plot, thus the datum points are not shown. The actual datum points are shown in the surface plots previously.

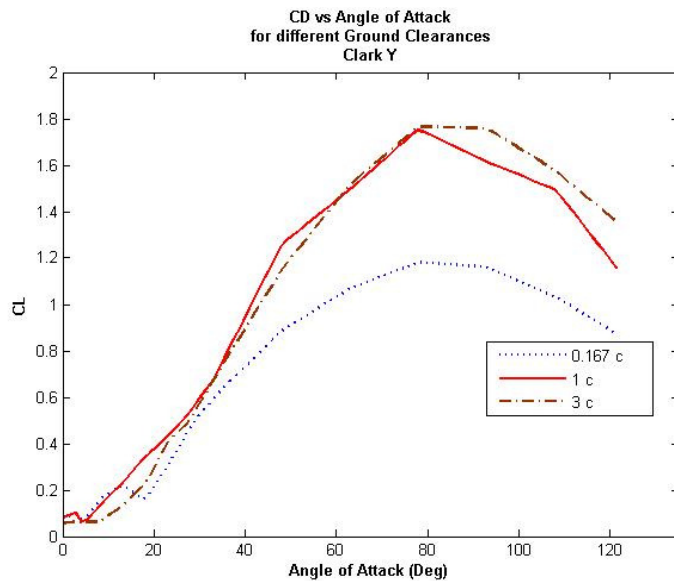


Figure 3.16 Drag coefficient variation with AoA as a function of non-dimensionalised ground clearance - Clark Y

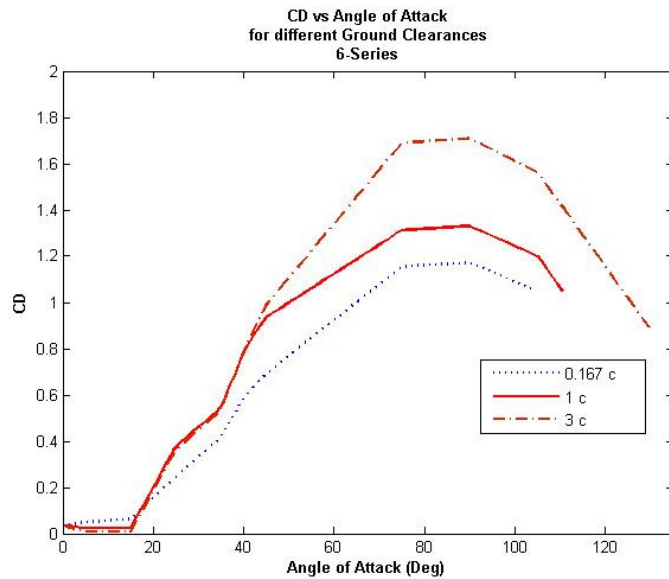


Figure 3.17 Drag coefficient variation with AoA as a function of non-dimensionalised ground clearance - 6 Series

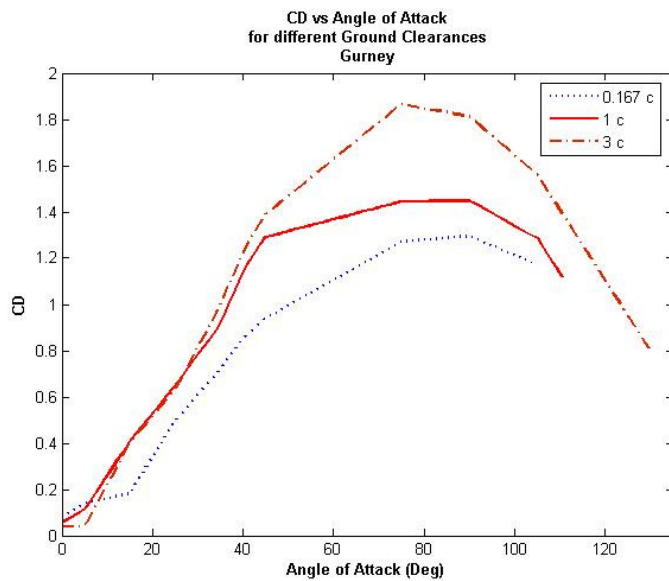


Figure 3.18 Drag coefficient variation with AoA as a function of non-dimensionalised ground clearance – 6-Series with Gurney

The drag coefficient for all aerofoils follows the same general trend. The coefficient post stall shows a curve broadly similar to a cosine function, showing similarity to a flat plate. Variation in clearance had an effect on the magnitude of the coefficient, but not the general trend.

3.4.2.2 Drag variation with ground clearance

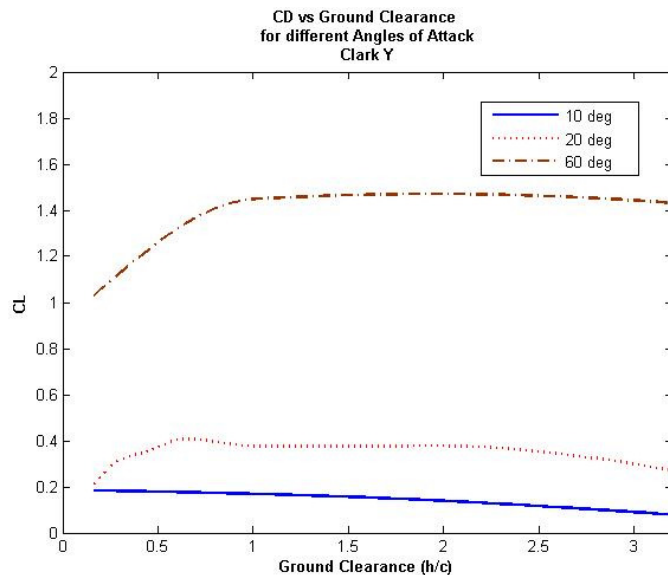


Figure 3.19 Drag coefficient variation with ground clearance as a function of AoA -

Clark Y

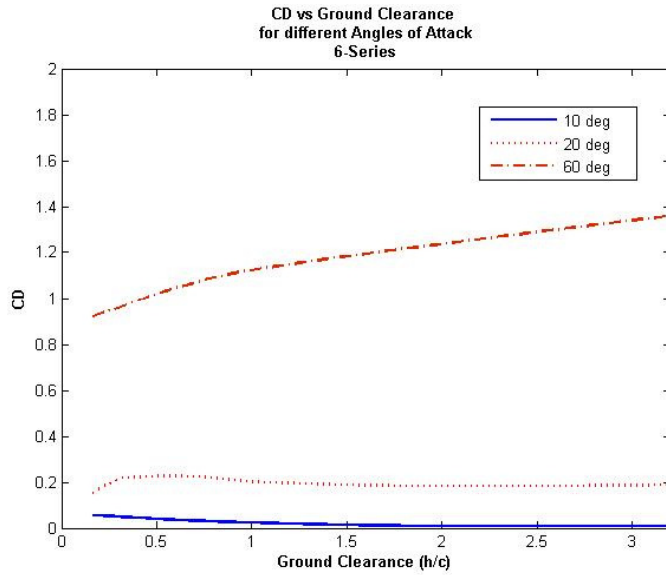


Figure 3.20 Drag coefficient variation with ground clearance as a function of AoA - 6

Series

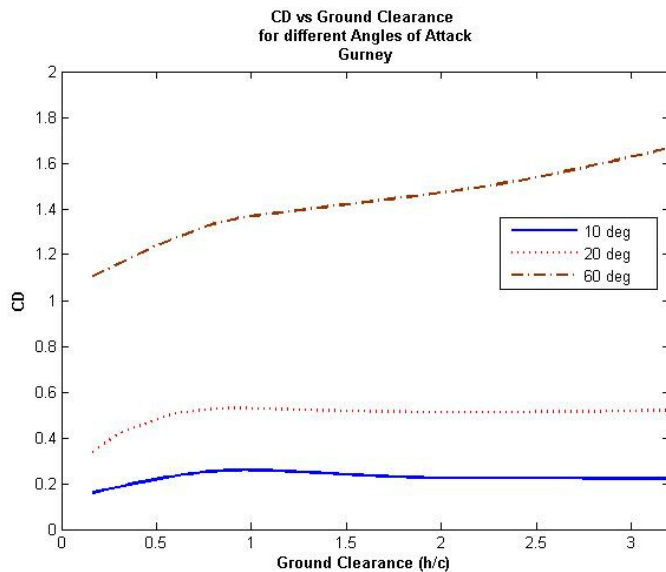


Figure 3.21 Drag coefficient variation with ground clearance as a function of AoA - 6-

Series with Gurney

The trend of increased post-stall drag with increased clearance is visible in Figure 3.19 to Figure 3.21. As in lift, this contrasts the pre-stall trend of decreasing drag with increasing clearance.

3.4.3 Moment coefficient variation

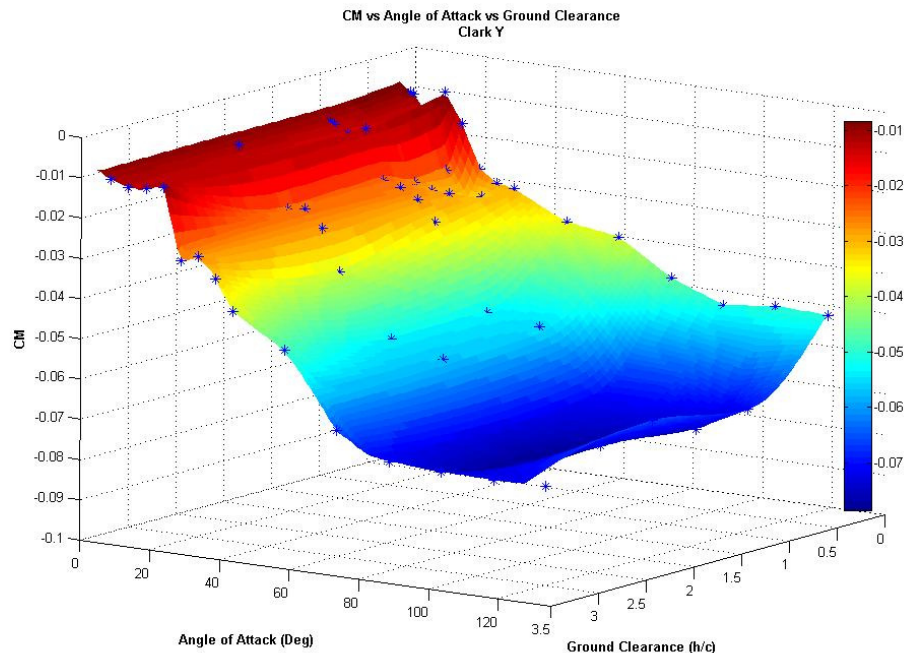


Figure 3.22 Moment coefficient variation - Clark Y

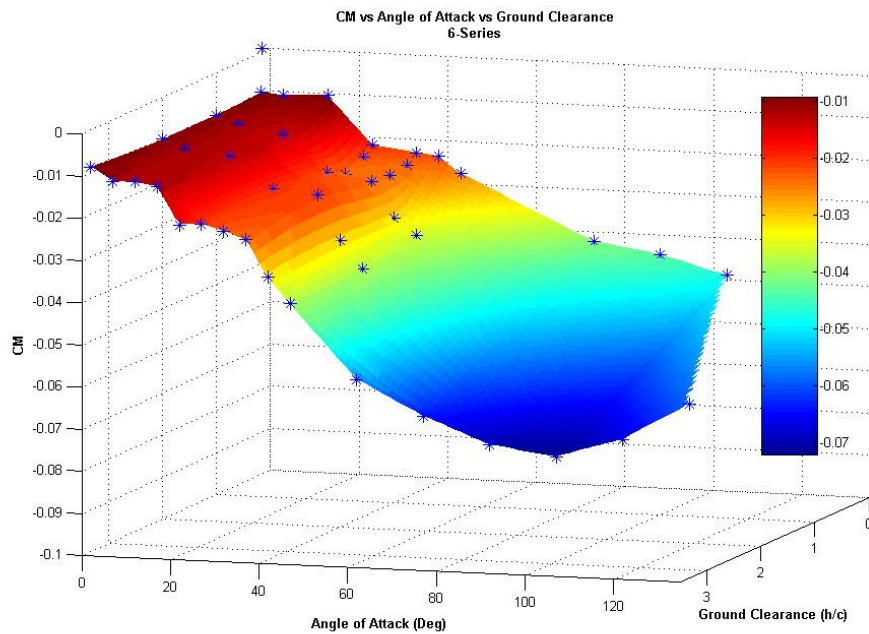


Figure 3.23 Moment coefficient variation - 6-Series

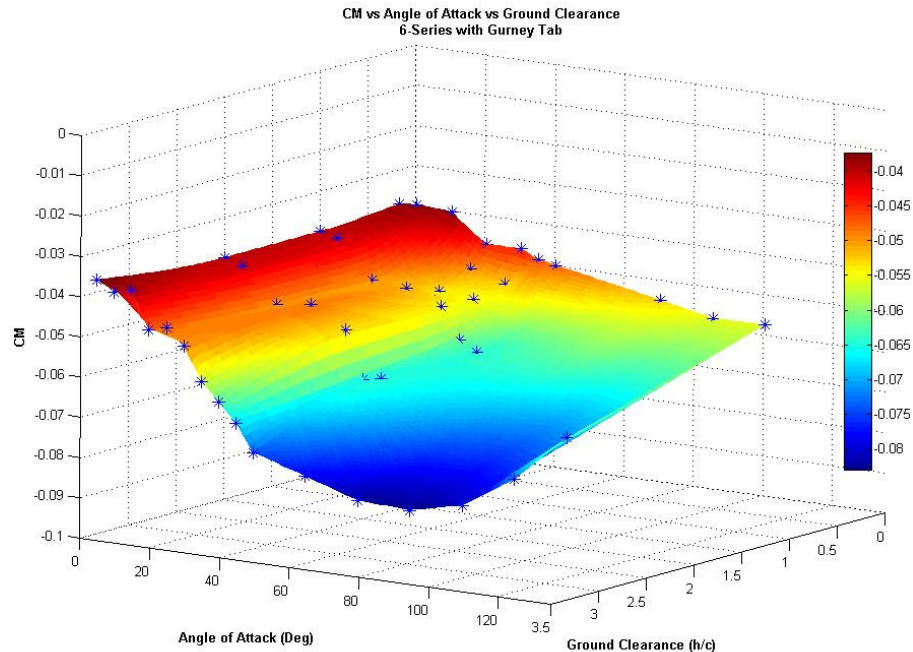


Figure 3.24 Moment coefficient variation - 6-Series with Gurney

Generally the moment coefficient became more negative (acting to reduce the angle of attack) with increased AoA. The variation of pitching moment was reduced with decreased ground clearance.

3.4.3.1 Moment variation with angle of attack

To facilitate the interpretation of the surface plots, cross plots were again made using spline interpolation and are presented in the next series of figures. These cross plots were generated from the 3D surface plot, thus the datum points are not shown. The actual datum points are shown in the surface plots previously.

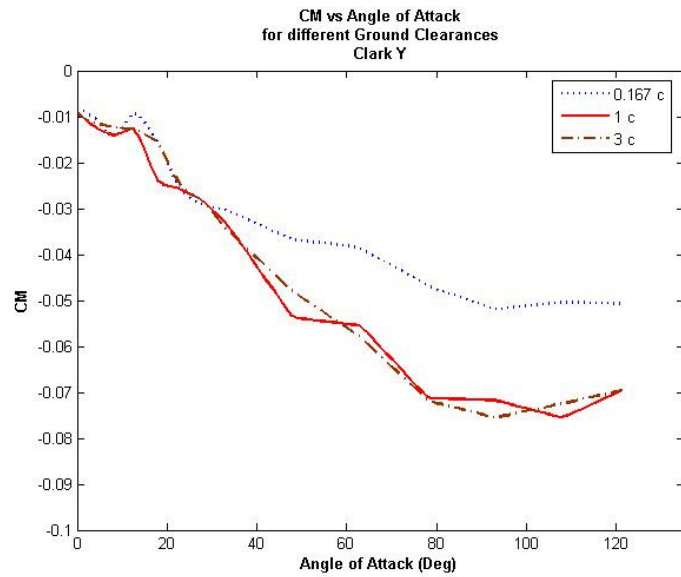


Figure 3.25 Moment coefficient variation with AoA as a function of non-dimensionalised ground clearance - Clark Y

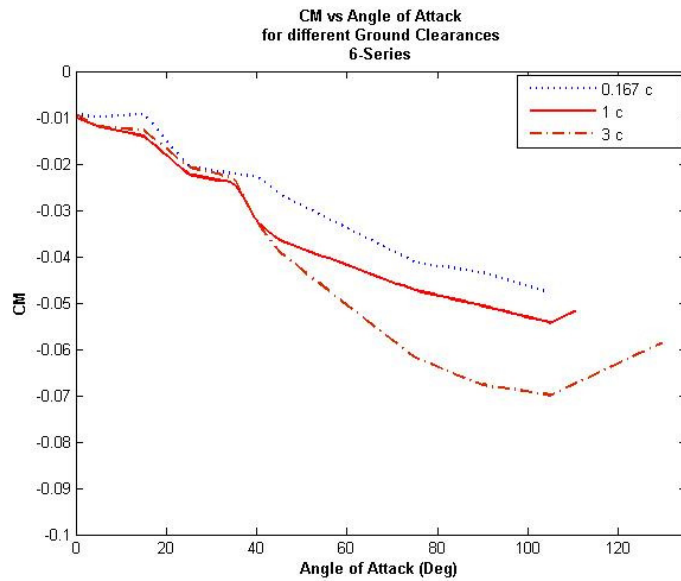


Figure 3.26 Moment coefficient variation with AoA as a function of non-dimensionalised ground clearance - 6 Series

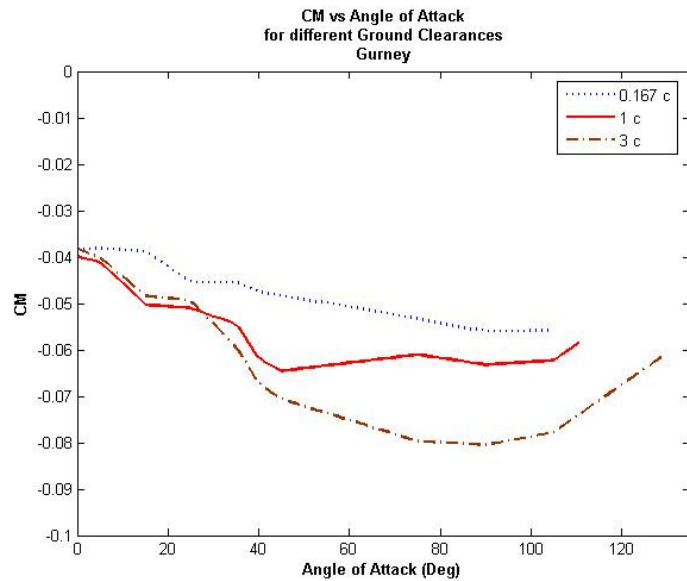


Figure 3.27 Moment coefficient variation with AoA as a function of non-dimensionalised ground clearance - 6-Series with Gurney

Figure 3.25 to Figure 3.27 show the variation of moment coefficient with AoA. While the actual values of C_m differed, the aerofoils all showed similar trends for the variation of pitching moment throughout the range of AoA. The location of the CoP moved aft post stall to a position approximately mid-chord at 90° AoA.

3.4.3.2 Moment variation with ground clearance

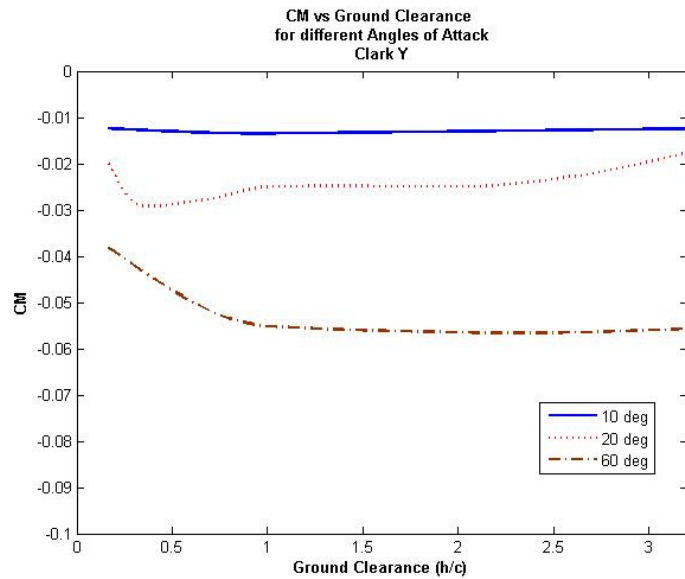


Figure 3.28 Moment coefficient variation with ground clearance as a function of AoA-

Clark Y

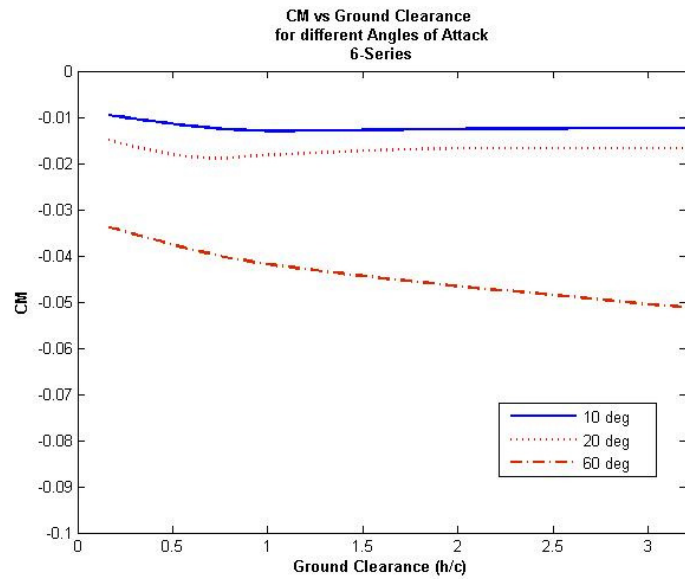


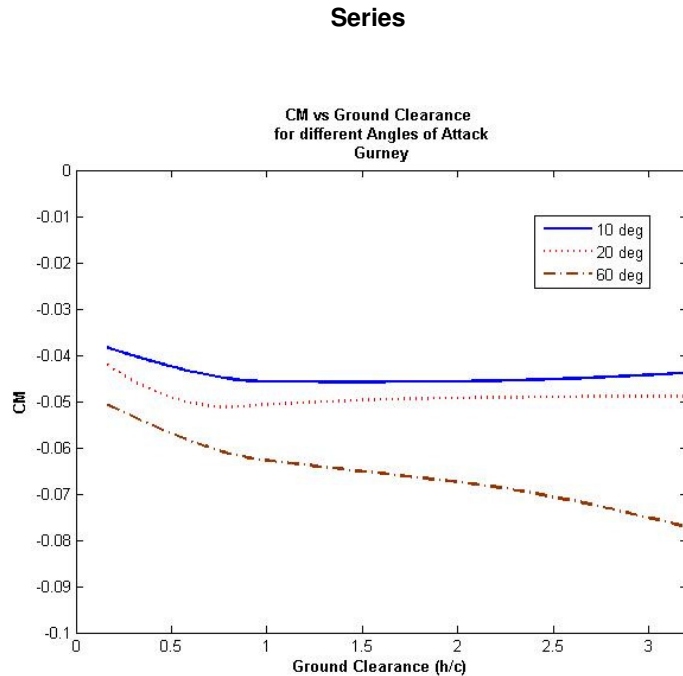
Figure 3.29 Moment coefficient variation with ground clearance as a function of AoA - 6

Figure 3.30 Moment coefficient variation with ground clearance as a function of AoA - 6-Series with Gurney

Figure 3.28 to Figure 3.30 show the variation of C_m with ground clearance. Close ground presence tended to reduce the magnitude of the C_m . The presence of the ground is most visible in the post-stall case (60° AoA); the C_m being reduced by approximately a third.

3.5 Aerofoil comparison

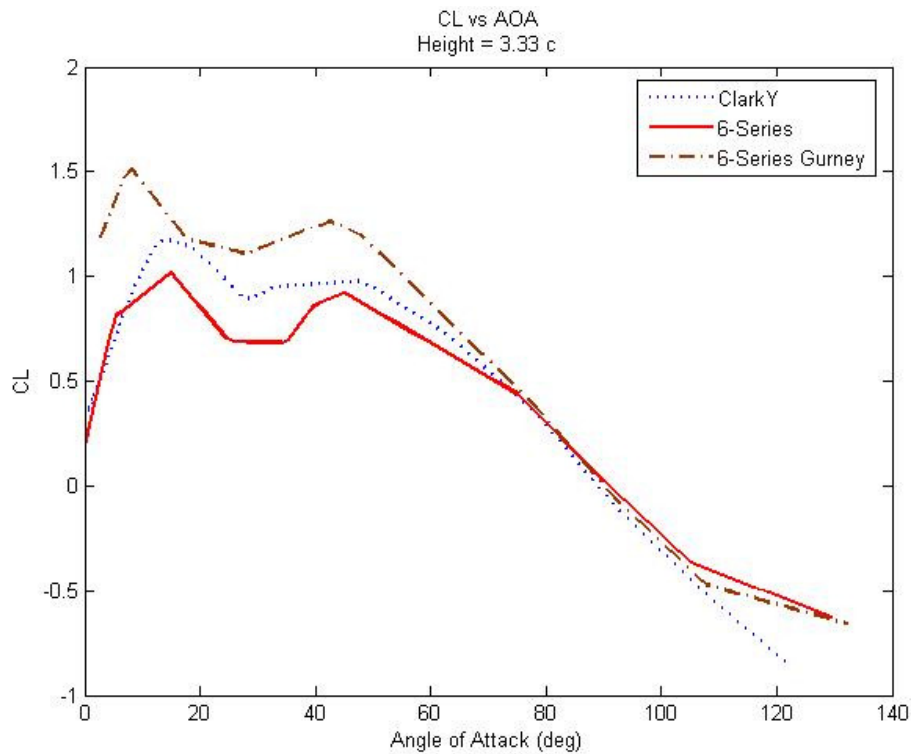


Figure 3.31 Lift coefficient comparison

Figure 3.31 shows the lift curves for all aerofoils tested outside ground effect. The lift is seen to increase up to stall, at which point the lift drops off. The lift increases again slightly post stall to another maxima at approximately 45° before dropping away steadily to 0 at 90°. The aerofoil with the Gurney tab provides the highest lift of the aerofoils tested. This was expected as the effective camber for this aerofoil is the highest. However it also shows the highest drag in Figure 3.32.

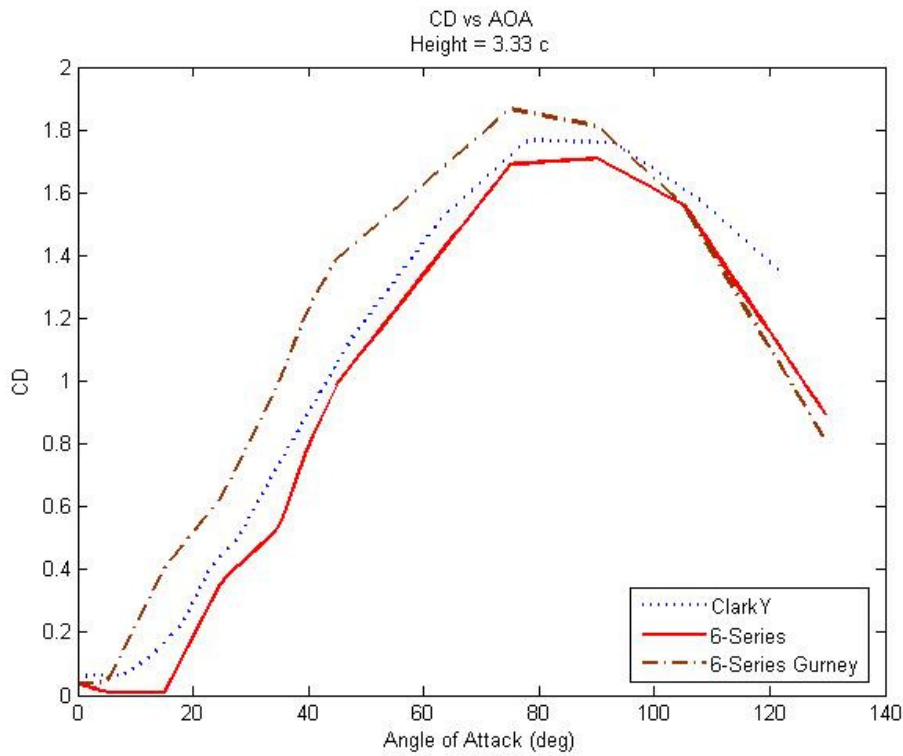


Figure 3.32 Drag coefficient comparison

The three aerofoils provided a similar trend of drag compared to AoA.

The drag for the third aerofoil was generally higher, and peaked 10° - 15° before the others.

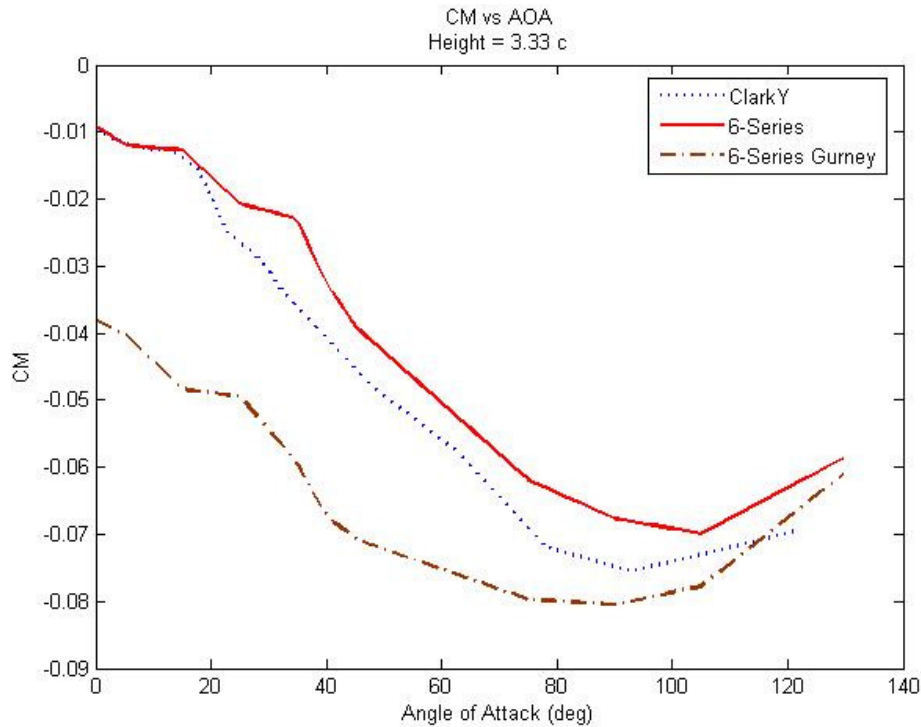


Figure 3.33 Moment coefficient comparison

The third aerofoil also shows a greater C_m than the other aerofoils, however the variation is slightly less across the range of AoA. The addition of the Gurney tab offset the CoP of the aerofoil rearward of the original position.

3.6 Discussion

There are a number of variables that may have had an impact on the results of this investigation. These are discussed in the following section. The application of these results in the automotive context are discussed in the next chapter.

3.6.1 Discussion of results

Close ground clearance appeared to delay the stall of the three aerofoils tested; however this effect could be a function of the ground simulation. The pre-stall trend of decreasing lift with decreased ground clearance is contrary to the expected increase in lift as the ground is approached. A possible explanation for both the stall delay and decrease in lift with decreased clearance would be interference from the ground boundary layer. Similar trends were found by Barber et al. (2002) at close ($<0.2c$) ground clearances with a fixed ground. The interaction with the ground boundary layer is complex, and the boundary layer thickness is a function of number of variables, including the pressure gradient and the suction of the aerofoil. The closer proximity to the boundary layer will give results similar to those of closer ground clearances without a boundary layer. The ground boundary layer may also help maintain attached flow on the suction side of the aerofoil. The thickness of the ground boundary layer and resultant displacement thickness are estimated in Equation 3.2 and Equation 3.3 respectively.

$$\text{Re} = \frac{\rho VL}{\mu} = \frac{1.2 \times 22 \times 1.05}{1.84 \times 10^{-5}} = 1.507 \times 10^6$$

Equation 3.1 Reynolds number of section

$$\delta_1 = \frac{0.3747x}{(\text{Re}_x)^{0.2}} = \frac{0.3747 \times 1.05}{(1.507 \times 10^6)^{0.2}} = 0.022869m$$

$$\delta_2 = \frac{0.3747x}{(\text{Re}_x)^{0.2}} = \frac{0.3747 \times 1.2}{(1.722 \times 10^6)^{0.2}} = 0.025448m$$

$$\Delta\delta = \delta_1 - \delta_2 = 2.579 \times 10^{-3} m$$

$$\Delta\delta = 17.2 \times 10^{-3} c$$

Equation 3.2 Ground boundary layer thickness

$$\delta^*_1 = \frac{1.72x}{\sqrt{\text{Re}_x}} = \frac{1.72 \times 1.05}{\sqrt{1.507 \times 10^6}} = 1.4712 \times 10^{-3}$$

$$\delta^*_2 = \frac{1.72x}{\sqrt{\text{Re}_x}} = \frac{1.72 \times 1.2}{\sqrt{1.722 \times 10^6}} = 1.57287 \times 10^{-3}$$

$$\Delta\delta^* = \delta^*_1 - \delta^*_2 = 0.1017 \times 10^{-3} m$$

$$\Delta\delta^* = 0.678 \times 10^{-3} c$$

Equation 3.3 Ground boundary layer displacement thickness

The results from Equation 3.2 and Equation 3.3 predict the variation in boundary layer thickness to be minor; however these calculations ignore the proximity of the aerofoil to the ground. The pressure gradient produced by the aerofoil will effect the growth of the ground boundary layer. It is expected that in this investigation the adverse pressure gradient from the aerofoil would increase the growth of the ground boundary layer. The interaction of these two phenomena is complex, and requires extensive investigation in its own right, beyond the scope of this work. Due to this the results at close ground clearance must be viewed with some uncertainty. Further investigation, ideally with moving ground to reduce / remove boundary layer effects would be

necessary to investigate the interaction of the aerofoil with the ground boundary layer, and thus validate results at close ground clearance.

The Reynolds number used for the testing is calculated in Equation 3.4.

$$Re = \frac{\rho VL}{\mu} = \frac{1.2 \times 22 \times 0.15}{1.84 \times 10^{-5}} = 2.15 \times 10^5$$

Equation 3.4 Reynolds Number of tests

While this is generally below the Reynolds number of the flows generally experienced by wings in automotive use, the difference should not cause large discrepancies between forces found in the investigation and those in the field. The Reynolds number typical of a FSAE race car at a speed of 48 km/h (design average track speed) are calculated below:

$$Re_{(Front)} = \frac{\rho VL}{\mu} = \frac{1.2 \times 13.333 \times 0.432}{1.84 \times 10^{-5}} = 3.84 \times 10^5$$

$$Re_{(Rear)} = \frac{\rho VL}{\mu} = \frac{1.2 \times 13.333 \times 0.780}{1.84 \times 10^{-5}} = 6.93 \times 10^5$$

Equation 3.5 Reynolds Number for typical FSAE wings

The wing geometries used for this calculation were those of the Monash University race car. These wings are large relative to the vehicle, but they are a competitive example of wings that comply with the competition rules. More information on the application of this research to FSAE is given in Chapter 4. Reynolds number effects will vary depending on AoA. At AoA near

90°, Reynolds number will have little effect as the separation points are effectively fixed; movement of the separation point around the leading edge of the aerofoil will have minimal impact on the forces experienced by the aerofoil. At AoA close to the stall of the aerofoil, the effects of Reynolds number will be important, but the magnitude of these effects would be insignificant compared to the instabilities due to the stall itself.

The forces acting on the wing were calculated by integrating the pressure contour, and thus results from this research do not include the effects of skin friction. Had a force-balance been used to directly measure the forces, skin friction would be included, but the results from a force-balance would be affected by the sealing of the aerofoil in the section, and it is for this reason the force-balance was not used. Drag due to skin friction is typically very small compared to the pressure drag on a bluff body such as an aerofoil post-stall. When the body is streamlined, such as an aerofoil pre-stall, the drag from skin friction is a larger component of the total drag, though the magnitude of drag from a streamlined body is typically small, thus the effect of skin friction is also small. Equation 3.6 presents an estimation of the skin friction acting on the aerofoils tested prior to stall. The method used calculates the friction on both sides of a flat plate in similar flow conditions. It is assumed that the flow is laminar over the length of the plate.

$$C_{sf} = 2 \times \frac{1.328}{\sqrt{\text{Re}_L}} = \frac{2.656}{\sqrt{2.16 \times 10^5}} = 5.715 \times 10^{-3}$$

Equation 3.6 Skin Friction Estimation

As demonstrated in Equation 3.6, the skin friction on an aerofoil pre-stall is much less than the range of pressure drag post-stall: 5.715×10^{-3} compared to a pressure drag coefficients ranging from 0.2 to 1.8.

As mentioned previously, the blockage ratio of the models tested was a function of the AoA. For 0° AoA the blockage ratio is 0.9% whilst the highest blockage (corresponding to 90° AoA) is 7.5%. At low AoA blockage effects are thought negligible, whereas this might not be the case for high AoA. Further study is required to determine the magnitude of the blockage effects on the results at high AoA.

It is expected the results from this investigation would be very similar to those experienced in the field, with some scepticism placed on the magnitude of the results collected at close ground clearance and at high blockage ratio ($\text{AoA} > 42^\circ$).

Chapter 4 Implications of results

4.1 Preamble

In this chapter the results found from the research will be reviewed in the context of a FSAE race car. A typical car will be simulated with and without active aerodynamics, and the performance benefit evaluated.

All the experiments were conducted for 2-D aerofoils; no 3-D effects have been investigated. The wings used on an automobile are obviously of finite AR, thus 3-D effects will modify the flow structure and hence the forces. In order to give an estimation of the potential benefits of an active aerodynamic system, some assumptions have to be made about the inherent differences between 2-D experimental and 3-D applications.

4.2 Wing size

The first assumption to be made is the physical size of the wing. FSAE rules (2006) dictate some rules on wing geometry. The sizes of the wings that are used in the following calculations are shown in Table 4-1.

Front Wing		Rear Wing	
Span	Chord	Span	Chord
1100	432	1400	780

Table 4-1 Wing geometry for performance evaluation

As mentioned previously in section 3.6.1, the wing geometries are those of a Monash University FSAE car. These wings were chosen as they represent a typical example of FSAE-specification wings.

4.3 Aspect ratio

Due to three dimensionality, an assumption as to the AR of the wings also needs to be made.

$$AR_{Actual} = \frac{b}{c}$$

Equation 4.1 Aspect ratio for rectangular wings

Where:

b = Wing span

c = Wing Chord

Equation 4.1 illustrates the basic definition of AR for rectangular wings. Using this relationship, and looking purely at the geometry of the wings used for these calculations, an AR in the order of 2 would be expected. However, this relationship does not include the effect of end plates on the wings. End plates tend to reduce 3-D effects, thus increasing the effective AR of the wing. The relationship between AR and end plate size is shown in Equation 4.2.

$$AR = AR_{Actual} \left(1 + 1.9 \frac{h}{b} \right)$$

Equation 4.2 End plate effect on wing AR (Hoerner, 1965)

Where:

h = Height of the end plate

b = Wing span

The endplates used on most FSAE wings will increase the effective AR to around 3.5, as per Equation 4.2. The end plate sizes used in the following example are as in Table 4-2:

Front Wing		Rear Wing	
Height	Width	Height	Width
240	420	660	876

Table 4-2 Wing end plate geometry for performance evaluation

<i>FrontWing</i>	<i>RearWing</i>
$AR_{(Actual)} = \frac{b}{c} = \frac{0.432}{1.1}$	$AR_{(Actual)} = \frac{b}{c} = \frac{0.78}{1.4}$
$AR_{(Actual)} = 2.546$	$AR_{(Actual)} = 1.795$

Equation 4.3 Aspect ratio of FSAE wings

<i>FrontWing</i>	<i>RearWing</i>
$AR = AR_{Actual} \left(1 + 1.9 \frac{h}{b} \right)$	$AR = AR_{Actual} \left(1 + 1.9 \frac{h}{b} \right)$
$AR = 2.546 \left(1 + 1.9 \frac{0.24}{0.432} \right)$	$AR = 1.795 \left(1 + 1.9 \frac{0.66}{0.78} \right)$
$AR = 3.602$	$AR = 3.403$

Equation 4.4 Aspect ratio of FSAE wings with endplates

The low ground clearance on the front will also have the effect of reducing 3-D effects; further increasing the effective AR of the front wings. A conservative AR of 3.6 for the front and 3.4 for the rear wings will be used for the calculations that follow.

4.4 Flow interaction

A final assumption that needs to be made is regarding the interaction of flows between the wings and the car body. Increasing the drag of the front wing can decrease the total drag experienced by the car via interaction of flow over the front wheels and car body. Also altering the flow from the front wing will alter the flow experienced by the rear wing. These interaction effects are the reason the aerodynamic characteristic of the total vehicle needs to be investigated for each setting. This is obviously a complex process, one

that is well beyond the scope of this research. The proximity of the front wing to rotating wheels can lead to interactions of the flows from wing and wheel. Rotating wheels tend to generate lift and vortices. Interaction between the wing and wheel can act to reduce this lift and increase the downforce generated by the wing, or the reverse, depending on wing location (S.Diasinos et. al. 2004). To aid comparison between a hypothetical vehicle without wings and one with wings, the interaction effects will be neglected.

4.5 Vehicle weight

Some assumptions also need to be made about the car. The rules for FSAE do not state a minimum weight for the class, thus the general trend of most competitors has been for weight reduction. The weight of the RMIT car for 2006 was approximately 230 kg with driver. The wheelbase will be assumed as 1.1m. It will be assumed that the CoG is in the centre of the wheelbase, at a height of 0.3 m. When comparing the winged case to the non-winged, it will be assumed that the front wing assembly weighs an additional 10 kg, and rear wing assembly weighs an additional 15 kg. The suspension will be assumed to be rigid. The simulated vehicle will not be permitted to lift more than one wheel of the ground at any one time as per FSAE rules.

4.6 Tyres

The tyres used for the calculations will be those mentioned previously in section 1.6.1. The effects of camber and rolling resistance will be ignored.

4.7 Vehicle aerodynamic characteristics

Jawad and Longnecker, (2001) give some typical values for the aerodynamic coefficients of FSAE vehicles. It will be assumed that the vehicle has a frontal area of 1m^2 , C_L of 0.4 and C_D of 1. It will be assumed that the CoP is in the centre of the wheelbase, at a height of 0.3 m.

4.8 Potential performance benefit

Given these assumptions, some estimation can be made on the forces an active system would be able to generate, and how those forces would alter the performance envelope.

4.8.1 Pre-stall 3-D wing coefficients

The lift coefficient for a 3-D wing pre-stall is:

$$C_L = C_{L\alpha}(\alpha + \alpha_{L0})$$

Equation 4.5 Pre-Stall lift coefficient for a 3-D wing (Katz, 1995)

Where:

α = AoA

α_{L0} = AoA increment due to camber

$C_{L\alpha}$ is the lift slope, defined in Equation 4.6.

$$C_{L\alpha} = \frac{2\pi}{1 + 2/(AR)}$$

Equation 4.6 Pre-stall lift slope of a 3-D wing for AR >6 (Katz, 1995)

Or alternatively:

$$C_{L\alpha} = \frac{2\pi}{\sqrt{1 + (2/AR)^2} + 2/(AR)}$$

Equation 4.7 Pre-stall lift slope of a 3-D wing for AR <4 (Anderson, 2001)

The pre-stall drag coefficient is a combination of the lift-induced drag and the viscous drag as in

$$C_D = C_{Di} + C_{D0}$$

Equation 4.8 Pre-stall drag coefficient for 3-D wing (Katz, 1995)

Where:

C_{Di} = Induced drag (refer Equation 4.9)

C_{D0} = Viscous drag (pressure and skin friction)

An approximation for the induced drag is found using Equation 4.9

$$C_{Di} = \frac{C_L^2}{\pi \cdot AR}$$

Equation 4.9 Induced drag for 3-D wing (Katz, 1995)

4.8.2 Post-stall 3-D wing coefficients

The lift coefficient for the post stall 3-D wing can be estimated by considering the normal forces acting on a flat plate. Figure 4.1 displays the effect of AR on the drag coefficient of a flat plate normal to the flow. The drag coefficient is plotted against the inverse of the AR, shown as “ h/b ”, with “ h ” representing the chord of the plate, and “ b ” the span.

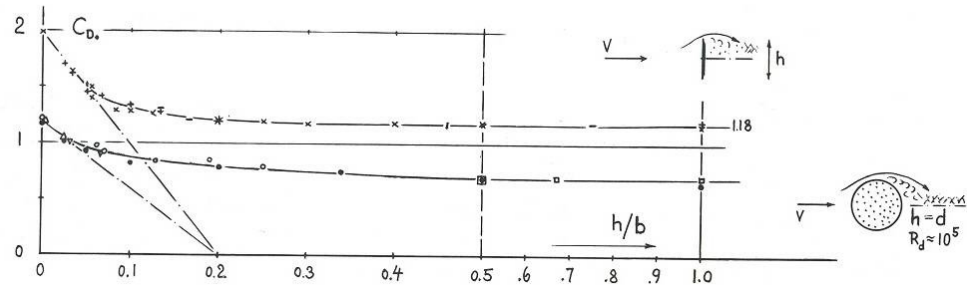


Figure 4.1 Drag coefficients of rectangular plates as a function of 1/AR (Hoerner, 1965)

In Figure 4.1 it can be seen that the majority of variation occurs between $h/b = 0$ and $h/b = 0.1$ (AR of ∞ to 10). Variation of drag coefficient is minor for an AR below 10. Thus while the effects of the end plates on the coefficients of a stalled wing are not known precisely, their effect can be assumed to be minor, and will be neglected. Following this principle, the pressure drag and lift coefficients for the stalled wing will be approximated by the relationships suggested by Hoerner (1965). (refer Equation 4.10 and Equation 4.11)

$$C_L = C_{D90} \cos(\alpha)$$

Equation 4.10 Lift coefficient for post-stall 3-D wing

$$C_D = C_{D90} \sin(\alpha)$$

Equation 4.11 Drag coefficient for post-stall 3-D wing

Where:

C_{D90} = Drag coefficient at 90° AoA

In the case of a flat plate, $C_{D90} = 1.98$ for 2-D and 1.17 for the AR of the 3-D rear wings used herein. Additionally the ground clearance of the front wing will reduce this by approximately 20% as found in this investigation, thus for the front wing, $C_{D90} = 0.94$

4.8.3 Potential forces and benefit from system

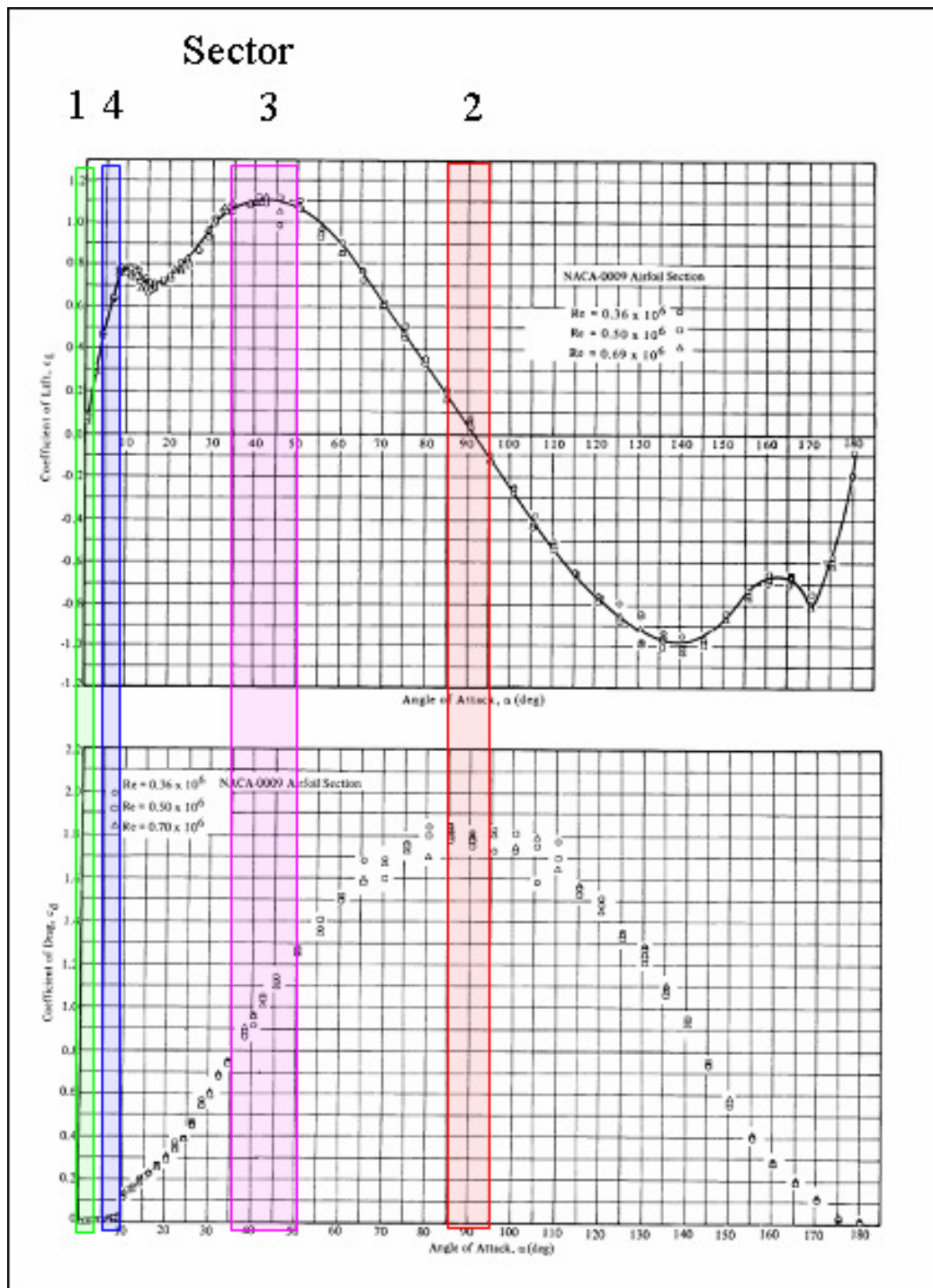
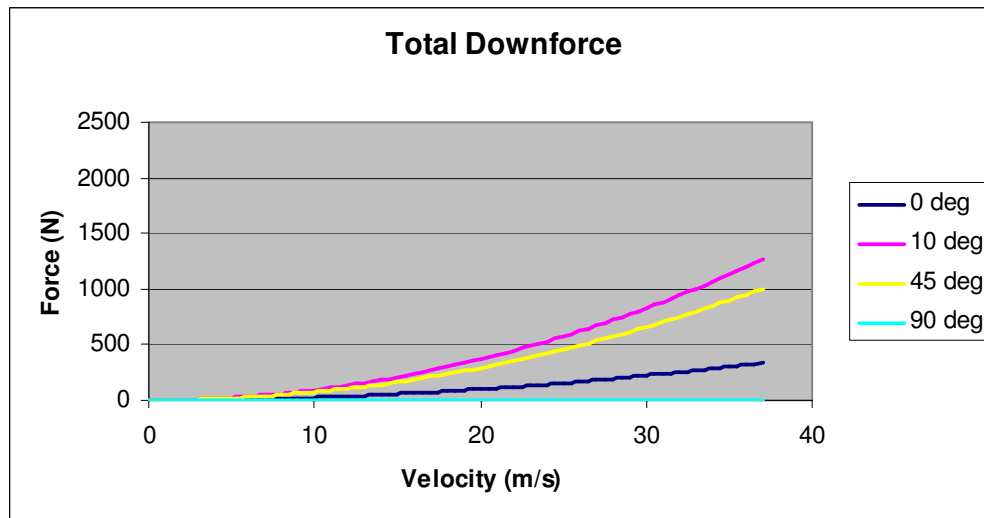
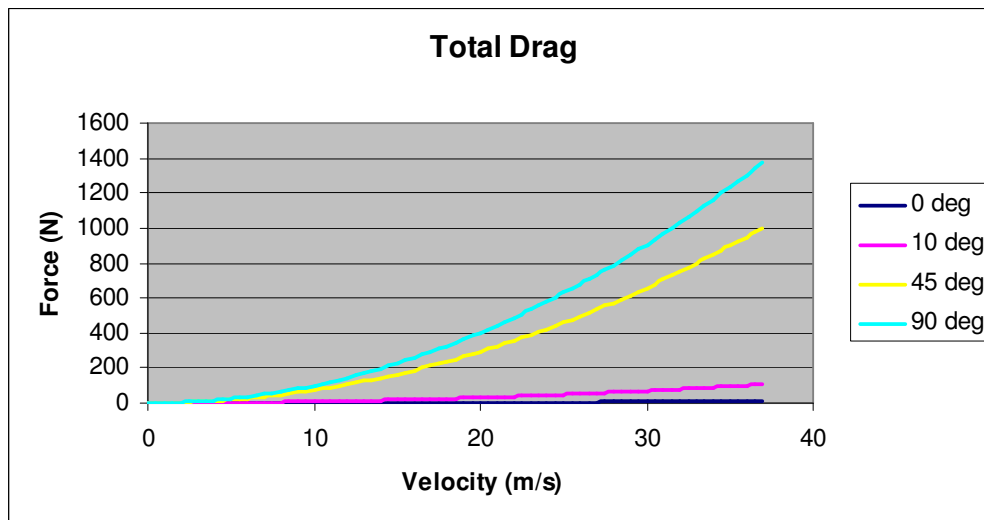


Figure 1.9 showed four wing positions that would be suitable in different regions of the track. Using the relationships for a 3-D wing (refer Equation 4.1 to Equation 4.11) the coefficients for lift and drag were calculated using the Clark Y profile. The calculated coefficients are tabulated in Table 4-3. Sample calculations are provided in Appendix 3.

AoA	C_L		C_D	
	Front	Rear	Front	Rear
0°	0.29	0.25	0.0074	0.0079
10°	1.07	0.94	0.075	0.085
45°	0.66	0.83	0.66	0.83
90°	0.0	0.0	0.94	1.17

Table 4-3 Coefficients of 3-D wings for varied AoA

Figure 4.2 shows the total downforce from both wings combined in each of these positions, while Figure 4.3 shows the total drag.

**Figure 4.2 Total downforce vs speed****Figure 4.3 Total drag vs speed**

As mentioned previously the speeds reached in competition tend to be fairly low. The FSAE rules (2006) for track layout are written with the intent of providing average speeds of 48 km/h. Figure 4.4 shows the percentage of lap-time spent at different speeds around a FSAE circuit. The plot represents a

lap of the endurance event for the RMIT car at the US FSAE competition in Detroit. These data were supplied by RMIT Racing and is used with permission.

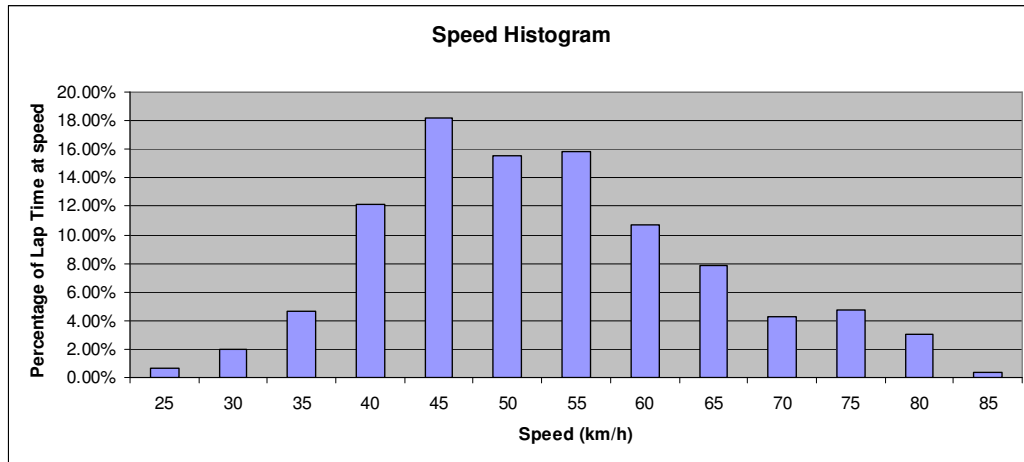


Figure 4.4 Speed histogram for an FSAE circuit

The data show the car spending almost 50% of the lap between 45-60 km/h. This is expected as the rules for the design of the track limit the length of any straights.

Given the assumptions and data previously discussed, without wings, the car would experience 56 N of lift and 140 N of drag at a speed of 55 km/h. This, combined with the tyre data give the car a steady state cornering potential of 1.73g or straight line braking potential of 1.85g.

If wings were fitted, the potential exists for a car travelling at 55km/h to improve its steady state cornering by 9% to 1.89g (wings @ 10°), or alternatively its braking by 10% to 2.04g (wings @ 45°). With the wings in the

low-drag position (0° AoA) the additional power requirement would be only 26.0W. It must be stressed however that this is merely an approximation and more complex simulation including the effects different AoA front and rear, and of moving CoP should be used to more accurately evaluate the potentials of the system.

Chapter 5 Conclusions and recommendations

5.1 Preamble

This chapter will revisit the objectives of the research, present conclusions and provide recommendations for further research.

The objectives of this research were as follows:

- How do the drag and lift forces vary with AoA in the range of 0° - 135° in ground effect?
- How does the Centre of Pressure location move with varied AoA within this range, in the presence of ground?
- How can this information potentially be used to enhance the performance of a Formula style car?

In the case of the Clark Y and 6-Series aerofoils, the lift force did not vary as expected prior to stall, with force decreasing with decreased ground clearance. The aerofoil with the Gurney tab displayed the typical characteristic of increased lift force with decreased ground clearance. All aerofoils displayed a decrease in drag with decreased ground clearance. The stall of the three aerofoils occurred at a higher AoA at close ground clearance than outside ground effect. Post-stall, the three aerofoils showed a decrease in lift and drag force with decreased ground clearance. Further study is required to determine how the ground simulation has affected these results. It is possible that the trends in the lift and drag data are a result of interaction with the ground

boundary layer, and further study conducted in the field or with more accurate ground simulation may produce alternate findings.

The CoPs of the aerofoils were found to move rearward with increased AoA. The magnitude of this effect was reduced with decreased ground clearance. This effect however may also be exaggerated by the ground simulation used, due to boundary layer interaction effects. The rearward movement of the CoP was expected for these aerofoils. Of interest would be a test with an aerofoil designed for zero / low pitch moment variation with AoA. A wing with this type of aerofoil could be mounted with a lighter actuator owing to the reduced moment throughout the range of AoA.

Simulating the potential effects of installing an active aerodynamic system on a FSAE race car showed potential to improve steady-state cornering by 9% and straight-line braking by 10%. An aerodynamic system that would allow tailoring the AoA of a wing for the requirements of a race or production car would increase the performance envelope of the vehicle in some circumstances, however the added performance would have to be seen to outweigh the increased cost, weight and complexity such a system would entail. The control system design is a very complex issue that would need to be addressed for proper implementation, as increasing the workload of the driver is not desirable. Further study such as lap-time simulation, control system design and cost analysis is required before further commitments are made to an active aerodynamic system.

An important phenomenon relating to stalled aerofoils is vortex shedding. This is a dynamic effect, thus not shown by the time averaged results in this investigation. The shedding of vortices leads to periodic loading of the aerofoil. Both the frequency and amplitude must be taken into account when designing a structure to support a stalled aerofoil, and determining the effects of this dynamic input to the race car. The frequency of the loading must not overly excite the structure, and the structure must withstand the addition of steady-state and periodic forces. The effect of ground proximity on the vortex shedding of a stalled aerofoil should be the topic of further research.

Another dynamic effect not covered by this research is dynamic stall. The stall of a wing is altered by rapid pitching. In the case of an inverted aerofoil, a nose-down pitch motion will tend to increase the AoA the stall occurs. A great deal of research has been done in the field of helicopter aerodynamics in this area. Any active aerodynamic system for a FSAE race car will need to alter AoA rapidly and thus may encounter this phenomenon. The effect of ground proximity on dynamic stall is beyond the scope of this research.

Any control system for varying AoA will require extensive design and testing to gain the potential benefits of reduced lap-times and perhaps integrate with the driver. There is also the compromise of added mass, volume and cost that would need to be assessed prior to a team attempting to incorporate such a system.

References and bibliography

1. J.D. Anderson, Jr. "**Fundamentals of Aerodynamics**," 3rd Ed. McGraw-Hill, New York, NY USA, 2001
2. J.D. Anderson, Jr. "**Introduction to Flight**," 5th Ed. McGraw-Hill, New York, NY USA, 2005
3. Anon. "**2006 Formula SAE Rules**," <http://www.sae-a.com.au/fsae/rules.htm>, Society of Automotive Engineers, Warrendale, USA, 2005, accessed 20/8/05
4. Anon. "**TFI Catalogue**," <http://www.turbulentflow.com.au>, Turbulent Flow Instrumentation P/L, 2005, accessed 20/8/05
5. T.J. Barber, E. Leonardi, R.D. Archer, "**Causes for Discrepancies in Ground Effect Analyses**," The Aeronautical Journal, Vol 106, No. 1066, December 2002
6. T.J. Barber, "**Aerodynamic Ground Effect: a Case Study of the Integration of CFD and Experiments**," International Journal of Vehicle Design, Vol. 40, No. 4, 2006
7. J.B. Barlow, W.H. Rae Jr, A. Pope, "**Low-Speed Wind Tunnel Testing, Third Ed.**" John Wiley & Sons inc, New York, USA, 1999.
8. R.H. Barnard "**Road Vehicle Aerodynamic Design: an Introduction, 2nd Ed.**" St Albans : MechAero, 2001

9. M.J. Berchak & M.W. Camosy, "**Comparison of Full-Scale Wing Wind Tunnel Test to Scale-Model Test for Open Wheel Race Cars,**" SAE 942495 Society of Automotive Engineers, Warrendale, USA, 1994
10. L Bjarke, J Del Frate & D Fisher, "**A Study of the Forebody High-Angle-of-Attack Aerodynamics Research on the F-18 and the X-29A Aircraft,**" NASA TM 104261, 1992
11. J.M Chen, Yuan-Cheng Fang, "**Strouhal Numbers of Inclined Plates,**" Journal of Wind Engineering and Industrial Aerodynamics, Vol 61, No. 2, July 1996
12. D.P. Coiro, F. Niccolosi, A. Amendola, D. Barbagallo, L. Paparone, S. Beccio, P. Castelli & S. Limone, "**Experiments and Numerical Investigation on a Multi-Component Airfoil Employed in a Racing Car Wing,**" SAE 970411, Society of Automotive Engineers, Warrendale, USA, 1997
13. K. Cooper, T. Bertenyi, G. Dutil, J Syms & G. Sovran, "**The Aerodynamic Performance of Automotive Underbody Diffusers,**" SAE 980030, Society of Automotive Engineers, Warrendale, USA, 1998
14. K. Cooper, G. Sovran & J Syms, "**Selecting Automotive Diffusers to Maximise Underbody Downforce,**" SAE 2000-01-0354, Society of Automotive Engineers, Warrendale, USA, 2000

15. S.Diasinos, T.J. Barber, E. Leonardi and S.D. Hall, "**A Two-Dimensional Analysis of the Effect of a Rotating Cylinder on an Inverted Aerofoil in Ground Effect.**" Australasian Fluid Mechanics Conference, Sydney, Australia, 2004
16. R.G. Dominy, A. Ryan, D.B. Sims-Williams, "**The Aerodynamic Stability of a Le Mans Prototype Race Car Under Off-Design Pitch Conditions**" SAE 2000-01-0872, Society of Automotive Engineers, Warrendale, USA, 2000
17. K.P. Garry, "**Some Effects of Ground Clearance and Ground Plane Boundary Layer Thickness on the Mean Base Pressure of a Bluff Vehicle Type Body,**" Journal of Wind Engineering and Industrial Aerodynamics, Vol. 62, No. 1, August 1996
18. A.P. Gaylard, A.J. Baxendale, J.P. Howell, "**The Use of CFD to Predict the Aerodynamic Characteristics of Simple Automotive Shapes,**" SAE 980036, Society of Automotive Engineers, Warrendale, USA, 1998
19. M. Gharib, "**Perspective: The Experimentalist and the Problem of Turbulence in the Age of Supercomputers,**" Journal of Fluids Engineering – Transactions of the ASME 118 (2): 233-242 JUN 1996
20. P.A.Gili, D.M.Pastone, F.B.Quagliotti, "**Blockage Corrections at High Angles of Attack in a Wind Tunnel,**" Journal of Aircraft, Vol. 27, No. 5, May 1990

21. H. Glauert, “**The Effect of the Static Pressure Gradient on the Drag of a Body Tested in a Wind Tunnel,**” Reports and Memoranda, No 1158, March 1928
22. S.F. Hoerner, “**Fluid-Dynamic Drag,**” Hoerner Fluid Dynamics, Vancouver, WA, 1965
23. S.F. Hoerner & H.V. Borst, “**Fluid Dynamic Lift,**” Hoerner Fluid Dynamics, Brick Town, N.J. USA, 1975
24. E.L.Houghton, N.B.Carruthers, “**Aerodynamics for Engineering Students, 2nd Ed.**” Edward Arnold Publishers Ltd, London, UK, 1982
25. J. Howell & D. Hickman, “**The Influence of Ground Simulation on the Aerodynamics of a Simple Car Model,**” SAE 970134, Society of Automotive Engineers, Warrendale, USA, 1997
26. J.P. Howell, G.M. Le Good, “**The Influence of Aerodynamic Lift on High Speed Stability,**” SAE 1999-01-0651, Society of Automotive Engineers, Warrendale, USA, 1999
27. W.H.Hucho, “**Aerodynamics of Road Vehicles: From Fluid Mechanics to Vehicle Engineering 4th Ed.**” Society of Automotive Engineers, Warrendale, USA, 1998
28. D.W Hurst, “**Modern Wind Tunnel Testing of Indycars,**” SAE 942497, Society of Automotive Engineers, Warrendale, USA, 1994

29. W. Jasinski, M. Selig, "**Experimental Study of Open_Wheel Race-Car Front Wings,**" SAE 983042, Society of Automotive Engineers, Warrendale, USA, 1998
30. Jawad, B.A, Longnecker, M.M, "**Aerodynamic Evaluation on Formula SAE Vehicles,**" SAE 2001-01-1270, Society of Automotive Engineers, Warrendale, USA, 2001
31. J. Katz, "**Aerodynamic Model for Wing-Generated Down Force on Open-Wheel-Racing-Car Configurations,**" SAE 860218, Society of Automotive Engineers, Warrendale, USA, 1986
32. J. Katz, L Dykstra, "**Effect of Wing/Body Interaction on the Aerodynamics of Two Generic Racing Cars,**" SAE 920349, Society of Automotive Engineers, Warrendale, USA, 1992
33. J. Katz, L. Dykstra, "**Application of Computational Methods to the Aerodynamic Development of a Prototype Race Car,**" SAE 942498, Society of Automotive Engineers, Warrendale, USA, 1994
34. J. Katz , "**High-Lift Wing design for Race-Car Applications,**" SAE 951976, Society of Automotive Engineers, Warrendale, USA, 1995
35. J. Katz , "**Race Car Aerodynamics: Designing for speed,**" Bentley Publishers, Massachusetts, USA, 1995
36. J. Katz, R. Walters, "**Effects of Large Blockage in Wind-Tunnel Testing,**" Journal of Aircraft, Vol 32, No 5, 1995

37. J. Katz, H. Luo, E. Mestreau, J. Baum & R. Lohner, "**Viscous-Flow Simulation of an Open-Wheel Race Car**," SAE 983041, Society of Automotive Engineers, Warrendale, USA, 1998
38. J. Katz, D. Garcia, "**Aerodynamic effects of Indy car components**," SAE 2002-01-3311, Society of Automotive Engineers, Warrendale, USA, 2002
39. R. Knowles, A. Saddington & K. Knowles, "**On the near wake of rotating, 40%-scale champ car wheels**," SAE 2002-01-3293, Society of Automotive Engineers, Warrendale, USA, 2002
40. D. Landman & C. Britcher, "**Development of race car testing at the Langley full-scale tunnel**," SAE 983040, Society of Automotive Engineers, Warrendale, USA, 1998
41. G.M. Le Good, A. McArthur, "**On-Road Measurements of Aerodynamic Lift Compared with Wind Tunnel Data**," SAE 960900, Society of Automotive Engineers, Warrendale, USA, 1996
42. C. Lindenburg, "**Stall Coefficients**," IEA symposium on the aerodynamics of wind turbines, December 4-5 2000, NREL, CO, USA
43. G.G. Mateer, D.J. Monson, F.R. Menter, "**Skin-Friction Measurements and Calculations on a Lifting Airfoil**," AIAA Journal, Vol 34, No 2, Feb 1996.

44. N. McKay, A. Gopalarathnam, "**The Effects of Wing Aerodynamics on Race Vehicle Performance**," SAE 2002-01-3294, Society of Automotive Engineers, Warrendale, USA, 2002
45. A.P. Mears, R.G. Dominy & D.B.Sims-Williams, "**The Air Flow about an Exposed Racing Wheel**," SAE 2002-01-3290, Society of Automotive Engineers, Warrendale, USA, 2002
46. E. Mercker, N. Breuer, H. Berneburg & H.J. Emmelmann, "**On the Aerodynamic Interference Due to the Rolling Wheels of Passenger Cars**," SAE 910311, Society of Automotive Engineers, Warrendale, USA, 1991
47. Milliken, W.F and Milliken, D.L, "**Race Car Vehicle Dynamics.**" Society of Automotive Engineers, Warrendale, USA, 1995
48. W. Mokhtar, "**A Numerical Study of High-Lift Single Element Airfoils with Ground Effect for Racing Cars**," SAE 2005-01-0607, Society of Automotive Engineers, Warrendale, USA, 2005
49. A.S.Ramamurthy, R.Balachandar, Diep Ngoc Vo, "**Blockage Correction for Sharp-Edged Bluff Bodies**," Journal of Engineering Mechanics, Vol. 115, No.7, July 1989
50. W.H. Jr Rae, A. Pope, "**Low-Speed Wind Tunnel Testing**," Wiley, New York, 1984

51. R. Ranzenbach, J. B. Barlow, "**Two-Dimensional Airfoil in Ground Effect, An Experimental and Computational Study,**" SAE 942509, Society of Automotive Engineers, Warrendale, USA, 1994
52. R. Ranzenbach, J. B. Barlow, "**Cambered Airfoil in Ground Effect – An Experimental and Computational Study,**" SAE 960909, Society of Automotive Engineers, Warrendale, USA, 1996
53. F.Riegels "**Airfoil Sections : Results from wind-tunnel investigations, theoretical foundations,**" Butterworth, London, 1961
54. P.E. Roach, J.T. Turner, "**Premature Boundary Layer Transition Caused by Surface Static Pressure Tappings,**" Aeronautical Journal, Feb 1988
55. J.Scott. "**NACA Airfoil Series,**"
<http://www.aerospaceweb.org/question/airfoils/q0041.shtml>, Aug 2001, accessed 20/8/05
56. R.E Sheldahl, P.C. Klimas, "**Aerodynamic Characteristics of Seven Symmetrical Airfoil Sections Through 180-Degree Angle of Attack for Use in Aerodynamic Analysis of Vertical Axis Wind Turbines,**" SAND 80-2114, Sandia National Laboratories, Albuquerque, NM, 1981
57. M. Soso, M. Selig, "**An Angle of Attack Correction Scheme for the Design of Low Aspect Ratio Wings with Endplates,**" SAE 2002-01-3292, Society of Automotive Engineers, Warrendale, USA, 2002

58. D. Steinbach, K. Jacob, "**Some Aerodynamic Aspects of Wings near Ground,**" Transactions of the Japan Society for Aeronautical and Space Sciences, Vol 34, No 104, Aug 1991
59. D. Steinbach, "**Comment on "Aerodynamic Characteristics of a Two-Dimensional Airfoil in Ground Effect",**" Journal of Aircraft, Vol 34, No 3, May-June 1997
60. K.E. Swalwell, J. Sheridan and W.H. Melbourne "**Frequency Analysis of Surface Pressures on an Airfoil after Stall,**" AIAA-2003-3416, 21st AIAA Applied Aerodynamics Conference, Orlando, Florida, June 23-26, 2003
61. E. van Opstal, P. Sandkuijl, S. Aubin "**The WIG Page,**" <http://www.setechnology.com/wig>, 2003, accessed 20/8/05
62. Visconti, Fedeli & Longhi, "**Aerodynamics Drives Chassis Design on Ferrari 360 Modena,**" SAE 2000-01-0093, Society of Automotive Engineers, Warrendale, USA, 2000
63. G. Wickern, K. Zwicker & M. Pfadenhauer, "**Rotating Wheels - Their Impact on Wing Tunnel Test Techniques and on Vehicle Drag Results,**" SAE 970133,
64. G. Wickern, A. Wagner & C. Zoerner, "**Induced Drag of Ground Vehicles and its Interaction with Ground Simulation,**" SAE 2005-01-0872, Society of Automotive Engineers, Warrendale, USA, 2005

65. S. Wordley, J. Saunders, "**Aerodynamics for Formula SAE: Initial Design and Performance Prediction,**" SAE 2006-01-0806, Society of Automotive Engineers, Warrendale, USA, 2006
66. X. Zhang & J. Zerihan, "**Turbulent Wake behind a Single Element Wing in Ground Effect,**" 10th International Symposium on Applications of Laser Techniques to Fluid Mechanics, 10-13 July, 2000
67. X.Zhang, J. Zerihan, A. Ruhrmann & M. Deviese, "**Tip Vortices Generated by a Wing In Ground Effect,**" 11th International Symposium on Applications of Laser Techniques to Fluid Mechanics, 8-11 July, 2002

Appendix 1 Calibration

A1.1 Dynamic Cobra probe calibration

“The Cobra Probe is a 4-hole pressure probe that provides dynamic, 3-component velocity and local pressure measurements in real-time.” (TFI Catalogue). “The Cobra Probe incorporates four 0.5 mm pressure taps in a multi-faceted head, with the pressure taps connected via tubing to pressure transducers in the body of the Probe. The frequency response of the Probe is linearised to provide dynamic capabilities from the mean velocity component (0 Hz) to more than 2000 Hz. The ratios of the tap pressures are then related to the instantaneous velocity vector and static pressure at the Probe head via calibration tables.“

The Dynamic Cobra probes were calibrated with the aid of a pitot-static tube and inclined manometer. A Pitot - static tube was mounted in the IWT tunnel section. The manometer was levelled and zeroed, then the air velocity in the wind tunnel was set to 22 m/s (the wind speed used in this research) as measured by the pitot-static arrangement. The Pitot - static tube was then replaced by a Dynamic Cobra probe, and the air velocity at the same location was measured by the Dynamic Cobra probe. The Cobra probe was then removed and the Pitot - static tube was replaced to confirm the tunnel speed had not varied during the test. The process was repeated for each Cobra probe.

A1.2 DPMS calibration

“The Dynamic Pressure Measurement System (DPMS) is a multi-channel pressure measurement system that provides simultaneous measurement of both time-averaged (mean) and time-varying (fluctuating) pressure measurements in real-time.” (TFI Catalogue). “As with other similar systems, the DPMS measures pressure using separate pressure transducers for each channel located in the DP modules. However, the DPMS also corrects the signals for amplitude and phase distortions of fluctuating pressures that occur in the tubing used to connect the measurement points (pressure taps) to the modules. This process is termed ‘linearisation’. Linearisation allows the DPMS to provide accurate pressure measurements from 0 Hz (mean pressure) to several kHz, depending on tube dimensions. The linearisation is performed automatically as data is acquired by the included Device Control software after the user has entered details of the tubing.”

The DPMS is accurate to within $\pm 0.3\%$ for pressure measurements within 0 – 50 °C.

All the channels of the DPMS are plumbed to the same reference port, thus applying a known negative (gauge) pressure to the reference port causes all the channels read the same positive pressure difference.

The first step in the process was to level and zero the inclined manometer.

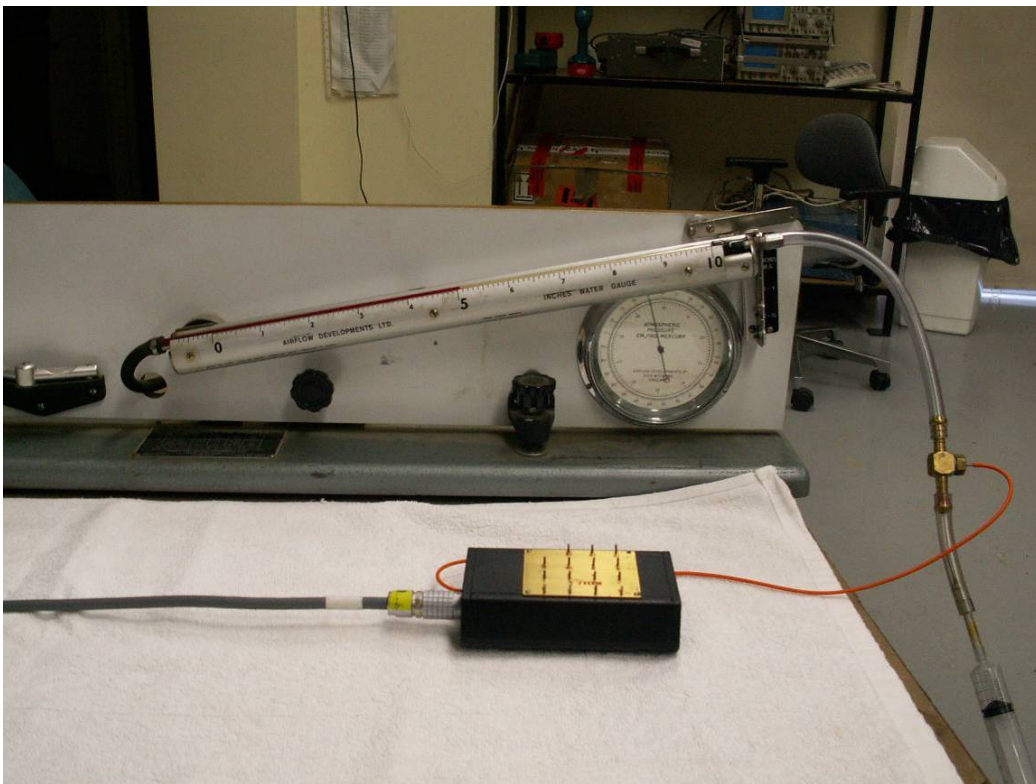


Figure A 1 DPMS during calibration

Once the manometer had been properly set up, tubes were attached, as in Figure A 1 to allow the vacuum drawn by a syringe to be applied to both the manometer and DPMS.

NOTE: To avoid potential damage to the DPMS, the tube to the reference port was be the last to be connected. Care was also taken with the syringe, as it is possible to damage the DPMS with overpressure.

Having checked for any leaks in the setup, the DPMS was zeroed before applying vacuum with the syringe. The reading on the manometer was noted, and compared to the results from the DPMS. At least three different

pressure readings were taken to check the error was a scalar factor. This process was repeated for each DPMS module.

A1.3 Tunnel calibration

Prior to testing, a Cobra probe was traversed across a vertical plane in the section where the wing was to be mounted. This provided a map of the flow velocity within the section, allowing it to be calibrated. It was found that outside of the boundary layers, the flow was fairly homogenous. There was little variation in the vertical direction, and the velocity contour was relatively flat across the central region (both within +/- 2%).

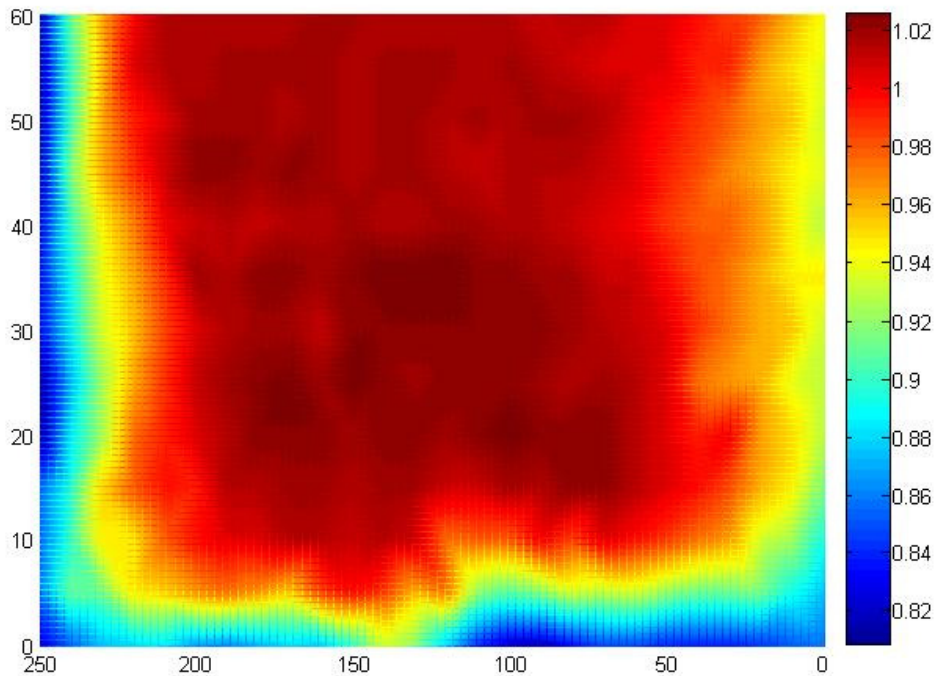


Figure A 2 Velocity contour of 2-D section

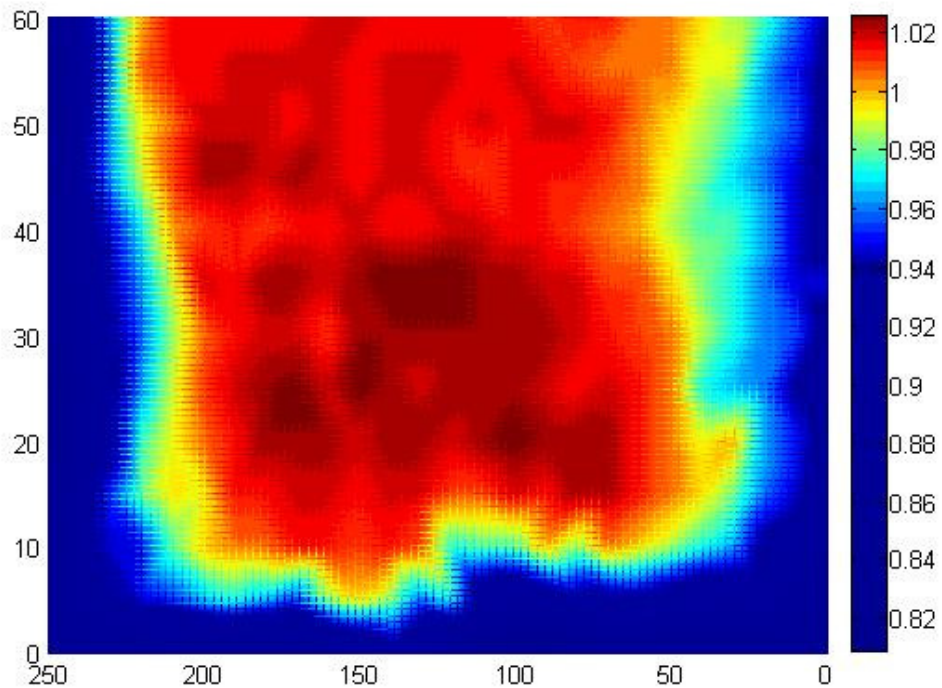


Figure A 3 Velocity contour of 2-D section (more refined)

The walls of the tunnel were tapped to allow monitoring of the static pressure gradient along the section. This gives an indication of corrections necessary for horizontal buoyancy and wake blockage. Holes were first drilled in the walls of the tunnel at 1 chord (150mm) intervals. The tube was next passed through the holes with some overhang and glued in place.

Figure A 4 shows the outside of the tunnel with pressure taps exiting the section.



Figure A 4 Pressure tapped tunnel wall

A total of 28 taps were used along the tunnel. The 8th tap was in line with the slot the aerofoil was mounted in. Figure A 5 shows a plot of the pressure gradient (normalised with dynamic pressure) down the tunnel section. A plot is shown for the empty tunnel, along with a plot taken when the aerofoil was at 90° AoA (full blockage). As can be seen, very little difference is visible between the two plots, implying little wake blockage.

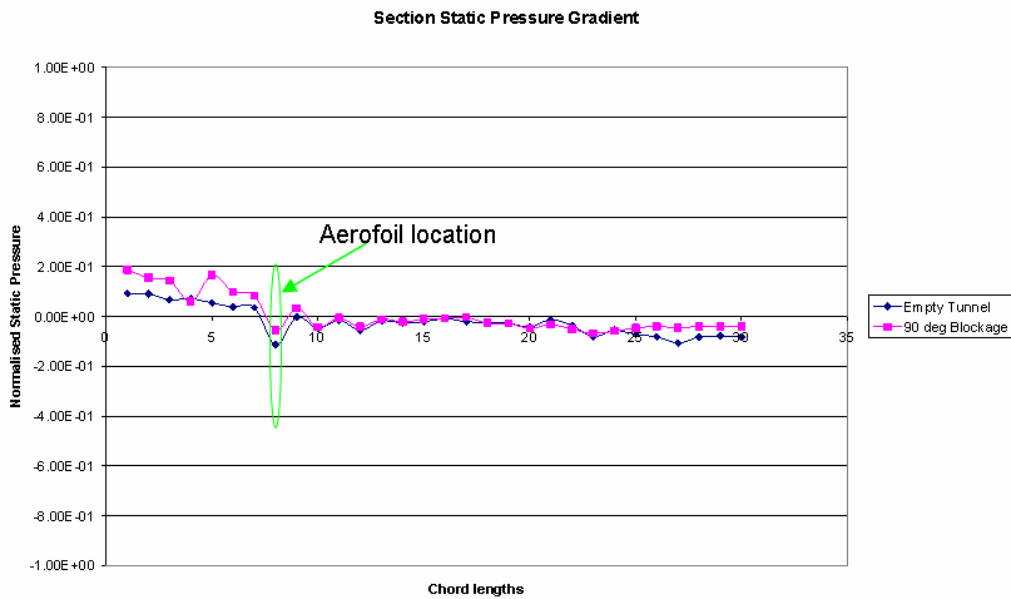


Figure A 5 Tunnel pressure gradient

The static pressure drops approximately 2 Pa per chord length down the tunnel, meaning any buoyancy effects would be minimal.

Appendix 2 Errors

A2.1 Aerofoil geometry

The aerofoil models were made in-house. In order to check geometric accuracy and allow comparison to official co-ordinate data, the aerofoil shapes were measured with a 3-D GOM. A 3-D “point cloud” of the aerofoil surface (Figure A 6) was created by the scanner, which was in turn condensed into 5 splines (Figure A 7) across the width of the wing. This allows comparison of the cross-section to literature, and a check of the two-dimensionality of the wing.

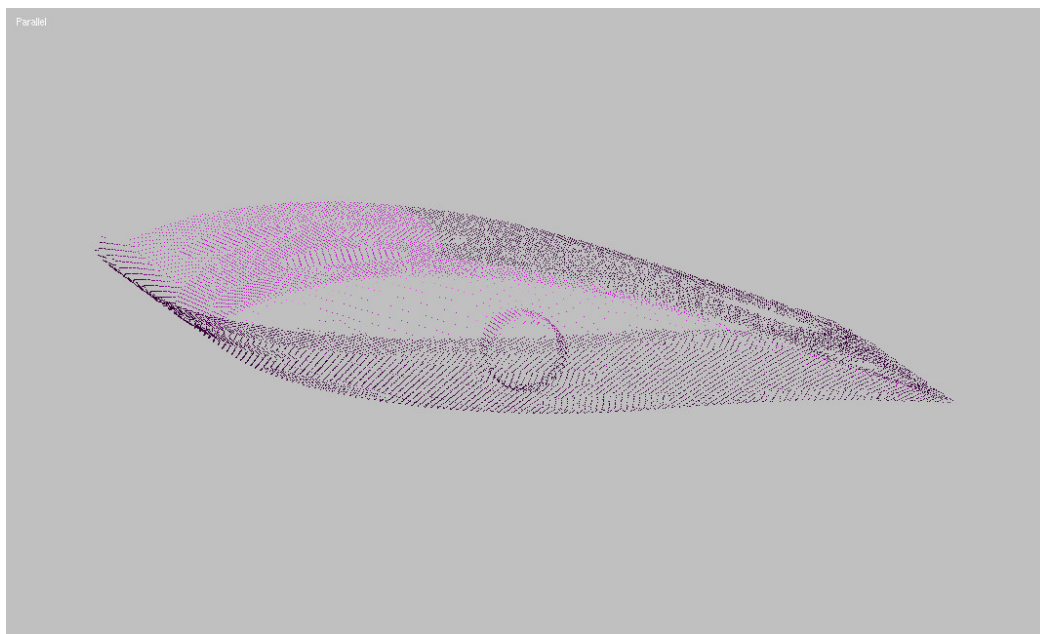


Figure A 6 Aerofoil point cloud

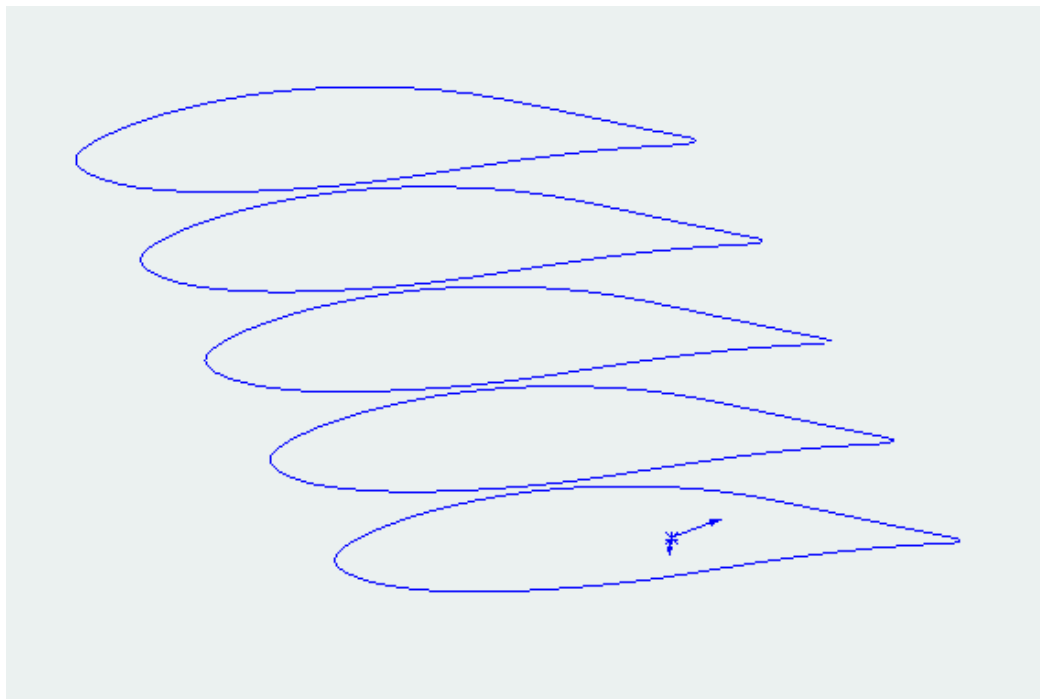


Figure A 7 Aerofoil splines

Both aerofoils were found to be within 2% of the published shape, and 2-D to within 1%. One of the splines generated from the Clark Y aerofoil is shown superimposed on the shape from literature in Figure A 8. The agreement between the two geometries is seen to be very good.

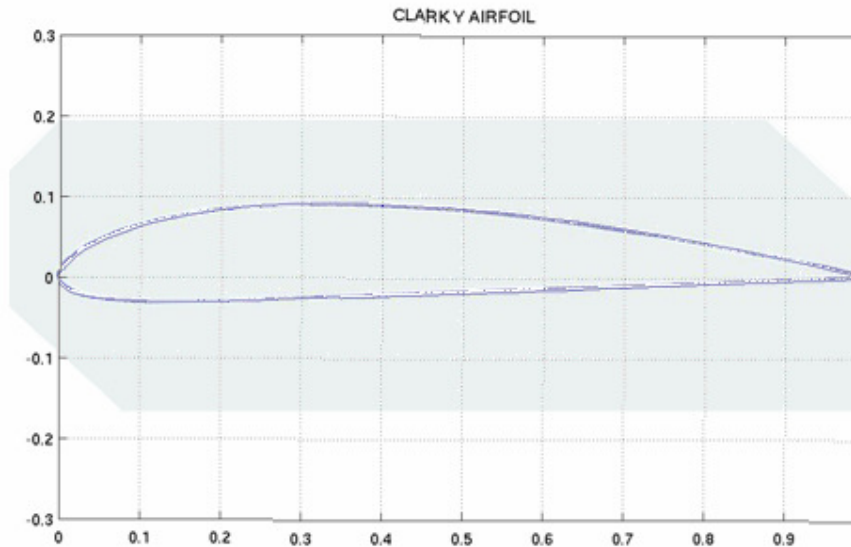


Figure A 8 Aerofoil overlay

A2.2 Measurement of AoA

The protractor used in the measuring of AoA (described in section 2.6) was graduated down to 1 deg increments. The AoA was checked before and after each run to make sure any play in the apparatus did not affect the results. A grub-screw located the shaft in the slide-block, and another screw located the slide blocks on the rails.

A2.3 Pressure measurement

Pressure data from the pressure taps on the aerofoils were captured with the DPMS; the calibration of which is discussed in Section A1.2. The DPMS is capable of collecting both dynamic and time-averaged data,

however only time-averaged was used in this investigation. Testing has shown the DPMS is accurate to +/- 0.3 %.

A2.4 Measurement of ground clearance

The ground clearance was measured with the aid of purpose built spacers, cut to the appropriate lengths. The spacer length was accurate to +/- 0.5 %. For each run, the AoA was adjusted, and then the height was set. In this manner, the height of the aerofoil above ground was always a measure of distance between the ground and the closest point on the aerofoil, rather than the ground and the pivot of the aerofoil, as has been the case with some other studies. The model was lowered until it rested on the spacer, then the locating screw was tightened, and the spacer was removed. Careful use of the spacers in this manner should give accuracy of height to within +/- 0.1 %., a running fit.

A2.5 Measurement of flow velocity

Flow velocity was measured with the aid of a Dynamic Cobra probe. The Cobra probe is a multi-holed probe that has been developed to give both time averaged and dynamic measurement of velocity, turbulence. See Section Appendix 1 for more details.

A2.6 Environmental variables

Environmental variables such as air temperature and density are quite hard to control, but do not effect the coefficient results, provided the variation

is not too large. During testing the ambient temperature varied from 15° to 28°. The ambient temperature, along with the ambient pressure is entered into the TFI software that samples the Dynamic Cobra probe and DPMS. Any effects from the variation in air density were cancelled when the pressure data were non-dimensionalised with the dynamic pressure.

A2.7 Repeatability study

In an effort to get an idea of the repeatability of the study, a number of trial runs were repeated at different times throughout the study. Table 5-1 shows the schedule for the four different tests at a set AoA of 60 deg and ground clearance of 500mm (3.33 c). Both the AoA and ground clearance were changed and reset between runs.

The tests were taken as follows

Test	1	2	3	4
Date Sampled	18-May-06	23-May-06	23-May-06	20-Aug-06
Time Sampled	21:16:15.109	12:29:37.281	14:18:33.000	20:10:29.015

Table 5-1 Repeatability test schedule

It should be noted that the whole apparatus was removed from the wind-tunnel and re-installed between the 3rd and 4th tests.

Figure A 10 shows the pressure recorded by each channel for the four runs. The first 15 channels are located on the underside of the aerofoil, with the following channels located on the top. See Figure A 9.

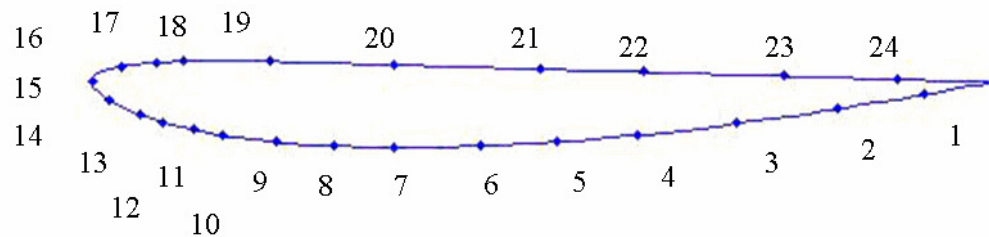


Figure A 9 Pressure tap layout for repeatability study

It is interesting to note in Figure A 11 that the majority of variation occurs in channels 16 through to 24. These were the pressure taps on the flat side of the aerofoil, and thus were subjected to less turbulent flow. Channels 1 through to 15 were on the curved surface of the aerofoil. As the aerofoil had stalled, these taps were in a turbulent wake region; however the variation of the time averaged pressures was small between the runs. It is thought the reason for this is due to high pressure gradients, the pressures on the side with attached flow are more sensitive to changes in AoA, especially near the leading edge (Channels 16 – 19). The time averaged pressures for regions in the wake will remain fairly similar across a wide range of AoA.

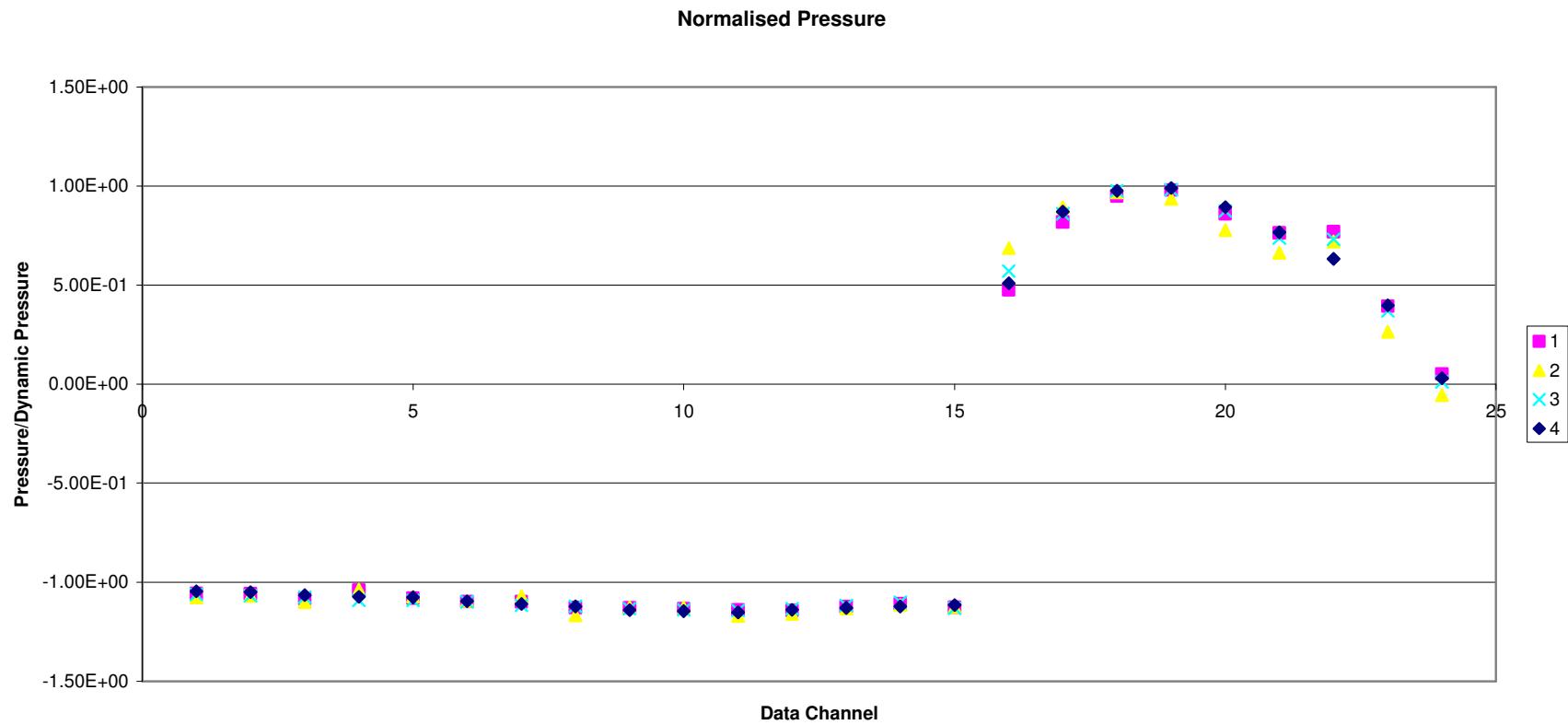


Figure A 10 Normalised pressure acquired per channel

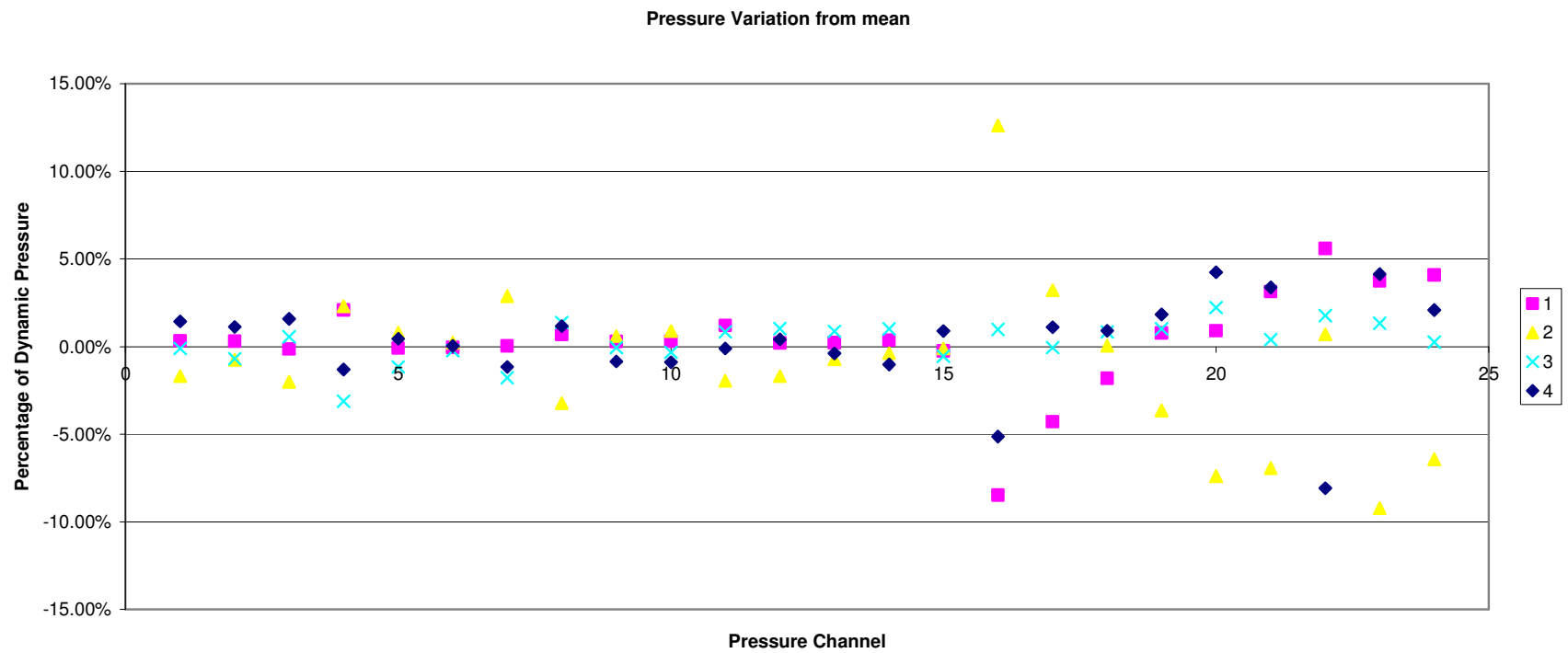


Figure A 11 Pressure variation between runs per channel

The pressure contours for each of the four runs were used to calculate the relevant force and moment coefficients. These are shown in Table 5-2.

Test	C_l	C_d	C_m
1	0.70617	1.8764	-0.061391
2	0.67675	1.8218	-0.05706
3	0.70101	1.8694	-0.059601
4	0.70105	1.8714	-0.05994
\bar{x} (mean)	0.69625	1.8598	-0.059498
σ (std. dev.)	0.01322	0.0255	0.001801

Table 5-2 Coefficient results from repeated trials

Table 5-2 shows the coefficients obtained from the 4 runs to be very similar. Run 2 showed the highest difference, the other 3 runs being much closer.

Appendix 3 Sample wing calculations

A3.1 Pre-Stall coefficients

Lift Coefficient

$$C_{L\alpha} = \frac{2\pi}{\sqrt{1 + (2/AR)^2} + 2/(AR)}$$

$$C_{L\alpha} = \frac{2\pi}{\sqrt{1 + (2/3.602)^2} + 2/(3.602)}$$

$$C_{L\alpha} = 3.698$$

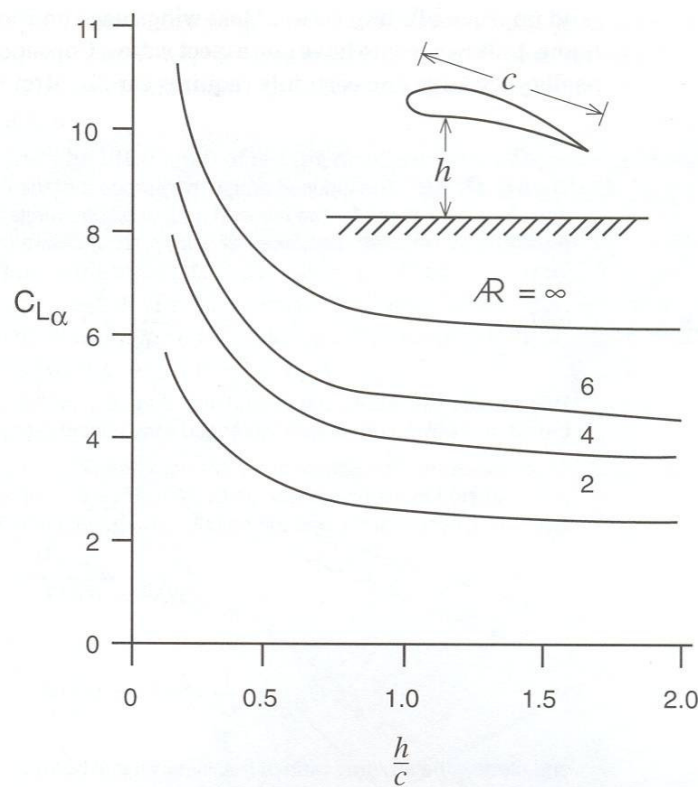


Figure A 12 Lift coefficient slope vs ground proximity

Figure A 12 shows the effect of ground proximity on the lift coefficient slope of rectangular wings. A simplification of this would be the addition of the basic (outside ground effect) $C_{L\alpha}$ with the curve shown in Figure A 13.

$$C_{L\alpha} = C_{L\alpha(Basic)} + \frac{\left(\frac{1}{(h/c)^2} - \frac{1}{4} \right)}{5}$$

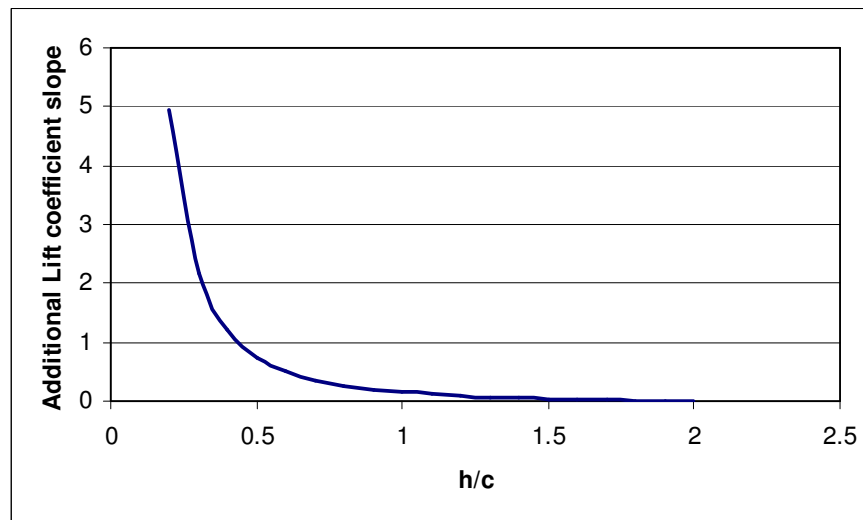


Figure A 13 Additional lift coefficient slope due to ground proximity

Using this method to account for the effect of ground proximity, the $C_{L\alpha}$ becomes:

$$F=9.48, R=3.67$$

Thus referring to Equation 4.5,

$$\begin{aligned} C_L &= C_{L\alpha}(\alpha + \alpha_{L0}) \\ C_L &= 9.48(10^\circ + 4^\circ) \times \frac{\pi}{180^\circ} \\ C_L &= 0.904 \end{aligned}$$

Drag Coefficient

$$\begin{aligned} C_{Di} &= \frac{C_L^2}{\pi \cdot AR} \\ C_{Di} &= \frac{0.904^2}{\pi \cdot 3.602} \\ C_{Di} &= 0.0722 \end{aligned}$$

$$\begin{aligned} C_{D0} &\cong C_{sf} \\ C_{D0} &\cong 2 \times \frac{1.328}{\sqrt{Re_L}} = \frac{2.656}{\sqrt{3.84 \times 10^5}} = 4.286 \times 10^{-3} \end{aligned}$$

$$\begin{aligned} C_D &= C_{Di} + C_{D0} \\ C_D &= 0.0722 + 4.286 \times 10^{-3} \\ C_D &= 0.07645 \end{aligned}$$

A3.2 Post-Stall Coefficients

Lift Coefficient

$$\begin{aligned} C_L &= C_{D90} \cos(\alpha) \\ C_L &= 0.94 \cos(45^\circ) \\ C_L &= 0.66 \end{aligned}$$

Drag Coefficient

$$C_D = C_{D90} \sin(\alpha)$$

$$C_D = 0.94 \sin(45^\circ)$$

$$C_D = 0.83$$